

STATE OF THE CLIMATE IN 2004

D. H. LEVINSON,¹⁹ Ed.

AFFILIATIONS (alphabetical by author)

1. PETER AMBENJE, Drought Monitoring Centre, Nairobi, Kenya
2. OMAR BADDOUR, National Meteorology Direction, Rabat, Morocco
3. GENNADY I. BELCHANSKY, Institute of Ecology, Moscow, Russia
4. GERALD D. BELL, MUTHUVEL CHELLIAH, MICHAEL S. HALPERT, KINGTSE MO, AND WASSILA M. THIAW, NOAA/NWS/NCEP Climate Prediction Center, Washington, D.C.
5. MICHAEL A. BELL, SUZANA J. CAMARGO, AND EMILY K. GROVER-KOPEC, International Research Institute for Climate Prediction, New York, New York
6. ERIC BLAKE AND RICHARD PASCH, NOAA/NWS National Hurricane Center, Miami, Florida
7. JASON E. BOX, Byrd Polar Research Center, The Ohio State University, Columbus, Ohio
8. OLGA N. BULYGINA, NATALIA N. KORSHUNOVA, AND VYACHESLAV N. RAZUVAEV, All Russian Research Institute of Hydro-meteorological Information, Obninsk, Russia
9. JOHN C. CHRISTY, University of Alabama, Huntsville, Alabama
10. EDWARD R. COOK, Lamont Doherty Earth Laboratory, Palisades, New York
11. MIGUEL CORTEZ VÁZQUEZ, Servicio Meteorológico Nacional, Mexico City, Mexico
12. BRUCE C. DOUGLAS, Laboratory for Coastal Research, Florida International University, Miami, Florida
13. DAVID C. DOUGLAS, USGS Alaska Science Center, Juneau, Alaska
14. SHELDON D. DROBOT, The National Academies, Washington, D.C.
15. C. MARK EAKIN AND CONNIE WOODHOUSE, NOAA/NESDIS National Climatic Data Center, Paleoclimatology Branch, Boulder, Colorado
16. RICHARD A. FEELY AND MICHAEL J. MCPHADDEEN, NOAA Pacific Marine Environmental Laboratory, Seattle, Washington
17. MICHAEL A. FORTUNE, Climate Science Forum, Silver Spring, Maryland
18. BRAD GARANGANGA, Drought Monitoring Centre, Belvedere, Harare, Zimbabwe
19. KARIN L. GLEASON, JAY H. LAWRIK, DAVID H. LEVINSON, MATTHEW J. MENNE, RICHARD W. REYNOLDS, SCOTT E. STEPHENS, AND ANNE M. WAPLE, (STG, Inc.), NOAA/NESDIS National Climatic Data Center, Asheville, North Carolina
20. STANLEY GOLDENBERG AND CHRISTOPHER LANDSEA, NOAA/OAR/AOML Hurricane Research Division, Miami, Florida
21. JOHN KENNEDY, Hadley Centre for Climate Prediction and Research, Met Office, Exeter, United Kingdom
22. CHRIS KOCOT, DAVID PHILLIPS, AND ROBERT WHITEWOOD, Environment Canada, Ottawa, Ontario, Canada
23. K. RUPA KUMAR, Indian Institute for Tropical Meteorology, Pune, India
24. WILLEM LANDMAN, South African Weather Service, Pretoria, South Africa
25. NIKOLAI MAXIMENKO, International Pacific Research Center, University of Hawaii at Manoa, Honolulu, Hawaii
26. LAURY MILLER, NOAA/OAR Laboratory for Satellite Altimetry, Silver Spring, Maryland
27. PETER NIILER AND LYNNE TALLEY, Scripps Institute of Oceanography, University of California, La Jolla, California
28. ANDREW K. NJOGU, IGAD Climate Prediction and Applications Centre, Nairobi, Kenya
29. FATIMA RAHIMZADEH, Atmospheric Science and Meteorological Research Center, Tehran, Iran
30. MADHAVAN RAJEEVAN, India Meteorological Department, Pune, India
31. JACKIE RICHTER-MENGE, Cold Regions Research and Engineering Laboratory, Hanover, New Hampshire
32. ERIC RIGNOT, NASA Jet Propulsion Laboratory, Pasadena, California
33. IGNATIUS G. RIGOR, University of Washington, Seattle, Washington
34. DAVID A. ROBINSON, Rutgers University, New Brunswick, New Jersey
35. MATILDE RUSTICUCCI, University of Buenos Aires, Buenos Aires, Argentina
36. M. JAMES SALINGER, National Institute of Water and Atmospheric Research, Newmarket, Auckland, New Zealand
37. RUSSELL C. SCHNELL AND ROBERT S. STONE, NOAA/ERL Climate Monitoring and Diagnostics Laboratory, Boulder, Colorado
38. DIANE STANITSKI, NOAA/OAR Office of Global Programs, Silver Spring, Maryland
39. AFSANEH TAGHIPOUR, Iran Meteorological Organization, Tehran, Iran
40. RIK WANNINKHOF, NOAA/OAR/AOML Ocean Chemistry Division, Miami, Florida
41. ANDREW B. WATKINS AND BLAIR TREWIN, Australian Bureau of Meteorology, Melbourne, Australia
42. PANMAO ZHAI AND XUKAI ZOU, National Climate Center, Beijing, China

CORRESPONDING AUTHOR ADDRESS: Dr. David Levinson, Climate Monitoring Branch, National Climatic Data Center, NOAA/NESDIS, Asheville, NC 28801
E-mail: David.Levinson@noaa.gov

TABLE OF CONTENTS

1. Introduction.....	7
2. Global climate	8
a. Global surface temperature	8
b. Upper-air temperature	10
i) Low–midtroposphere.....	11
ii) Midtroposphere.....	11
iii) Lower stratosphere	11
c. Global precipitation	11
d. Northern Hemisphere snow cover.....	14
e. Climate of the oceans.....	14
i) Global sea level rise	14
ii) Sea surface temperatures	16
iii) Ocean heat and freshwater content and transports.....	17
iv) Evolution of the 2004 El Niño.....	17
v) Global ocean carbon cycle: Inventories, sources, and sinks	17
vi) Surface current observations.....	18
vii) Sea ice extent and thickness	19
3. Trends in trace gases	20
a. Carbon dioxide.....	20
b. Methane	21
c. Carbon monoxide	21
d. Halocarbons.....	21
e. N ₂ O and SF ₆	22
4. The Tropics	23
a. ENSO and the tropical Pacific	23
i) Overview.....	23
ii) Equatorial Pacific Ocean sea surface and subsurface temperature evolution	24
iii) The MJO, Kelvin wave activity, and atmospheric circulation	24
b. Tropical storms.....	26
i) Atlantic hurricane season	26
ii) North Pacific tropical storms.....	29
iii) South Pacific and Australia region tropical cyclones	35
iv) Indian Ocean tropical cyclones	37

TABLE OF CONTENTS

5. Polar climate.....	39
a. Arctic.....	39
i) Temperature.....	39
ii) Sea ice.....	39
iii) Greenland.....	41
b. Antarctic.....	42
i) Surface climate.....	43
ii) Stratospheric ozone.....	43
6. Regional climate.....	44
a. North America.....	44
i) Canada.....	44
ii) United States of America.....	48
iii) Mexico.....	53
b. Central America.....	54
c. South America.....	55
d. Europe.....	55
e. Africa.....	58
i) North Africa.....	58
ii) West Africa.....	59
iii) East Africa and the Greater Horn.....	61
iv) Southern Africa.....	62
f. Asia.....	64
i) China.....	64
ii) Southwest Asia.....	66
iii) Russia.....	68
iv) South Asian monsoon.....	70
g. Australasia and the Southwest Pacific.....	73
i) Australia.....	73
ii) New Zealand.....	75
iii) Southwest Pacific.....	75
7. Seasonal summaries.....	77
Acknowledgments.....	81
Appendix: Contributors.....	81
References.....	81

From a global perspective, the annual average surface temperature in 2004 was the fourth highest value observed since regular instrumental records began in 1880. Global surface air temperatures in 2004 were 0.44°C (0.79°F) above the 1961–90 mean, according to both the U.S. and U.K. archives. Observations of the global annual mean temperature in 2004 from the combined lower and middle troposphere was 0.38°C (0.68°F)—the fourth warmest year in the 47-yr archive of worldwide radiosonde observations, and the ninth warmest year out of the past 26 based on satellite measurements.

The average precipitation anomaly over global land areas in 2004 was 10.7 mm above average, which was ~1% above the 1961–90 mean, and the first year since 2000 that the global mean value was wetter than average. Northern Hemisphere sea ice extent was the third lowest on record for the year, dating back to 1973. The annual snow cover extent over Northern Hemisphere land areas was 25.1 million km², which was the 25th most extensive snow cover during the period of record.

Levels of carbon dioxide (CO₂) continue to increase in the atmosphere at the NOAA/Climate Modeling and Diagnostics Laboratory (CMDL) Mauna Loa Observatory on the Big Island of Hawaii; CO₂ rose approximately 1.3 parts per million (ppm) in 2004, to reach a preliminary value of 377.6 ppm. However, the 2004 increase was below the long-term average increase of 1.5 ppm yr⁻¹. A minimum ozone concentration of 138 Dobson units (DU)

was measured on 4 October 2004 at South Pole station, which was above the 1986–2004 average minimum value of 117 ±26 DU.

Sea levels continued to rise globally, increasing at a rate of 2.8 ±0.4 mm yr⁻¹ based on satellite altimeter measurements. The satellite measurements since 1993 have recorded a significantly higher rise in sea level than the overall twentieth-century rate of 1.8 ±0.3 mm yr⁻¹, determined from tide gauge observations during the past century.

The climate of 2004 was influenced by the development of a weak El Niño (i.e., ENSO warm event) in the western and central equatorial Pacific Ocean during the second half of the year. A series of westerly wind bursts during July–October, which were initiated by Madden–Julian oscillation activity in the tropical western Pacific, generated several Kelvin waves in the oceanic mixed layer that aided in the formation of the warm event. Only limited regional-scale impacts associated with El Niño occurred during the boreal autumn, because the event did not develop basinwide.

Tropical cyclone activity was above average in the North Atlantic, west North Pacific, and South Indian Ocean basins in 2004. The hurricane season was extremely active in the North Atlantic basin, with a total of 15 named storms, nine hurricanes, and six major hurricanes in 2004. Nine of these tropical cyclones struck the Atlantic and Gulf of Mexico coasts of the United States, with three of these landfalling as major hurricanes. The

first documented hurricane developed in the South Atlantic Ocean (cyclone “Catarina”), which made landfall along the southern coast of Brazil in late March. The west North Pacific typhoon season was also very active, with 10 tropical systems making landfall in Japan, breaking the previous record of 6 during a single season. In the South Indian Ocean, Tropical Cyclone Gafilo devastated Madagascar, making landfall as a category 5 supercyclone.

From a regional perspective, the annual mean temperature across Europe as a whole in 2004 was 0.98°C above the 1961–90 base period average, with temperature anomalies in excess of 1°C measured across parts of northwest Europe and Scandinavia. Temperatures were also warm across South America and parts of Asia. The annual average temperature in Russia was 0.8°C above the long term mean, but temperatures in 2004 were anomalously cold in Asian Russia.

Drought conditions continued across western North America, although conditions improved in the southwest United States and California late in the year, while the multiyear drought persisted in parts of the Pacific Northwest and Northern Rockies. Drought conditions also persisted across a majority of the Greater Horn and southern Africa. Monsoonal rains were deficient across the Indian subcontinent in 2004; only 87% of the long period average rainfall was recorded. In contrast, above-normal rainfall across parts of Southwest Asia helped ease some of the long-running drought conditions in the region.

I. INTRODUCTION—D. H. Levinson¹⁹

This special section of *BAMS* includes analyses of the global climate system for 2004, and the significant regional climatic events that occurred during this past year. The purpose of the State of the Climate article each year is to summarize the annual climate conditions, and to put the global and regional aspects of the observed climate into historical perspective.

Overall, this is the 15th yearly State of the Climate article (known as the Climate Assessment until 2001) and the ninth year that the article has appeared in *BAMS*. This is also the fifth year that the National Climatic Data Center (NCDC) has taken the lead in the article's development and production. However, this has truly been an international effort, and the contributors to the article this year include scientists from numerous institutions around the world, who have provided data, figures, and/or text to this article. Special effort has been made to acknowledge all contributions to the article, and authorship has been noted through citation of individual sections, as well as in the list of contributors in the appendix.

It should be noted that, given the complexity and variability of the global climate system, it is impossible to accurately cover all aspects of the observed annual climate in an article of this length. However, the authors and contributors to this special section of *BAMS* have addressed the most important aspects and events related to the climate of 2004, and have attempted to convey these to a broad audience.

Each year we have tried to include new or unusual topics that help to broaden the coverage of the past year's climate conditions. This year, we have added a new section on the climate of the oceans, which includes discussions of the important parameters related to the observed conditions in the global oceans. We have also added two new sections to cover all Southern Hemisphere and Indian Ocean tropical cyclones, so that the state of the climate of these important weather systems now encompasses all regions of tropical cyclogenesis around the world.

The following is an executive summary that highlights many of the most important topics and statistics of the climate of 2004.

Chapter 2: Global Climate

SURFACE TEMPERATURE

- The global mean surface air temperature in 2004 was among the fourth highest observed during the period of worldwide instrumental records (beginning in approximately 1880); about 0.44°C above the 1961–90 base period mean, but approximately 0.1°C below the record high value in 1998.

- The 10 highest mean annual global temperatures have occurred since 1990, and, calculated as a linear trend, the rise in global surface temperatures since 1900 is about 0.6°C century⁻¹.

UPPER-AIR TEMPERATURE

- The global annual average temperature in 2004 of the combined lower and middle troposphere was the ninth warmest year (out of 26) in the satellite archive, and the fourth warmest year (out of 47) in the radiosonde archive; about 0.38°C below the maximum (observed in 1998) in both the satellite and radiosonde archives.
- Midtropospheric temperatures have increased since satellite records began in 1979, and the rate of increase has been reported to be as small as +0.044°C decade⁻¹ and as large as +0.127°C decade⁻¹.
- The global lower-stratospheric temperature in 2004 remained well below average, and is the 12th consecutive year in which the annual average was below that of the base period (1984–90).

PRECIPITATION

- The surface precipitation anomaly over global land areas in 2004 was 10.7 mm, a departure of ~1% above the 1961–90 base period mean, and the first year since 2000 that the global mean value was wetter than average.
- Above-normal global seasonal precipitation was measured in three of the four seasons, with the only exception during the June through August period, which has had 10 consecutive years of below-average global precipitation.

SNOW COVER

- Annual snow cover extent over Northern Hemisphere land areas in 2004 averaged 25.1 million km²—0.5 million km² below the 38-yr average, and the 14th least extensive annual snow cover during the period of record.

OCEANS

- Satellite altimeter observations since 1993 show that global sea level has risen almost steadily at a rate of 2.8 ± 0.4 mm yr⁻¹, which was significantly higher than the twentieth-century rate of 1.8 ± 0.3 mm yr⁻¹ determined from tide gauge observations during the past century.

Chapter 3: Trends in Trace Gases

- Carbon dioxide (CO₂) rose approximately 1.3 parts per million (ppm) in 2004, to reach a preliminary value of 377.6 ppm, which is below the long-term average increase of 1.5 ppm yr⁻¹ at the National Oceanic and Atmospheric Administration (NOAA)/Climate Modeling and Diagnostics

Laboratory (CMDL) Mauna Loa Observatory on the Big Island of Hawaii.

- The most abundant ozone (O₃)-depleting gases in the troposphere continued to decline through 2004, but the so-called chlorofluorocarbon (CFC) replacements [hydro-CFCs (HCFCs)] increased globally.

Chapter 4: The Tropics

- An El Niño developed during the boreal summer and fall in 2004, and weak warm event conditions persisted in the central equatorial Pacific region for the remainder of the year.
- Atlantic tropical storm and hurricane activity was well above average in 2004, with 15 named storms, 9 hurricanes, and 6 major hurricanes. Nine of these systems struck the Atlantic and Gulf of Mexico coasts of the United States, with three of these landfalling as major hurricanes.
- The west North Pacific typhoon season was also very active in 2004, with 10 tropical systems making landfall in Japan, breaking the previous record of 6 (set in 1990 and 1993).
- The first documented tropical cyclone developed in the South Atlantic Ocean (cyclone “Catarina”), making landfall along the southern coast of Brazil in March.
- Below-average tropical cyclone activity was observed in the east North Pacific, South Pacific, and Australian regions, while near-normal activity occurred in the North Indian Ocean, and slightly above normal activity was observed in the South Indian basin.

Chapter 5: The Poles

- At the South Pole station, the minimum ozone concentration of 138 Dobson units (DU), measured on 4 October 2004, was above the 1986–2004 average minimum value of 117 ±26 DU.
- The annual average extent of Northern Hemisphere sea ice has decreased by 8% over the past 30 yr, and these decreases were larger (15%–20%) during summer. September sea ice extent has decreased by about 19% since the late 1970s, and 2004 marked the third consecutive year of extreme spring sea ice retreat.
- Land surface temperatures in 2004 north of 60°N were the 21st warmest since 1900, and followed the record warm year of 2003.
- A trend of warming temperatures around Greenland that began in the early 1980s continued through 2004, and summer temperatures for Alaska were the warmest since reliable statewide records began in 1918.

Chapter 6: Regional Climate

- *North America:* Drought continued across western North America, although conditions improved in the southwest United States and California late in the year, while the multiyear drought persisted in parts of the Pacific Northwest and Northern Rockies. Anomalously warm and dry conditions in late spring and summer led to one of the worst fire seasons in the historical record in Alaska and the Yukon.
- *South America:* The continent-wide annual mean temperature for 2004 was 0.53°C above the 1961–90 base period average.
- *Europe:* The annual mean temperature across Europe as a whole in 2004 was 0.98°C above the 1961–90 base period average, and temperature anomalies in excess of 1°C occurred across parts of northwest Europe and Scandinavia.
- *Africa:* Sahel rains were near normal during 2004, and this, along with well-timed precipitation in both North and West Africa, helped foster the worst desert locust outbreak since 1987–89. Drought conditions persisted across a majority of the Greater Horn and southern Africa. Tropical Cyclone Gafilo devastated Madagascar, making landfall as a category 5 supercyclone.
- *Asia:* The temperature across China was warmer than average in 2004, with an annual average of 0.8°C above the 1971–2000 base period. Above-normal rainfall across parts of Southwest Asia helped ease some of the long-running drought conditions in the region. Russia as a whole was warmer than average for the year (0.8°C above average), but temperatures in 2004 were anomalously cold in Asian Russia. Monsoonal rains were deficient across the Indian subcontinent in 2004—only 87% of the long period average.
- *Australasia:* Above-normal daytime temperatures and below-average rainfall were observed across most of the eastern half of Australia in 2004, allowing long-term dry conditions to persist. Temperatures across New Zealand were the coolest since 1993, and above-normal temperatures were recorded across the southwest Pacific in conjunction with warm sea surface temperatures (SSTs) in the central and western equatorial Pacific basin.

2. GLOBAL CLIMATE

a. Global surface temperature—M. J. Menne¹⁹

According to surface temperature records maintained independently by institutions in the United Kingdom (Hadley Centre of the Met Office and the Climate Research Unit at the University of East

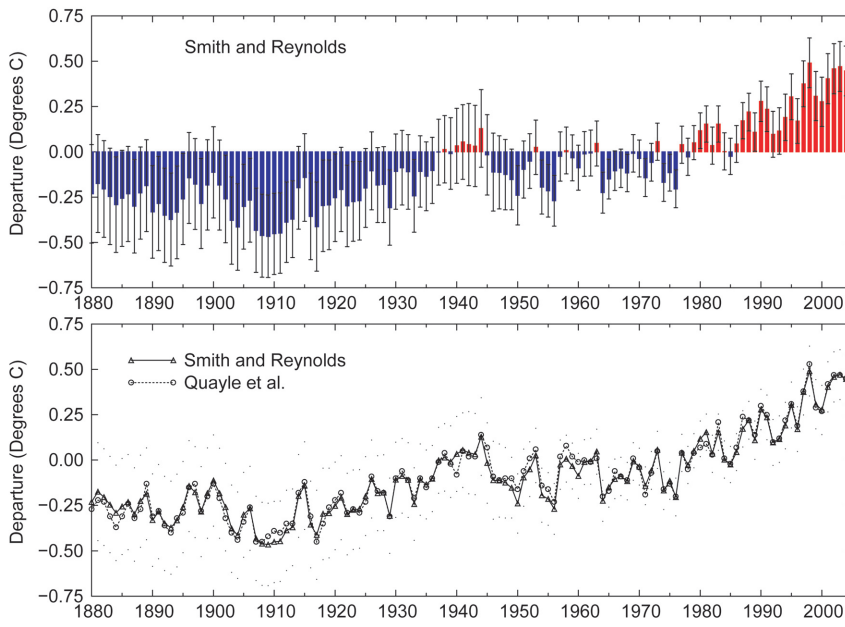


FIG. 2.1. (a) Global annual surface temperature departures from the 1961 to 1990 base period average. Error bars represent the 95% confidence limits for annual average temperature values calculated according to Smith and Reynolds (2005). (b) Comparison between the formerly used Quayle et al. (1999) annual surface temperature series and the recent Smith and Reynolds (2005) analysis (source: NOAA/NCDC).

Anglia) and in the United States (NOAA's National Climatic Data Center), the global mean surface temperature in 2004 was the fourth highest in the period of widespread instrumental records (dating to the midnineteenth century). Surface temperatures in 2004 averaged about 0.44°C above the 1961–90 mean value in both the U.K. record (Folland et al. 2001; Parker et al. 1995; Jones 1994; Jones et al. 2001; Jones and Moberg 2003) and in the NOAA/NCDC U.S. record (Smith and Reynolds 2005). This departure was about 0.1°C less than the record high value observed in 1998 (Fig. 2.1). Calculated as a linear trend, the rise in global surface temperatures since 1900 is about 0.6°C century⁻¹.

Serial monthly temperature anomalies from the U.S. surface temperature archive are shown in Fig. 2.2 for the period since 1961. A calendar-month record high global average was observed in November 2004, when the global mean surface temperature was estimated to be about 0.09°C higher than the former November record

set in 2001. Average land surface temperature records were also set for the months of October and November during 2004.

Worldwide, land surface temperatures were the fourth highest on record in 2004, while the average SST ranked as third highest (not shown). Most regions across the globe recorded temperatures in excess of the 1961–90 mean, as shown in Fig. 2.3. In some regions, especially in the Northern Hemisphere, the average exceeded the 90th or 98th percentiles of the mean annual temperature distribution estimated using 1961–90 observations (Horton et al. 2001). Averaged separately by hemisphere, 2004 surface temperatures ranked as second highest on record in the Northern Hemisphere and as the sixth highest on

record in the Southern Hemisphere, according to the NOAA/NCDC archive.

From a regional perspective, a prolonged period of much above-normal temperatures occurred across Alaska during boreal summer, when average surface temperatures were the highest on record (see section 6b, North America). Prolonged heat waves also occurred in parts of Europe, India, and Australia (see sections 6d, 6frv, and 6gi, respectively). In contrast, parts of the Andes region and South Asia experienced exceptionally cold conditions during the local winter season (see sections 6c and 6fii, respectively).

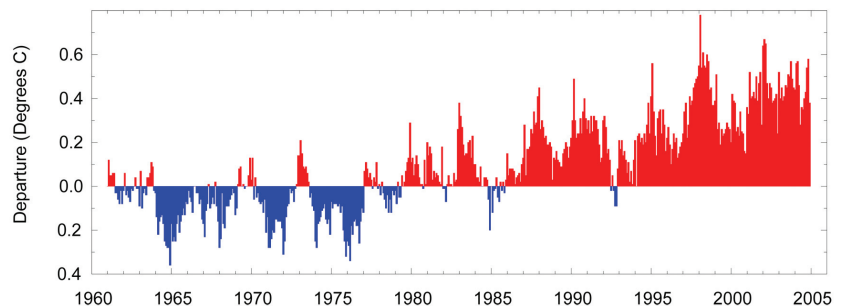


FIG. 2.2. Serial monthly surface temperature anomalies from 1961 to 2004, based on Quayle et al. (1999). Departures were determined with respect to a 1961–90 base period (source: NOAA/NCDC).

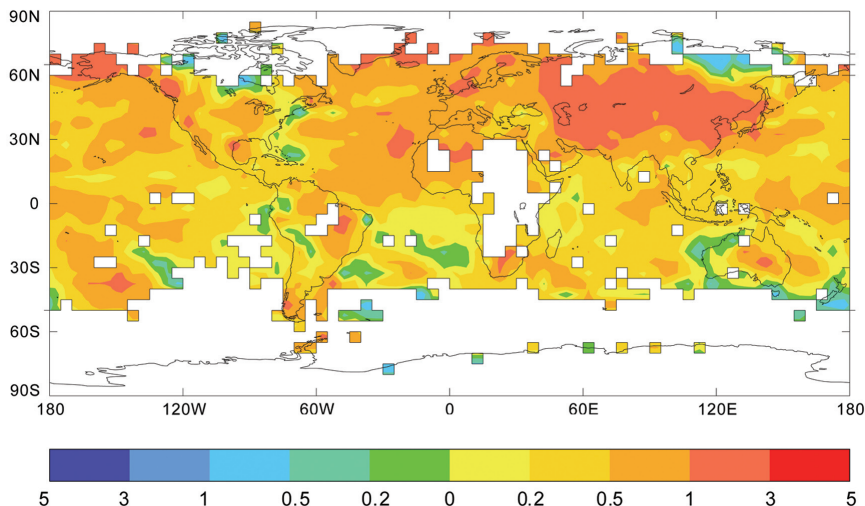


FIG. 2.3. Geographic distribution of temperature anomalies in 2004 expressed as a departure from the 1961 to 1990 base period mean value. The temperature value of each 5° lat × 5° lon pixel was derived from at least 1 month of data in each of four 3-month seasons (source: The Hadley Centre for Climate Prediction and Research).

b. Upper-air temperature—J. R. Christy⁹

Although no single reference dataset of long-term global upper-air temperature observations exists at this time, several datasets based on radiosonde (balloon) or satellite observations have become available that are suitable for climate-monitoring purposes. The discrepancies in the variations and trends depicted by the various datasets may result from differences in the characteristics of the source data, spatial and temporal sampling, and the types of bias adjustments that are applied (Christy and Norris 2004; Seidel et al. 2004; M. Free 2005, personal communication). Consequently, the use of multiple datasets for monitoring the temperature of the free atmosphere can serve as a means for assessing the uncertainty in the estimates of both anomalies and trends.

Bulk atmospheric temperatures for three atmospheric layers—low-midtroposphere ($T_{\text{Low-Trop}}$), midtroposphere ($T_{\text{Mid-Trop}}$), and lower stratosphere ($T_{\text{Low-Strat}}$)—are derived from satellite measurements of the microwave emissions of atmospheric oxygen. Specifically, the measurements are made by the Microwave Sounding Units (MSUs) and the Advanced MSUs (AMSUs) since 1998 that are flown as part of the instrument suite on NOAA polar-orbiting weather satellites. The University of Alabama

in Huntsville (UAH) generates all three products (UAH v5.1; Christy et al. 2003), and Remote Sensing Systems (RSS) produces $T_{\text{Mid-Trop}}$ and $T_{\text{Low-Strat}}$ (RSS v1.3; Mears et al. 2003). Biases and errors due to spacecraft drift (both horizontal and vertical) and on-orbit calibration changes have been identified and removed. Any differences in trends derived from these datasets are related to choices made in the construction process (Thorne et al. 2005a, manuscript submitted to *BAMS*).

Two radiosonde-based datasets have recently been made available by NOAA Radiosonde Atmospheric Tem-

perature Products for Assessing Climate (RATPAC) and the Hadley Centre (HadAT2). RATPAC utilizes 87 globally distributed stations and consists of the Lanzante et al. (2003) manually homogenized dataset for 1958–97, appended with post-1997 data that are homogenized through statistical analysis (M. Free 2005, personal communication). HadAT2 incorporates data from 676 stations where each station's time series was homogenized through a complex statistical analysis procedure using nearby station information and reports of operational changes (Thorne et al. 2005b). The results shown in this section include the RATPAC and HadAT2 time series of temperature of the tropospheric layer from 850 to 300 hPa ($T_{850-300}$), which corresponds to ~1.5 to 9 km.

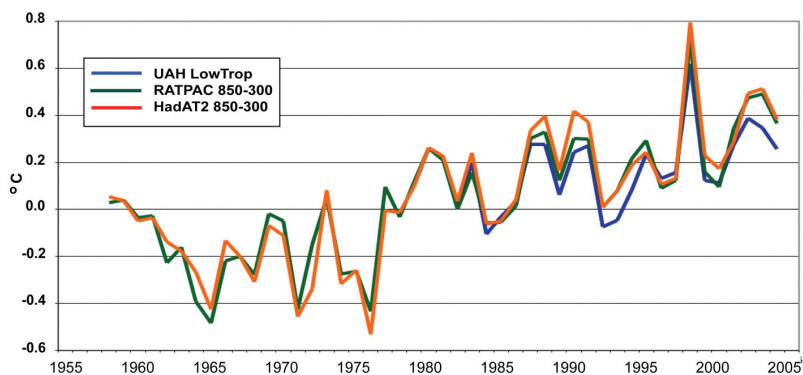


FIG. 2.4. Annual global $T_{850-300}$ anomalies from the RATPAC and HadAT2 datasets, and $T_{\text{Low-Trop}}$ from UAH.

i) LOW-MIDTROPOSPHERE

Globally, UAH $T_{\text{Low-Trop}}$ (surface to 8 km) in 2004 was the ninth warmest year (out of 26), while both radiosonde-based datasets of $T_{850-300}$ had their fourth warmest year (out of 47; Fig. 2.4). Using a measurement error of $\pm 0.08^\circ\text{C}$ (Christy et al. 2003), the value estimated for the UAH annual mean could rank from 13th to 4th warmest, because many annual values cluster near that of 2004. Using global annual anomalies since 1978 from all three datasets, the difference between the warmest and coldest years is approximately 0.80°C , and the UAH value for 2004 was about 0.38°C below the maximum (observed in 1998).

For the 26-yr period, global UAH $T_{\text{Low-Trop}}$, RATPAC $T_{850-300}$, and HadAT $T_{850-300}$ indicate trends of $+0.08$, $+0.12$, and $+0.12^\circ\text{C decade}^{-1}$, respectively. The largest discrepancies between UAH $T_{\text{Low-Trop}}$ and the two radiosonde datasets of $T_{850-300}$ occurred after 2000. Beginning in 1958, the RATPAC and HadAT2 datasets have shown $T_{850-300}$ trends of $+0.13$ and $+0.14^\circ\text{C decade}^{-1}$, respectively.

The most rapid temperature changes observed in the troposphere since 1978 have occurred in the polar regions (see section 5 for more information). The seasonal anomalies of the UAH lower-tropospheric temperature for the $62.5^\circ\text{--}85^\circ\text{N}$ latitude band indicate that the north polar region has warmed at a rate of $+0.38^\circ\text{C decade}^{-1}$, with notable warming since 1993, while the south polar region has cooled at $-0.13^\circ\text{C decade}^{-1}$ (not shown).

ii) MIDTROPOSPHERE

A very broad layer from the surface to the lower stratosphere (up to ~ 18 km) is represented by $T_{\text{Mid-Trop}}$. Variations in either the troposphere or the stratosphere (or both) can therefore contribute to variations in $T_{\text{Mid-Trop}}$. The two realizations of $T_{\text{Mid-Trop}}$ are depicted in Fig. 2.5. The global average 2004 $T_{\text{Mid-Trop}}$

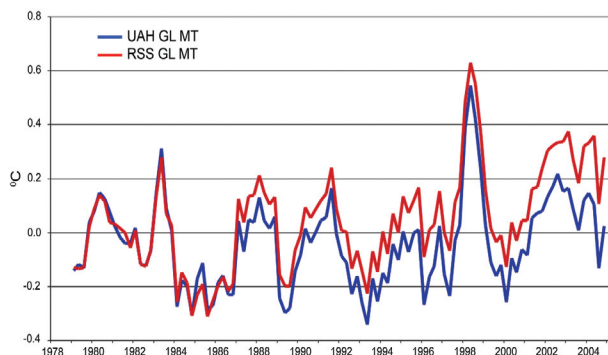


FIG. 2.5. Global seasonal $T_{\text{Mid-Trop}}$ temperature anomalies from RSS and UAH.

were 10th and 4th warmest since 1978 for UAH v5.1 and RSS v1.3, respectively. Again, using the UAH global, annual error estimate of $\pm 0.08^\circ\text{C}$, the UAH ranking for 2004 could vary between 14th and 6th warmest. The overall global trends of $T_{\text{Mid-Trop}}$ were $+0.127^\circ\text{C decade}^{-1}$ for RSS and $+0.044^\circ\text{C decade}^{-1}$ for UAH. In Fig. 2.5, the base period was set as 1979–81 so the divergence at the end is more readily apparent. The main differences between the two datasets occurred around 1987 and after 2001.

iii) LOWER STRATOSPHERE

Globally, 2004 $T_{\text{Low-Strat}}$ (15–24 km) represented the sixth and ninth coolest years in the UAH and RSS datasets. The trends for 1979–2004 were -0.45 and $-0.34^\circ\text{C decade}^{-1}$ for the two datasets, respectively (Fig. 2.6). The main difference occurred as a drift between 1992 and 1997, where UAH cooled relative to RSS.

As in the lower troposphere, the polar regions ($62.5^\circ\text{--}85^\circ\text{N}$ and $^\circ\text{S}$) have experienced the largest regional temperature variations and trends (not shown). However, the negative trends have moderated in the past few years. In fact, the anomalies for December–February 2003–04 in the north and September–November 2002 in the south represent the maximum positive seasonal temperature anomalies on record in the polar regions.

c. Global precipitation—D. H. Levinson,¹⁹ S. E. Stephens,¹⁹ and J. H. Lawrimore¹⁹

The annual precipitation anomaly and percent change, analyzed using gauge data from the Global Historical Climatology Network (GHCN), are shown for global land areas in Figs. 2.7a–e. For the year as a whole, the annual precipitation averaged over global

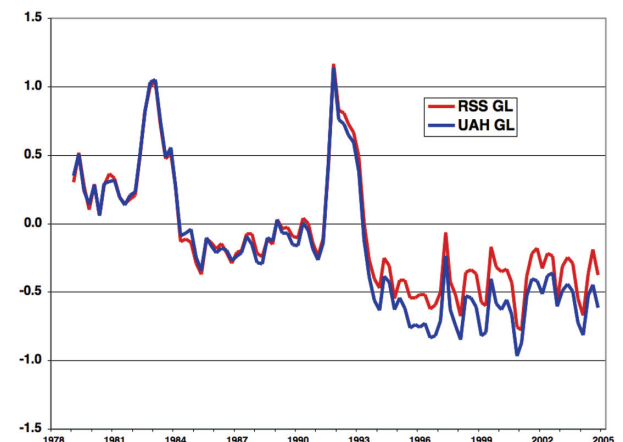


FIG. 2.6. Global seasonal lower-stratospheric temperature ($T_{\text{Low-Strat}}$) anomalies from RSS and UAH.

land areas was above normal in 2004, with an annual mean value of 1030.8 mm, which was $\sim 1.05\%$ above average (Fig. 2.7a). Annual anomalies were calculated from the GHCN precipitation dataset, and were determined with respect to the 1961–90 mean using stations with a minimum of 25 yr of data during the base period (Peterson and Vose 1997; Vose et al. 1992). In 2004, the global anomaly was positive (wet), exceeding 10.7 mm above the climatological base period.

As can be seen in the time series in Fig. 2.7, global annual and seasonal precipitation have shown sig-

nificant interannual variability, especially over the past decade, with several multiyear periods that fluctuated between anomalously wet and dry conditions (shown on each graph as positive and negative anomalies, respectively). The current annual wet anomaly in 2004 followed three consecutive years of below-normal global precipitation that began in 2001 (Fig. 2.7a). In addition, above-normal seasonal precipitation was measured during the boreal winter (December–February), spring (March–May), and autumn (September–November) in 2004 (Figs. 2.7b,c,e). The only season with below-normal precipitation

this past year was summer (June–August), which was part of a long-term, multidecadal period of below-normal global precipitation observed during the boreal summer that began in the mid-1970s (Fig. 2.7d).

Global precipitation over both ocean and land surfaces is shown in Fig. 2.8 using satellite–gauge blended data from the Climate Anomaly Monitoring System and Outgoing Longwave Radiation (OLR) Precipitation Index (CAMS_OPI; Janowiak and Xie 1999). Numerous positive precipitation anomalies were measured during the past year (Fig. 2.8b), including several anomalously wet areas across the United States. Overall, most of the eastern half of the United States was wet in 2004, with the largest wet anomalies exceeding 200 mm (observed over Texas and the southern Plains). The wet conditions in this region occurred primarily during the late summer and fall (not shown), and were associated with a period of enhanced convection and transient storm activity. Southeast U.S. precipitation anomalies were enhanced by an active landfalling North Atlantic Ocean tropical cyclone season (see section 4b1), aided by a stronger-than-normal western extension of the subtropical ridge over the western North Atlantic. In addition, Hawaii and western Alaska were anomalously wet in 2004. However, abnormally dry conditions were observed over central and eastern Alaska during the summer (June–August), which led to a record fire season across the state

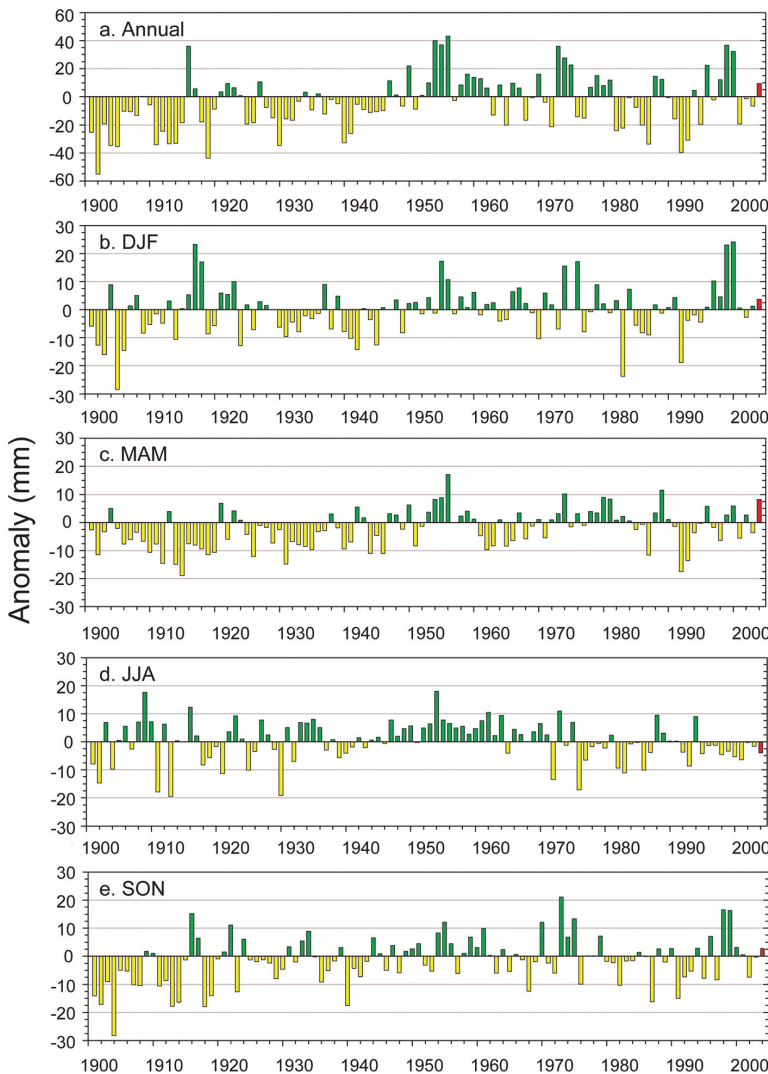


FIG. 2.7. Time series of annual and seasonal global precipitation anomalies displayed over the period of 1901–2004 using observations from the GHCN dataset: (a) annual, (b) Dec–Jan–Feb (DJF), (c) Mar–Apr–May (MAM), (d) Jun–Jul–Aug (JJA), and (e) Sep–Oct–Nov (SON). The precipitation anomalies were calculated in mm with respect to the 1961–90 base period, with green bars indicating positive anomalies and yellow bars indicating negative anomalies (the red bar denotes the 2004 anomaly).

(for further details see section 6a11). Other notable annual wet anomalies observed in 2004 included most of the United Kingdom and northern Europe, Iceland, Tahiti, and parts of Chile and Bolivia, as well as southern Japan and the Korean peninsula, which were affected by precipitation generated by numerous landfalling typhoons in 2004.

Significant negative precipitation anomalies and dry conditions over the past year were observed across the Iberian Peninsula, eastern areas of Australia, and regions just east of the Andes Mountains in South America. Significant annual dry anomalies also occurred across northern India and Pakistan, which were the result of below-normal monsoon rains in 2004 (see section 6fiv). In Southeast Asia, below-average tropical cyclone activity contributed to acute dryness in parts of Indochina. Despite the active typhoon season in 2004, the majority of the tropical cyclones in the west North Pacific basin followed recurvature paths, which brought them farther north into areas such as Japan, which had a record number of landfalling tropical systems, as opposed to areas of Vietnam, Laos, Thailand, Cambodia, and Myanmar [see section 4b11(i) for further details on the western North Pacific typhoon season].

The obvious advantage of the CAMS_OPI dataset is the near-global coverage over the oceans, as well as coverage over land areas where limited gauge observations are available. In 2004, the largest annual precipitation accumulations coincided with regions that typically receive large-scale tropical convection (Fig. 2.8a): the intertropical convergence zones (ITCZs), the south Pacific convergence zone (SPCZ), and monsoon troughs over the equatorial oceans, Southeast Asia and the Indonesian archipelago, equatorial Africa, and South America.

Precipitation anomalies observed over the oceans in 2004 included a very large region with

positive annual anomalies (wet conditions) across the tropical western Pacific Ocean (Fig. 2.8b). As mentioned above, these wet anomalies were due to enhanced tropical cyclone activity in this region. Negative anomalies (dry conditions) in 2004 included the western North Atlantic Ocean and Gulf Stream region, the near-equatorial region of the Pacific basin, the Coral Sea and convection associated with the SPCZ, along with portions of the eastern Indian Ocean.

Only limited regional precipitation affects were observed in 2004 related to the weak El Niño event

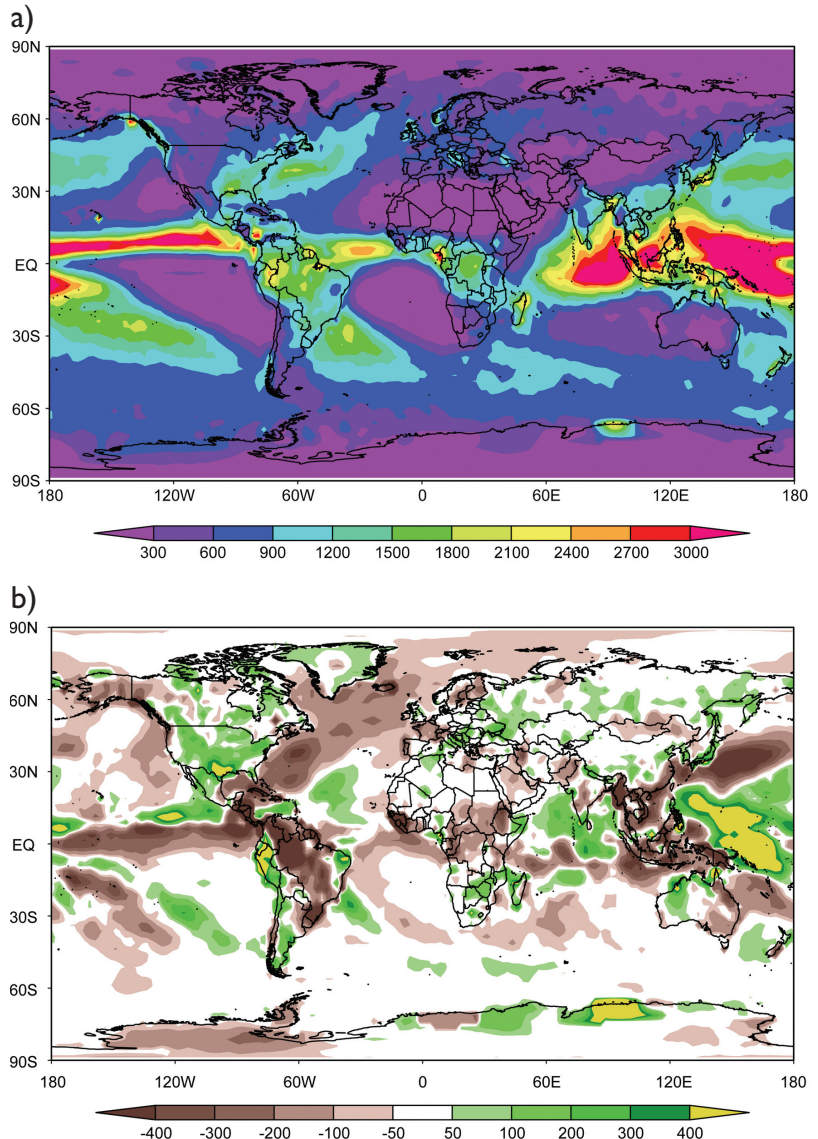


FIG. 2.8. Global precipitation (mm) determined from the CAMS_OPI dataset: (a) total accumulated annual precipitation observed during 2004, and (b) annual precipitation anomalies (mm) observed during 2004. Anomalies were determined with respect to the 1979–2000 base period, where positive anomalies (wet conditions) are shown in green and yellow shading, and negative anomalies (dry conditions) are shown in brown shading.

that developed in the equatorial Pacific basin during the boreal summer and fall. One region that typically has suppressed precipitation and dry conditions during El Niño events is eastern Australia (Ropelewski and Halpert 1987, 1989, and 1996), which had anomalously dry conditions in 2004 (Fig. 2.8b). However, the below-normal precipitation anomalies were present before the advent of the warm event in the equatorial western and central Pacific, and the dry conditions had peaked during the austral fall [for further details on El Niño–Southern Oscillation (ENSO) in 2004, see section 4a, and for more information on Australian climate see section 6g1].

d. Northern Hemisphere snow cover—D. A. Robinson³⁴

Annual snow cover extent over Northern Hemisphere land areas averaged 25.1 million km² in 2004. This was 0.5 million km² below the 38-yr average, and ranked 2004 as having the 25th most extensive snow cover of record (Table 2.1). This evaluation includes snow over the continents and the Greenland ice sheet. The area covered by snow in 2004 ranged from a maximum of 46.9 million km² in January to a minimum of 3.6 million km² in August. Monthly snow cover extent values are routinely calculated at Rutgers University^{2,1} from weekly maps of cover produced by NOAA meteorologists, who construct these maps primarily by utilizing daily visible satellite imagery.

Despite the fact that snow cover was close to or above average at the beginning and end of 2004, the 12-month running means of Northern Hemisphere snow extent were below the long-term average throughout most of the year (Fig. 2.9). This was a reversal from 2003, when the 12-month running means were above average for the first time since the mid-1990s. For most of 2004, both Eurasian and North American snow cover extent were below their respective long-term averages (Table 2.1).

Significant temporal and spatial variability was observed in 2004. For example, hemispheric snow coverage was above average in October and December, while it was below average in November. The December snow cover anomaly was positive for the Northern Hemisphere due to the sixth largest extent over Eurasia, and despite a below-average rank of 29th for North America. In addition, a marked decrease

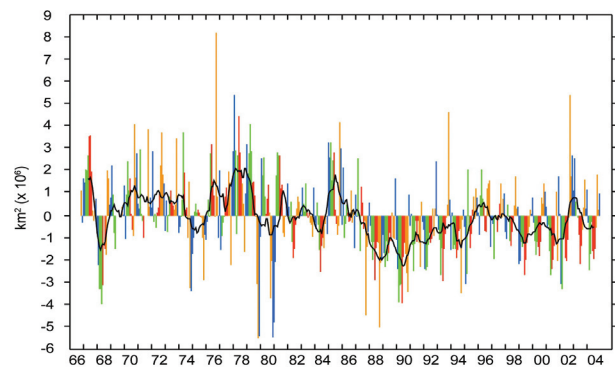


FIG. 2.9. Anomalies of monthly snow cover extent over Northern Hemisphere land areas (including Greenland) between Nov 1966 and Dec 2004. Also shown are 12-month running anomalies of hemispheric snow cover extent, plotted on the seventh month of a given interval. Mean hemispheric snow extent was 25.6 million km² over the full period of record. The monthly means for the period of record were used for nine missing months between 1968 and 1971 in order to create a continuous time series of running means (all missing months fell between Jun and Oct).

in monthly anomalies was noted over North America between February (7th most extensive) and March (26th most extensive). This was a result of an early spring loss of cover in the central and western United States, while the smaller northeastern United States had above-average snow cover persist into March (not shown).

The snow cover extent ranks for both the Eurasian and North American continents were within the same terciles in 8 months during 2004 (Table 2.1). The continental extents differed by two terciles in February and December, with a mirrorlike reversal of continental rankings between these months (i.e., Eurasia and North America ranked 29:7 and 6:29, respectively).

e. Climate of the oceans—D. H. Levinson¹⁹ and D. Stanitski,³⁸ Eds.

1) GLOBAL SEA LEVEL RISE—L. Miller²⁶ and B. C. Douglas¹²

Satellite altimeter observations since 1993 show that global sea level has risen almost steadily at a rate of 2.8 ± 0.4 mm yr⁻¹ (Fig. 2.10). This trend was significantly higher than the twentieth-century rate of 1.8 ± 0.3 mm yr⁻¹ determined from tide gauge observations made over the past 50–100 yr (Douglas 1997; Peltier 2001; Miller and Douglas 2004; Church et al. 2004; Holgate and Woodworth 2004; White et al. 2005). However, it is unclear whether the increased rate observed by satellite altimeters reflects a long-term change with respect to the historical rate or is

^{2,1} Maps depicting weekly and monthly conditions, monthly anomalies, and monthly climatologies of snow cover extent for the entire period of record, along with gridded products, may be viewed online at the Rutgers Global Snow Lab Web site: <http://climate.rutgers.edu/snowcover>.

some manifestation of interdecadal variability.

A map of the altimeter-measured trends (Fig. 2.11) shows that all of the ocean basins experienced rising sea levels over the past decade, but large regional variations are also evident. The tropical western Pacific and Southern Ocean exhibited large positive trends ($> 10 \text{ mm yr}^{-1}$), while the northern Pacific was distinctly negative. The geographical pattern of trends was roughly similar to that observed in the change in upper-ocean heat content as determined from in situ hydrographic measurements (Cabanes et al. 2001), suggesting that, at least on decadal time scales, regional sea level trends have been largely controlled by thermal processes. Mean warming of the upper 750 m of the water column in all of the ocean basins can account for 1.6

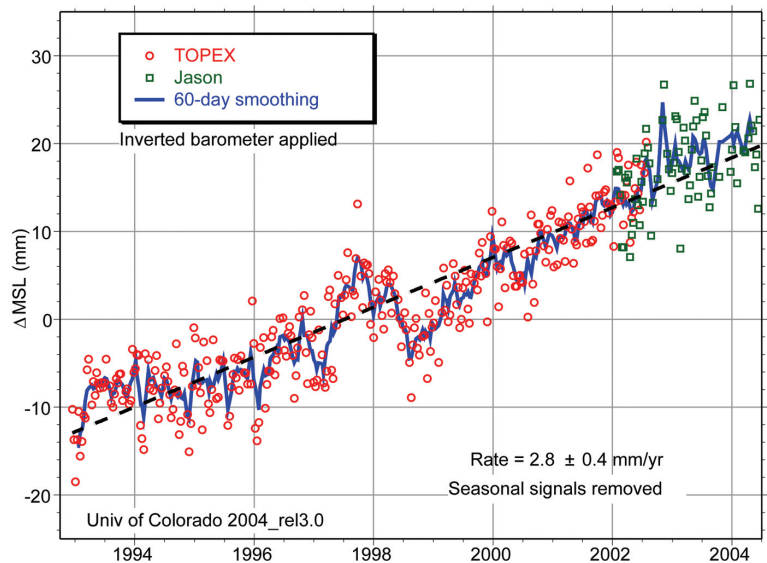


FIG. 2.10. Global mean sea level variations determined using altimeter measurements from the TOPEX (1993–2002) and Jason-1 (since 2002) satellites. (source: <http://sealevel.colorado.edu>; Leuliette et al. 2004).

TABLE 2.1. Monthly and annual Northern Hemisphere and continental (Eurasia and North America, which includes Greenland) snow cover extent between Nov 1966 and Dec 2004. Included are the numbers of years with data used in the extent calculations, means, standard deviations, the 2004 values and rankings. Areas are shown in millions of km^2 . Note that the data from 1968, 1969, and 1971 have one, five, and three missing months, respectively, and thus are not included in the annual (Ann) calculations.

	Yrs	Mean	Std dev	2004	2004 NH rank	Eurasia rank	North American rank
Jan	38	46.9	1.5	48.0	8	10	12
Feb	38	45.9	1.9	45.6	18	29	7
Mar	38	41.0	1.9	38.7	34	34	26
Apr	38	31.4	1.7	29.9	31	23	33
May	38	20.5	1.8	20.4	19	19	18
Jun	37	11.1	2.1	9.8	26	26	25
Jul	35	4.9	1.4	3.3	31	31	32
Aug	36	3.6	1.0	5.2	24	33	36
Sep	36	5.7	1.0	5.2	24	26	20
Oct	37	18.4	2.7	20.0	7	10	8
Nov	39	34.2	2.1	34.4	23	19	25
Dec	39	43.4	1.9	44.3	12	6	29
Ann	35	25.6	1.0	25.1	25	22	26

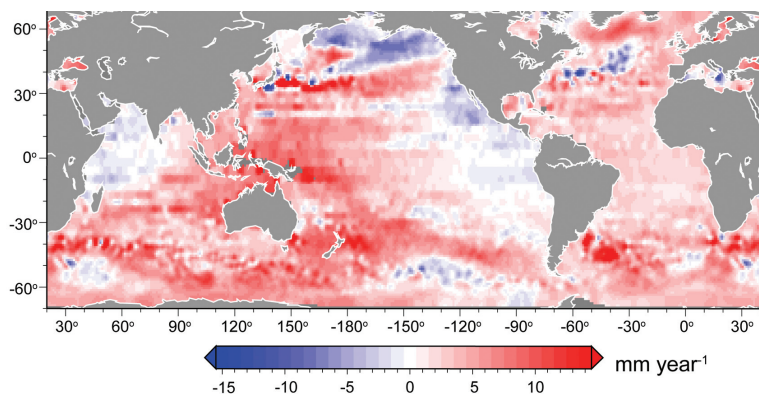


FIG. 2.11. Sea level trends over the period 1993–2004 determined from TOPEX and Jason-1 satellite altimeter observations. The global mean of this map gives the 2.8 mm yr⁻¹ value shown in Fig. 2.10.

±0.2 mm yr⁻¹ of global sea level change between 1993 and 2003 (Willis et al. 2004). This contrasts sharply with the average twentieth-century contribution to sea level rise from thermal expansion, estimated to be about 0.5 mm yr⁻¹ (Antonov et al. 2002). The remaining portion of the total trend for the past decade, roughly 1.2 mm yr⁻¹, was likely due to the melting of grounded ice on Greenland and/or Antarctica and, to a lesser extent, from mountain glaciers, which is a result consistent with the average twentieth-century mass contribution to sea level rise estimated by Miller and Douglas (2004).

ii) SEA SURFACE TEMPERATURES—R. W. Reynolds¹⁹

SST variability during 2004 was examined using the weekly optimum interpolation (OI) analysis of Reynolds et al. (2002). This analysis combines in situ SST data (i.e., ship and buoy data) with satellite SST retrievals from the infrared (IR) channels of the Advanced Very High Resolution Radiometer (AVHRR).

The general change in SSTs over the past several decades has been a slow warming with several large fluctuations of 1–3 yr. The climatological base period used is 1971–2000, so the overall warming tends to favor positive over negative anomalies toward the end of the record. Fluctuations of 1–3 yr are usually due to the warm and cold SST anomalies in the tropical Pacific associated with strong El Niño and large La Niña events, respectively. Impacts from these events often influence the tropical Indian SST anomalies and may influence the tropical Atlantic SST anomalies, but the “phase” of the SST relationship appears to have varied. For example, the El Niño event of 1982–83 occurred along with cold tropical Atlantic SST anomalies, while the El Niño event of 1997–98 occurred along with warm tropical Atlantic SST

anomalies. However, the SST anomaly curve was relatively flat from 2001 through 2004, which suggests that overall warming trends were small over this period and that no large El Niño or La Niña events occurred during this time (see section 4a for further information).

The mean and standard deviation of the weekly anomaly for 2004 are shown in Fig. 2.12. The mean anomalies in the upper panel show positive SST anomalies in the central Pacific, the North Atlantic, and, to a weaker extent, the tropical Indian Ocean and the western Indian Ocean near 35°S. The standard deviation of the anomaly (Fig. 2.12, lower panel) shows the strongest variability between roughly 30° and 70°N, and in the eastern tropical Pacific. In addition, there was more modest variability along the equator in the eastern

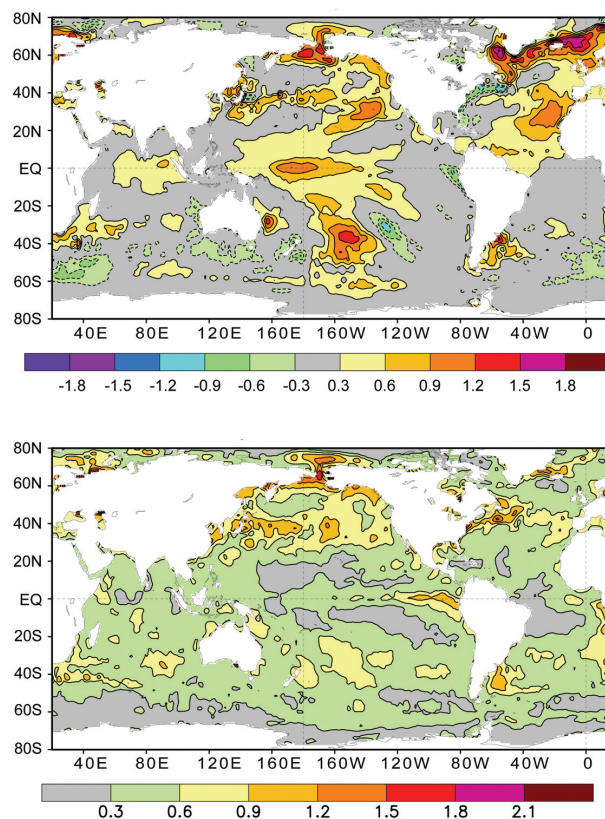


FIG. 2.12. Weekly SST anomalies for the period of 7 Jan 2004 through 29 Dec 2004: (top) mean and (bottom) standard deviation. The anomalies were computed relative to a 1971–2000 base period. The contour interval shown is 0.3°C, and the 0°C contour is not shown.

Pacific, and between 30° and 50°S east of South America, and both east and west of the Cape of Good Hope near the southern tip of Africa.

The most important signal observed in 2004 associated with extratropical SST variability, which also occurred in 2003, was along 60°N latitude. These positive SST anomalies between August and October were the oceanic response to large and warm summer and fall air masses, and their associated positive land surface air temperatures anomalies are found along this same latitude band (for further details on seasonal surface temperatures see section 7).

III) OCEAN HEAT AND FRESHWATER CONTENT AND TRANSPORTS—L. Talley²⁷

Operational products of subsurface temperature and salinity fields are produced for the Atlantic basin, and the subsurface temperature field is produced only for the North Pacific basin. Water temperature changes in the upper ocean had important regional variations in 2004, with warming in the subtropics and highest polar latitudes, and cooling at subpolar latitudes in the Northern Hemisphere (both in the North Pacific and North Atlantic). Global ocean heat content calculated from combined datasets increased monotonically from 1993 to 2003 (Fig. 2.13), and since 1999 in the Tropics.

Freshening of upper-ocean waters around the high-latitude North Atlantic has been reported over the past several decades (Dickson et al. 2003; Curry et al. 2003). The observed salinity decreases persisted into 2004 (not shown), along with continued thinning of Arctic sea ice (see sections 2eVI and 5c). Freshening

of surface and intermediate water north of the Antarctic Circumpolar Current, and increased salinity in surface waters south of the current over the past decade have also been observed.

IV) EVOLUTION OF THE 2004 EL NIÑO—M. J. McPhaden¹⁶

A weak El Niño developed in the second half of 2004 in the equatorial Pacific Ocean. Anomalous warming of the ocean mixed layer and surface conditions was, for the most part, centered near the international date line, with near-normal SSTs in the equatorial cold tongue of the eastern Pacific and along the west coast of South America. SST anomalies in the Niño-3.4 index region (5°N–5°S, 120°–170°W) were approximately 0.8°C above average from August to December 2004. The Southern Oscillation Index (SOI) was consistently negative during the latter half of 2004 (–0.6 average index value during August–December; see Fig. 6.49), which is indicative of the warm phase of ENSO. The near-equatorial trade winds were unusually weak west of the date line, associated with the elevated central and western Pacific SSTs and negative SOI values. In contrast, the trade winds in the eastern Pacific were near to above normal throughout much of 2004.

The 2004 El Niño event was unusual in that it followed the moderate-amplitude 2002–03 El Niño by only 1 yr (McPhaden 2004). Factors contributing to the quick development of the 2004 El Niño after the termination of the previous event are not fully understood. However, it is noteworthy that the 2002–03 El Niño was followed by an extended period of excess warm water volume (i.e., heat content) in the equatorial zone, which was atypical of conditions following most previous El Niños. It is likely that the presence of weak, positive heat content anomalies following the 2002–03 El Niño generated large-scale conditions that were favorable for the recurrence of another warm event earlier than would otherwise have been expected. Episodic westerly wind forcing (i.e., westerly wind bursts) in the boreal spring and summer of 2004 (Fig. 2.14) may have served as the stimulus for the development of the observed warm anomalies by displacing the western Pacific warm pool toward the east (e.g., Kessler et al. 1995; see section 4a for a complete overview of the conditions associated with ENSO in 2004).

V) GLOBAL OCEAN CARBON CYCLE: INVENTORIES, SOURCES, AND SINKS—R. A. Feely¹⁶ and R. Wanninkhof⁴⁰

As a result of the measurements during the global CO₂ survey in the 1990s, and current improved

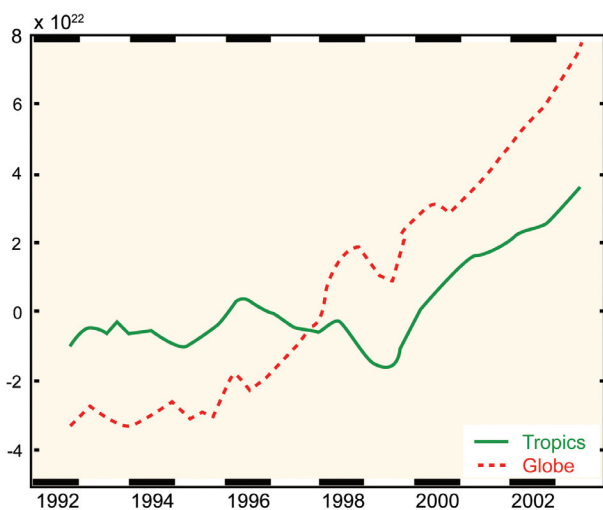


FIG. 2.13. Total oceanic heat content (in J × 10²²) integrated over the Tropics (green line) and the globe (red line) since late 1992 (adapted from Willis et al. 2004).

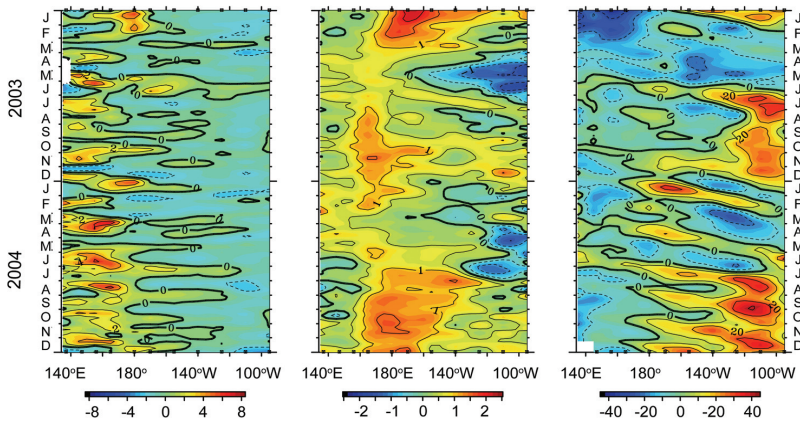


Fig. 2.14. Five-day-averaged anomalies: (left) zonal wind (m s^{-1}), (center) SST ($^{\circ}\text{C}$), and (right) 20°C isotherm depth (m; which corresponds to the depth of the thermocline) relative to the mean seasonal cycle. The data were averaged over the 2°N – 2°S region, and based on Tropical Atmosphere–Ocean (TAO) project Triangle Trans-Ocean Buoy Network (TRITON) moored-buoy time series data. Tick marks on the horizontal axis indicate those longitudes sampled at the (top) start and (bottom) end of record.

methods of quantifying the anthropogenic CO_2 signal above the large natural background, the first measurement-based inventory of anthropogenic CO_2 in the ocean is now available (Fig. 2.15).

Anthropogenic CO_2 is unevenly distributed throughout the oceans, and the highest vertically integrated concentrations are found in the North Atlantic. The Southern Ocean south of 50°S has very low vertically integrated anthropogenic CO_2 concentrations. Approximately 60% of the total oceanic anthropogenic CO_2 inventory is stored in the South-

ern Hemisphere oceans, roughly in proportion to the larger ocean area of this hemisphere. Approximately 30% of the anthropogenic CO_2 is found at depths shallower than 200 m and nearly 50% is above a 400-m depth. The global average depth of the $5 \mu\text{mol kg}^{-1}$ contour is approximately 1000 m. Therefore, the majority of the anthropogenic CO_2 in the ocean is confined to the thermocline region.

From cruises in the North Pacific, the difference between the Repeat Hydrography measurements in 2004 and those from the World Ocean Circulation Experiment (WOCE) in 1994 quantitatively document changes of natural and anthropogenic CO_2 over the past decade. Significant increases in dissolved inorganic carbon (DIC) of up to $35 \mu\text{mol kg}^{-1}$ were observed in surface waters and in intermediate depths ranging from 200 to 1000 m. The increases are due to the uptake of anthropogenic CO_2 , changes in the strength of ventilation and biological processes, and the influence of eddies in the region. On average, mixed layer DIC increases of $1.5 \pm 0.2 \mu\text{mol kg}^{-1} \text{yr}^{-1}$ were observed in the subtropical waters of the North Pacific over the past decade, indicating that the oceanic uptake of CO_2 in this part of the global oceans has been faster than the rate of growth of CO_2 in the atmosphere.

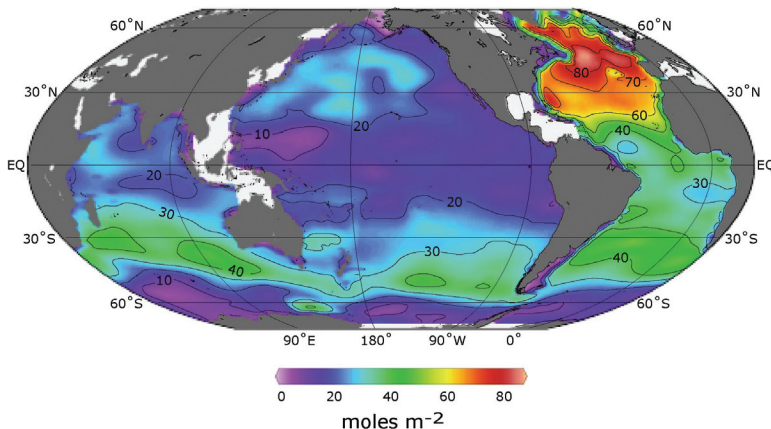


Fig. 2.15. Column inventory of anthropogenic CO_2 in the ocean. High inventories are associated with deep water formation in the North Atlantic, and intermediate inventories with mode water formation between 30° and 50°S . Total inventory of shaded regions is $106 \pm 17 \text{Pg C}$ (Sabine et al. 2004).

VI) SURFACE CURRENT OBSERVATIONS—P. Niiler²⁷ and N. Maximenko²⁵

The “Global Drifter Program” produces instrumental data records of the near-surface velocity of the global oceans (Niiler 2001), which are maintained at NOAA’s Atlantic Oceanographic and Meteorological Laboratory (AOML) for all drifters (8049 as of July 2004).

The western tropical Pacific circulation injects significant surface water from the Philippine Sea to the South China Sea through the Luzon Strait (Centurioni et al. 2004) during the October–December periods of the northeast monsoon. Drifters have observed significant interannual changes of the patterns of this inflow. A

comparison of the 2003 and 2004 drifter tracks during this monsoon period (Fig. 2.16) shows that the inflow in 2004 was much broader to the west, and stronger than observed in 2003. These changes were consistent with the altimeter observations of the differences of the sea level patterns in the Philippine Sea and the South China Sea (see section 2e1 above).

VII) SEA ICE EXTENT AND THICKNESS—I. G. Rigor³³ and J. Richter-Menge³¹

The annual average extent of Arctic sea ice has decreased by 8% over the past 30 yr and these decreases were larger (15%–20%) during summer (ACIA 2004).

The decline of Arctic Ocean sea ice has been attributed to the warmer air temperatures observed in the basin (e.g., Rigor et al. 2000; Jones et al. 1999), which may have thinned and decreased the extent of sea ice (ACIA 2004). However, there is also some evidence that changes in the circulation of sea ice on the Arctic Ocean, driven by changes in winds over the Northern Hemisphere, are important in explaining the recent minima in summer sea ice extent (see section 5c).

The last three summers have exhibited record low sea ice extent on the Arctic Ocean. The summer of 2002 set the record minimum for the Northern Hemisphere, while the summer of 2004 (Fig. 2.17; NSIDC 2004) had reduced sea ice over the Arctic Ocean than that observed in 2002, but more sea ice was observed in the Canadian archipelago and in the Laptev Sea. The age and thickness of sea ice explains more than half of the variance of the observed summer sea ice extent. The younger and thinner state of most of the sea ice on the Arctic Ocean persisted through 2004 (NSIDC 2004).

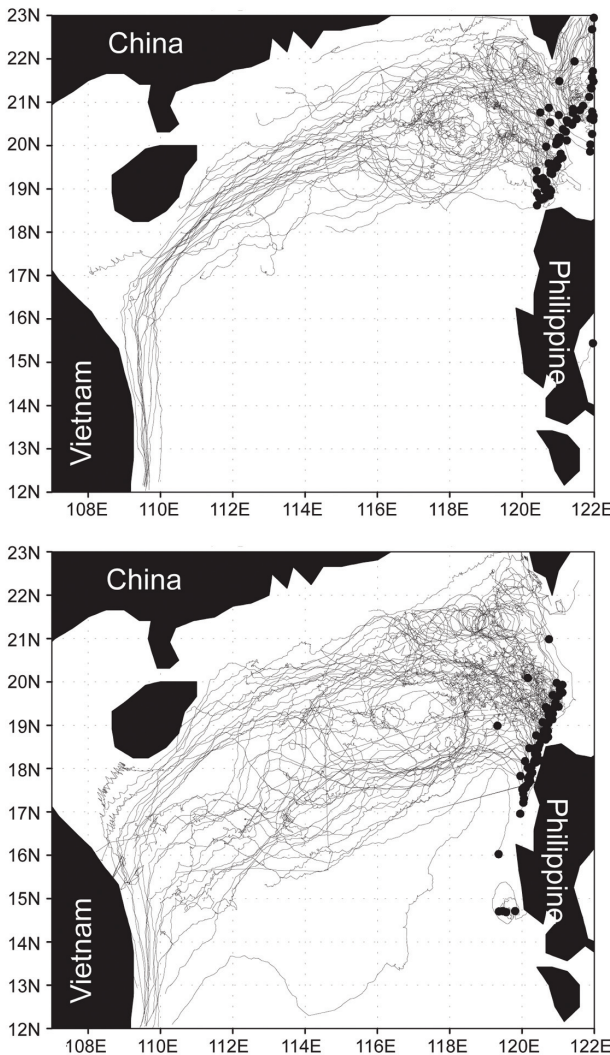


FIG. 2.16. Sep–Jan tracks of Argos drifters that were released in the vicinity of the Luzon Strait in 2003–04 [(top) 77 drifters, processed data] and in 2004–05 [(bottom) 85 drifters, raw data]. Note that significant interannual differences occurred in the north–south extent of the westward circulation in the South China Sea.

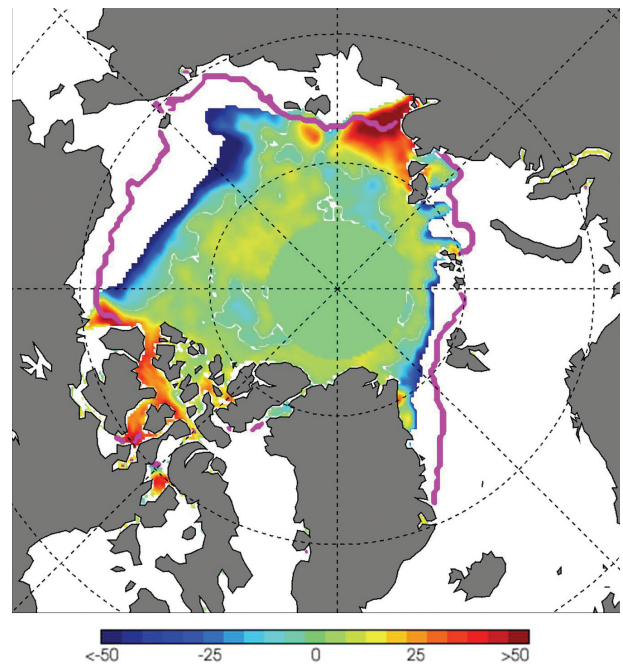


FIG. 2.17. Sea ice concentration anomalies (in %) in Sep 2004 over the Arctic basin. The 2004 anomalies were estimated as the difference in sea ice concentration in 2004 with respect to the 1979–2000 base period. The pink line indicates the 1979–2000 median Sep ice edge. Anomalies are not calculated north of the circle centered over the pole (shown as light green) where satellite coverage prior to 1988 is unavailable (source: the National Snow and Ice Data Center, University of Colorado at Boulder; http://nsidc.org/news/press/20041004_decline.html)

3. TRENDS IN TRACE GASES—R. C. SCHNELL²⁷

a. Carbon dioxide

Carbon dioxide emitted from fossil fuel burning is partitioned into three mobile reservoirs: the atmosphere, the oceans, and the terrestrial biosphere. As a result of fossil fuel combustion, atmospheric CO₂ has increased from about 280 ppm (ppm = parts in 10⁶ by dry-air mole fraction) at the start of the industrial revolution (~mid-1800s) to about 380 ppm in 2004. Roughly half of the emitted CO₂ remains in the atmosphere and the remainder has gone into two “sinks”—the oceans and land biosphere (which includes plants and soil carbon).

The amount of dissolved CO₂ in the oceans is relatively small; most of the carbon uptake in this reservoir occurs because dissolved CO₂ reacts with carbonate (and borate) ions in the ocean surface. Exchange between the atmosphere and the ocean surface occurs quickly, but the capacity of the ocean to take up carbon is small. Most of the fossil fuel–derived carbon eventually ends up in the deep ocean, but exchange between surface waters and the deep ocean is slow (on a time scale of centuries). So far, about 5% of conventional fossil fuels have been combusted. If combustion were stopped today, after a few hundred years ~15% of the total carbon that had been previously emitted would remain in the atmosphere, and the remainder would be in the oceans. However, as more of the fossil fuel reserves are burned, carbonate (and borate) will be depleted, and the airborne fraction of combusted carbon will increase. The airborne fraction would approach 75% as all known reserves were burned (Tans 1997). These simple calculations have assumed that ocean circulation and other processes in the ocean remain the same as the climate changes. However, there is no guarantee that this will happen.

There is strong observational evidence that the terrestrial biosphere is also a sink for fossil fuel–derived CO₂ (Tans and White 1998). The magnitude of that sink, on an annual basis, is currently comparable to that of the oceans. A doubling of the current terrestrial biosphere (including live plants and soil carbon) would be a sink for about one-third of the carbon emitted if all fossil fuels were burned (Tans and Bakwin 1995).

Currently, nearly 7 Pg (Pg = 10¹⁵g) of carbon is emitted into the atmosphere by fossil fuel combustion each year. During the 1990s, uptake by the oceans was estimated as 1.7 ± 0.5 Pg yr⁻¹ and by the land biosphere as 1.4 ± 0.7 Pg yr⁻¹ (Prentice et al. 2001). These are net fluxes; it is important to note that the gross fluxes between the atmosphere and oceans, and

the atmosphere and the terrestrial biosphere (through photosynthesis and respiration), are on the order of 100 Pg yr⁻¹. Interannual variations in the atmospheric increase of CO₂ (Fig. 3.1a; based on Conway et al. 1994) are not attributed to variations in fossil fuel emissions, but are due to small changes in these net fluxes. Most attempts to explain the interannual variability of the atmospheric CO₂ increase have focused on short-term climate fluctuations (e.g., ENSO; post-Mt. Pinatubo cooling), but the mechanisms, especially the role of the terrestrial biosphere, are not well understood. The annual increase in CO₂ at the NOAA/CMDL Mauna Loa Observatory near the summit of the Big Island of Hawaii was greater than 2 ppm yr⁻¹ during 2002 and 2003, but the preliminary data suggest that the increase at Mauna Loa during 2004 of 1.3 ppm (to 377.6 ppm) was below the long-term average increase of 1.5 ppm yr⁻¹.

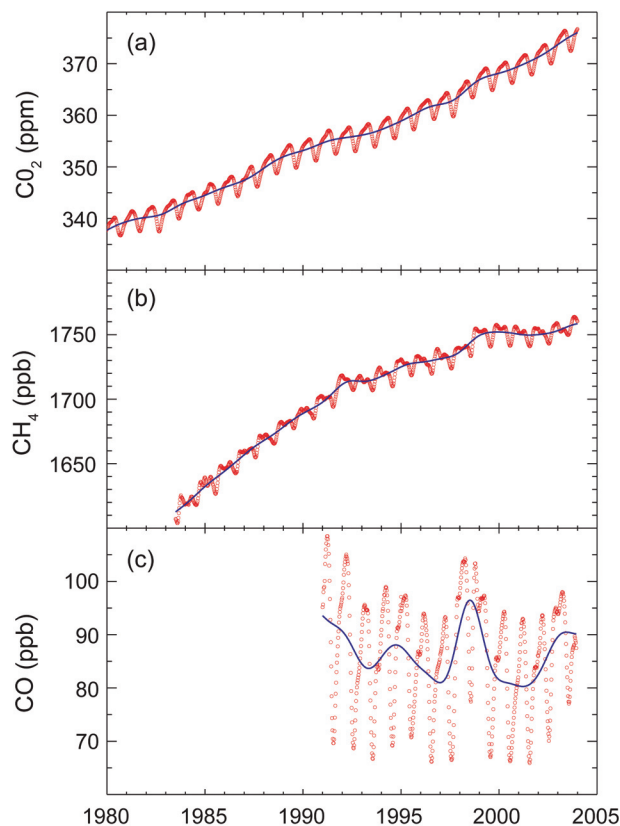


FIG. 3.1. Globally averaged trace gas mole fractions (red symbols) determined from samples collected as part of the NOAA/CMDL Global Cooperative Air Sampling Network: (a) CO₂ (data courtesy: T. J. Conway, NOAA/CMDL), (b) CH₄ (data courtesy: E. J. Dlugokencky, NOAA/CMDL), and (c) CO (data courtesy: P. C. Novelli, NOAA/CMDL). In all three panels the solid blue line is the deseasonalized trend (more information can be found online at <http://www.cmdl.noaa/ccgg>).

b. Methane

The contribution of methane (CH_4) to anthropogenic radiative forcing, including direct and indirect effects, is approximately 0.7 W m^{-2} , which is about half that of CO_2 . In addition, changes in the burden of CH_4 feed back into atmospheric chemistry affecting the concentrations of OH and O_3 . The increase in methane since the preindustrial era is responsible for about one-half the estimated increase in background tropospheric O_3 during that time. Changes in OH concentration affect the lifetimes of other greenhouse gases such as the widely used replacement refrigerants [hydrofluorocarbons (HFCs), HCFCs].

High-precision measurements of atmospheric methane provide climate modelers with current and past rates of CH_4 increase, and they are also useful in constraining the CH_4 budget and how it has changed with time. In Fig. 3.1b, smoothed values of globally averaged CH_4 mole fractions from the NOAA/CMDL air sampling network are plotted as a function of time. During 20 yr of measurements, CH_4 has increased, but the rate of increase has slowed since the early 1990s. The large increase in 1998 was likely the result of climatic conditions that resulted in increased emissions from wetlands and biomass burning. Globally averaged CH_4 since then remained almost constant from 1999 to 2002 (Dlugokencky et al. 2003). In 2003, CH_4 increased by about 5 ppb; this seems to have been driven by increased emissions in the Northern Hemisphere, because there was little corresponding change in the Southern Hemisphere. Preliminary results from 2004 suggest that atmospheric CH_4 levels were the same or slightly greater than those in 2003.

c. Carbon monoxide

Unlike CO_2 and CH_4 , carbon monoxide (CO) does not strongly absorb terrestrial IR radiation, but can still impact climate through its chemistry. The chemistry of CO affects OH (which influences the lifetimes of CH_4 and HFCs) and tropospheric O_3 (itself a greenhouse gas), so emissions of CO can be considered equivalent to emissions of CH_4 (Prather 1996). Current emissions of CO may contribute more to radiative forcing over decadal time scales than emissions of anthropogenic nitrous oxide (N_2O) (Daniel and Solomon 1998).

Globally averaged CO mole fractions are plotted as a function of time in Fig. 3.1c. There has been a long-term decrease in globally averaged CO, driven by a decrease in the Northern Hemisphere (Novelli et al. 2003). Superimposed on the decrease was a significant increase during 1997 and 1998, which was likely

the result of biomass burning in the Tropics (Langenfelds et al. 2002) and boreal forests (Kasischke et al. 2000). Because the lifetime of CO is relatively short (few months), the anomaly quickly disappeared and CO returned to pre-1997 levels shortly thereafter. Global CO continued to decrease slowly from 1999 to 2002 when more large boreal fires appear to have left their mark. These large fires were the likely cause of increasing CO starting in mid-2002. Preliminary measurements suggest that in 2004, CO levels were comparable to the early 2000s.

d. Halocarbons

Long-lived halocarbons containing chlorine (Cl) and bromine (Br) affect the radiative balance of the atmosphere because they efficiently absorb terrestrial IR radiation. These halocarbons also influence the radiative atmospheric balance indirectly through their destruction of stratospheric ozone. Due to concern over depleted stratospheric ozone, the production of many halocarbons has been restricted in recent years. The phase-out of halocarbons internationally was brought about through the 1987 Montreal Protocol on Substances that Deplete the Ozone Layer. As a result of these efforts, concentrations of many ozone-depleting gases have declined at the Earth's surface in recent years. A continued decline was observed for many gases in 2004 (Figs. 3.2a–c).

Despite the international efforts associated with the Montreal Protocol, the concentrations of some halocarbon gases have continued to increase globally (Fig. 3.2d). The most significant increases have been observed for HCFCs, because these chemicals are used as replacements for other gases that deplete ozone much more efficiently. Increases in HCFCs have slowed in recent years; by mid-2004, the chlorine in the three most abundant HCFCs amounted to 210 ppt, or 7.7% of all chlorine carried by long-lived, purely anthropogenic halocarbons. The influence of these disparate trends on future levels of stratospheric ozone can be gauged roughly from a sum of Cl and Br in long-lived halocarbons, provided the enhanced efficiency for Br to destroy ozone is considered. This sum is expressed here as equivalent chlorine (ECl; Fig. 3.2e) and was derived from surface-based measurements. ECl provides an estimate of the ozone-depleting power of the atmosphere a few years in the future, which is when air at the Earth's surface will have been transported and become mixed into the stratosphere where the ozone layer resides.

These observations (Fig. 3.2e) indicate that the ECl content of the lower atmosphere has declined fairly steadily over the past 10 yr at a mean rate of

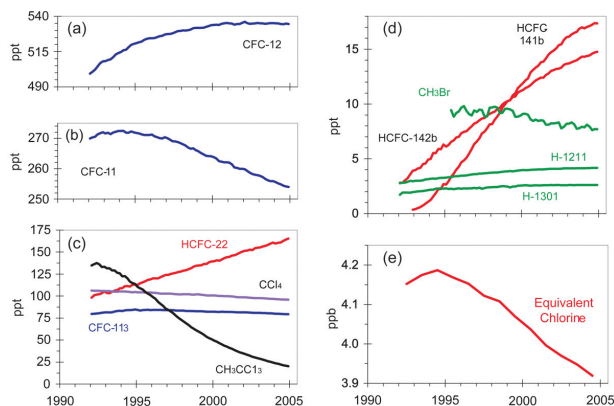


FIG. 3.2. Changes in global tropospheric mixing ratios (in ppt, or pmol mol^{-1}) of the most abundant CFCs (a), (b) and (c), and (d) HCFCs, chlorinated solvents, and brominated gases. These global changes were calculated from atmospheric measurements made at remote sites in both the Northern and Southern Hemispheres (source: NOAA/CMDL). (e) Secular changes in atmospheric equivalent chlorine (ECI; in ppb or nmol mol^{-1}), which is an estimate of the ozone-depleting power of atmospheric halocarbons. ECI was derived from observed mixing ratios of ozone depleting gases appearing in the other four panels, and it was derived from the sum of $[\text{Cl} + (\text{Br} \times 45)]$ contained in these gases (updated from Montzka et al. 2003b; courtesy of S. A. Montzka, J. H. Butler, T. Thompson, D. Mondeel, and J. W. Elkins, NOAA/CMDL).

27 ppt ECI yr^{-1} (or about $-0.66\% \text{ yr}^{-1}$). Scenarios projecting future halocarbon mixing ratios were derived based upon full compliance with the amended and revised Montreal Protocol and our understanding of the atmospheric lifetimes of these gases (Montzka et al. 2003a). These analyses suggest that over the next 40–50 yr ECI will decline to levels that were present before ozone depletion was observed.

Changes in the direct radiative influence of long-lived halocarbons can be estimated from observed changes in atmospheric mixing ratios with the knowledge of trace-gas radiative efficiencies. Such an analysis suggests that the direct radiative forcing of these gases was still increasing in 2004, although at a much slower rate than those observed from 1970 to 1990.

e. N_2O and SF_6

Nitrous oxide (N_2O) is an important greenhouse gas that influences the radiative balance of the atmosphere both directly and indirectly. Since preindustrial times, the radiative forcing from observed increases in atmospheric N_2O is about 0.15 W m^{-2} , or about one-tenth as large as the influence of CO_2 . Nitrous oxide is also the most important source of

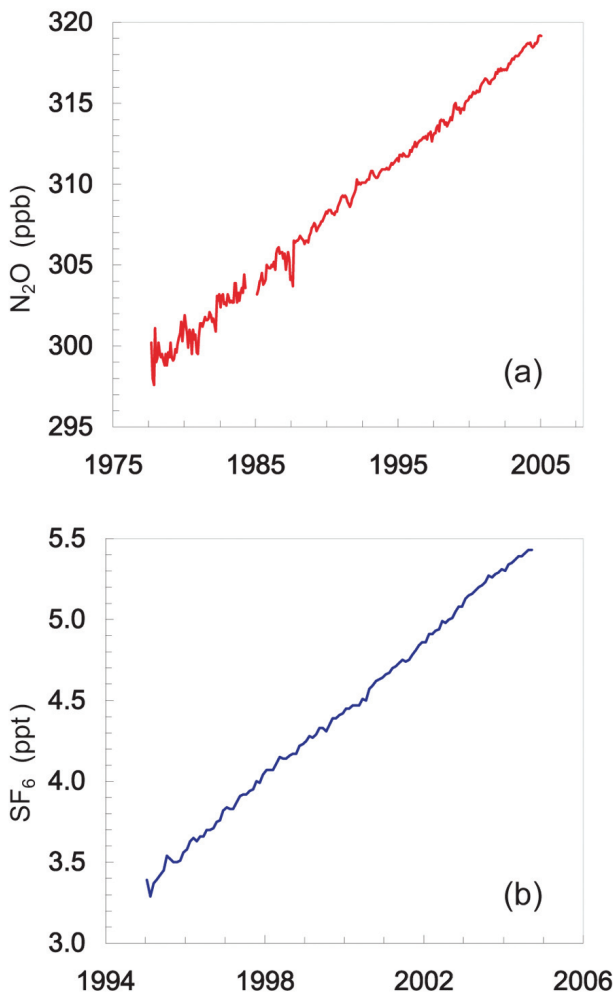


FIG. 3.3. Global tropospheric mixing ratios for (a) N_2O and (b) SF_6 , determined from the NOAA/CMDL Global Cooperative Air Sampling Network. Global means were determined from measurements made by on-site instrumentation and from air collected in flasks (updated from Geller et al. 1997; Thompson et al. 2004; courtesy of J. H. Butler, G. Dutton, J. W. Elkins, D. Mondeel, and T. Thompson, NOAA/CMDL).

stratospheric nitrogen oxides that play an important role in regulating the abundance of stratospheric ozone. Nitrous oxide is emitted to the atmosphere as a result of both natural processes and anthropogenic activities. Measurements from ice cores, firn air, and ambient air suggest that mixing ratios of N_2O have increased by approximately 50 ppb since preindustrial times. Since the late 1980s, the rate of increase in N_2O has averaged 0.7 ppb yr^{-1} (Fig. 3.4a). This increase was sustained in 2004; global surface mixing ratios of N_2O increased by 0.65 ppb in 2004 and reached 319.2 ppb at the end of the year.

Sulfur hexafluoride (SF_6) is a strong absorber of terrestrial IR radiation (Fig. 3.3b). Concern over

continued mixing ratio increases of this potent greenhouse gas stem, in part, from its long atmospheric residence time (> 500 yr). Sulfur hexafluoride is emitted to the atmosphere primarily as a result of anthropogenic production. Global mixing ratios increased throughout the 1990s and early 2000s. The mean rate of increase from 2003 to 2004 was 0.2 ppt yr^{-1} ; at the end of 2004, global surface mixing ratios of SF_6 reached 5.5 ppt.

4. THE TROPICS

a. ENSO and the tropical Pacific—

G. D. Bell⁴ and M. S. Halpert⁴

1) OVERVIEW

Conditions over the tropical Pacific during 2004 reflected the development of a weak warm episode (i.e., El Niño) during the second half of the year, and strong intraseasonal activity associated with the Madden–Julian oscillation (MJO) throughout the year. One precursor condition to the weak El Niño was the development of anomalously warm waters at approximately 110–130-m depth across most of the equatorial Pacific since June 2003, in association with a deepening of the oceanic thermocline (Fig. 4.1a). Increased depths of the thermocline are indicated by positive depth anomalies of the 20°C isotherm, which approximates the center of the thermocline across the eastern equatorial Pacific. Another precursor condition was the persistence of small positive SST anomalies across the central and east-central equatorial Pacific (Fig. 4.1c), which increased during July and August as the warm episode developed.

This evolution was associated with the development of westerly zonal wind anomalies at 850-hPa across the east-central equatorial Pacific (Fig. 4.1b), reflecting a reduction in strength of the equatorial easterlies. These reduced easterlies contributed to decreased equatorial upwelling and to the resulting deepening of the oceanic thermocline.

Despite the anomalously warm SSTs, there was little or no reflection in the average pattern of deep convection and associated precipitation over the central and east-central equatorial Pacific, as indicated by OLR anomalies (Fig. 4.1e). As a result, the warm SSTs had no discernible influence on the atmospheric circulation, as indicated by near-average 200-hPa heights across the central and east-central equatorial Pacific (Fig. 4.1d). Instead, the dominant signal in

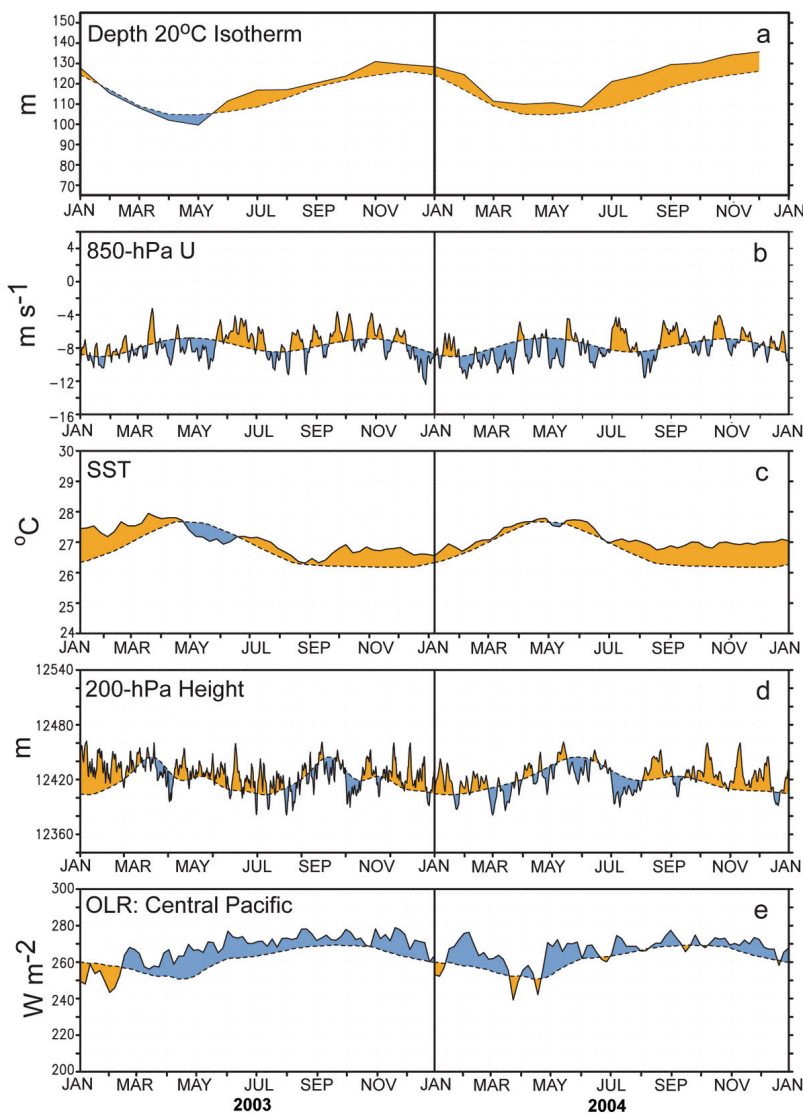


FIG. 4.1. Monthly time series of (a) the depth of the 20°C isotherm (m), (b) 850-hPa zonal wind speed (m s^{-1}), (c) SST ($^\circ\text{C}$), (d) 200-hPa height (m), and (e) OLR (W m^{-2}) over the central equatorial Pacific. Values were determined by averaging over the region bounded by 5°N – 5°S and 180° – 100°W . The solid curve in all panels shows the 5-day mean values and the dashed curve is the climatological mean. The anomalies are shown shaded, with orange (blue) shading indicating positive (negative) anomalies, except in (e) where the shading convention is reversed. The climatology and anomalies were computed with respect to the 1979–95 base period.

the 850-hPa zonal wind anomalies, 200-hPa height anomalies, and OLR anomalies, throughout the year reflected considerable intraseasonal variability related to the MJO.

ii) EQUATORIAL PACIFIC OCEAN SEA SURFACE AND SUB-SURFACE TEMPERATURE EVOLUTION

During the first half of 2004, slightly positive equatorial SST anomalies were observed near the date line, with the warmest SSTs and largest positive anomalies located well west of the date line (Figs. 4.2a–d). A slight retrogression of the warmest waters also occurred during the period, as the 30°C surface isotherm became situated just north of New Guinea during March–May (Fig. 4.2c). Despite this evolution, positive temperature anomalies of 0.5°–1.0°C persisted near the date line throughout the period (Figs. 4.2b,d).

During the latter half of 2004, SSTs warmed over the central and east-central equatorial Pacific, as temperatures above 29°C extended to well east of the date line and the 30°C isotherm reached the date line (Figs. 4.2e–h). This anomalous warming was indicated by a strengthening of positive SST departures across the central and east-central equatorial

Pacific, with the largest departures of 1°–2°C seen during September–November between 160°E and 145°W (Fig. 4.2h). This evolution into weak warm episode conditions was associated with a gradual eastward expansion of the anomalous warmth at thermocline depth. However, the subsurface temperature departures remained weak throughout the period, only slightly exceeding 2°C (Figs. 4.3c,d). The observed changes in the surface and subsurface temperatures did not have a notable influence on the atmospheric circulation across the tropical Pacific, whose variability was instead dominated by MJO activity throughout much of the year.

iii) THE MJO, KELVIN WAVE ACTIVITY, AND ATMOSPHERIC CIRCULATION

Low-frequency variability in the Tropics is strongly influenced by the MJO (Madden and Julian 1971, 1972, 1994), a tropical disturbance that modulates tropical convection and atmospheric circulation patterns with a typical period of 30–60 days. The MJO tends to be most active during ENSO-neutral years, especially just prior to El Niño, and can produce ENSO-like anomalies in the large-scale circulation over the Pacific Ocean (Mo and Kousky 1993; Kousky

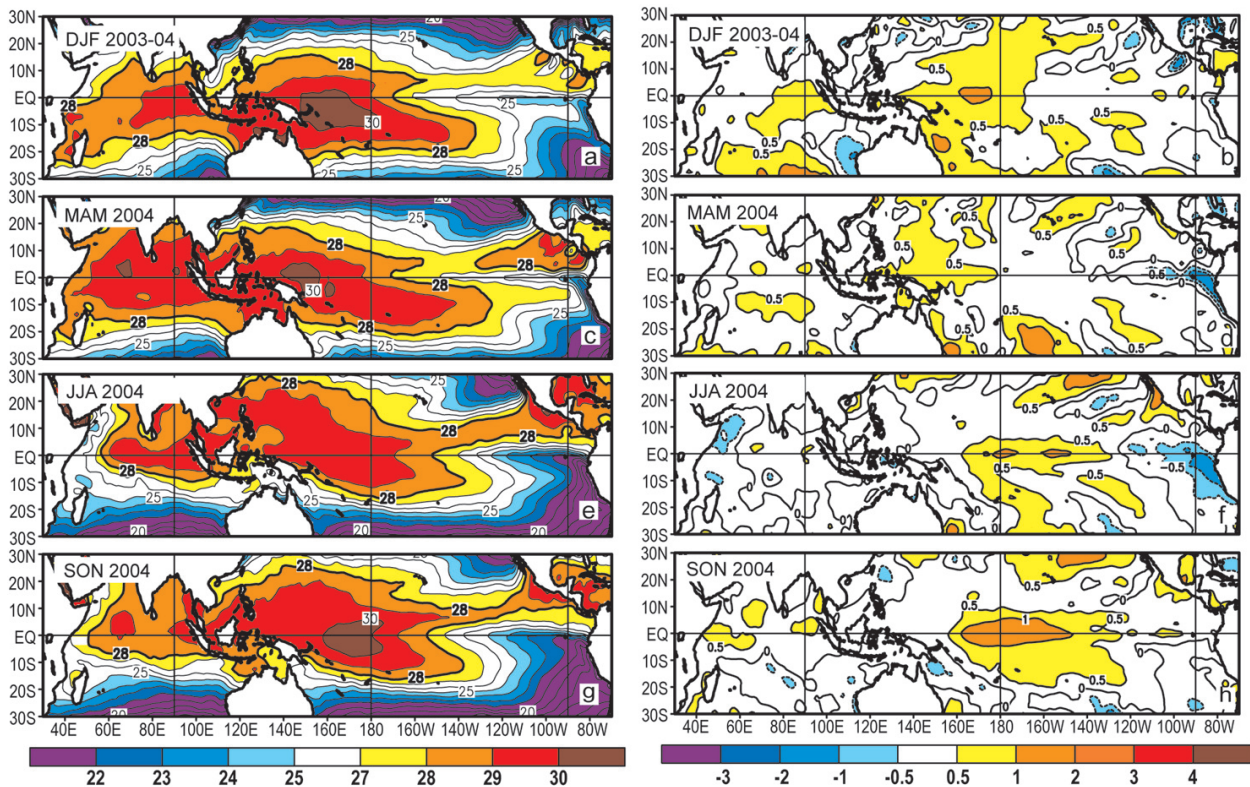


FIG. 4.2. Seasonal (left) SSTs and (right) anomalies for (a), (b) DJF 2003–04, (c), (d) MAM 2004, (e), (f) JJA 2004, and (g), (h) SON 2004. The contour interval is 1°C, with the 0.5°C anomaly contour included. Anomalies were determined as departures from the 1971–2000-adjusted OI climatology (Smith and Reynolds 1998).

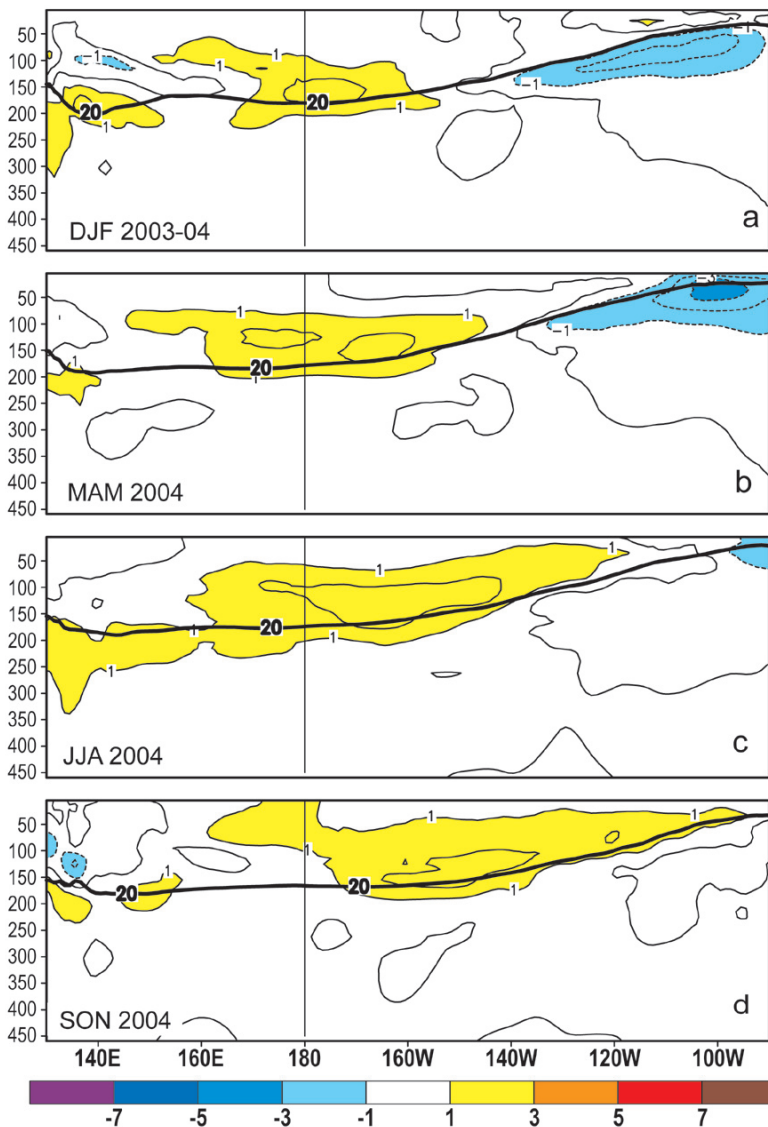


FIG. 4.3. Equatorial depth–longitude sections of ocean temperature anomalies for (a) DJF 2003–04, (b) MAM 2004, (c) JJA 2004, and (d) SON 2004. The contour interval is 1°C, and the dark line is the 20°C isotherm. The data were derived from an analysis system that assimilates oceanic observations into an oceanic GCM (Behringer et al. 1998). Anomalies were determined as departures from the 1981–2000 base period means.

and Kayano 1994) and western United States (Higgins et al. 2000).

During 2004, the low-level (850 hPa) and upper-level (200 hPa) equatorial zonal winds, 200-hPa streamfunction, 200-hPa velocity potential, and patterns of tropical convection exhibited considerable intraseasonal variability in association with the MJO (Figs. 4.1b,d,e). The MJO is indicated in the time–longitude section in Fig. 4.4 by continuous propagation of the 200-hPa velocity potential anomalies around the globe. This MJO activity contributed to alternating

periods of enhanced and suppressed convection from the Indian Ocean to the date line, and to alternating periods of low-level easterly and westerly wind anomalies across the tropical Pacific (see Fig. 2.14, left panel).

The low-level wind anomalies associated with the MJO may generate oceanic Kelvin waves, which are eastward-propagating oceanic gravity waves that feature downwelling in the mixed layer at their leading edge and upwelling in their wake (Zhang et al. 2001). A typical eastward-propagation rate for these waves is roughly 10° longitude per week. Several Kelvin waves occurred during 2004, each resulting in increased ocean temperatures at thermocline depth, followed later by a shoaling of the thermocline and cooler temperatures. These Kelvin waves were superimposed upon a trend of larger-than-average thermocline depths across the central and east-central equatorial Pacific (see Fig. 2.14, right panel), and a gradual increase and eastward shift in the upper-ocean heat content anomalies.

In the atmosphere, circulation anomalies over the eastern North Pacific and North America are known to be influenced by the East Asian jet stream, which exhibits large fluctuations in response to anomalous tropical convection over the central equatorial Pacific. Because the MJO is a propagating disturbance, its impacts on the East Asian jet stream and the downstream circulation anomalies over North America depend upon the eastward extent of the enhanced tropical convection. For example, when the

associated tropical convection moves to the date line and even farther east, as seen during both January and April, there was a resulting eastward extension of the East Asian jet stream and an eastward shift of the jet exit region.

When tropical convection is enhanced over the Indian Ocean and suppressed near the date line, as seen during February and May, the East Asian jet core and jet exit region retract westward, which leads to a westward shift of the mean upper-level ridge and trough positions across the eastern North Pacific

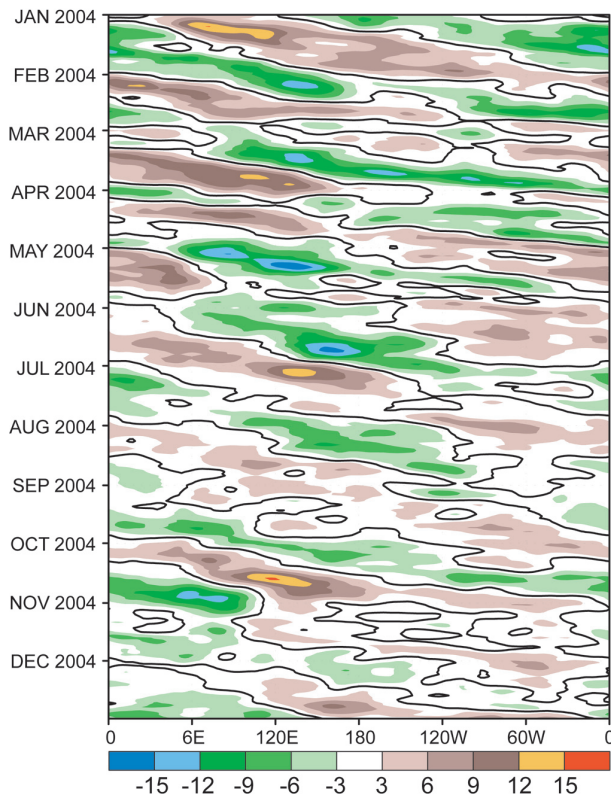


FIG. 4.4. Time–longitude section (5°N–5°S) of daily 200-hPa velocity potential anomalies during 2004. The shading interval is $3 \times 10^6 \text{ m}^2 \text{ s}^{-1}$, and the thick solid contour is the zero line. Anomalies were determined as departures from the 1971–2000 base period daily means, and plotted using a 5-day running mean smoother.

and North America. During May, these conditions contributed to one of the strongest negative phases of the Pacific–North American (PNA) teleconnection pattern on record for that month. Key aspects of this pattern included above-average 500-hPa heights over the Gulf of Alaska and southern United States, and below-average heights over the central subtropical North Pacific and Canada. This circulation brought a strong northwesterly flow of arctic air from Alaska and the Beaufort Sea into western Canada in the area downstream of the mean upper-level ridge axis, and led to near-record cold surface temperatures (2° – 5°C below average) across most of that country (see section 6a1).

b. Tropical storms

- 1) ATLANTIC HURRICANE SEASON—G. D. Bell,⁴ S. Goldenberg,²⁰ C. Landsea,²⁰ E. Blake,⁶ R. Pasch,⁶ M. Chelliah,⁴ and K. Mo⁴

(i) Overview

The 2004 Atlantic hurricane season had well above-normal activity, with 15 named storms,^{4,1} 9

hurricanes (Hs), and 6 major hurricanes (MHs; defined as categories 3–5 on the Saffir–Simpson scale; Simpson 1974). Nine of these systems struck the continental United States—three as tropical storms and six as hurricanes. Three of the hurricanes hit the United States as major hurricanes.

Five named storms hit Florida in 2004—one as a tropical storm (Bonnie) and four as hurricanes (Charley, Frances, Ivan, and Jeanne). This tied the record with Texas (in 1886) for the most hurricanes to hit one state in a single season. Also, all three landfalling major hurricanes struck Florida, which was the most ever recorded for that state in a single season since accurate records began in 1900.

(ii) 2004 seasonal activity

One measure of seasonal activity is NOAA’s Accumulated Cyclone Energy (ACE) Index (Bell et al. 2000), which accounts for the combined strength and duration of tropical storms and hurricanes during a given season. This wind energy index is calculated by summing the squares of the 6-h maximum sustained surface wind speed in knots ($\sum V_{\text{max}}^2$) for all periods while the system is either a tropical storm or hurricane. The total ACE Index value for the 2004 season was 257% of the 1951–2000 median (Fig. 4.5), which was the third-largest seasonal value in the 1950–2004 record, exceeded only by 1950 and 1995.

During above-normal Atlantic hurricane seasons, a large fraction of the total ACE value results from tropical storms that form in the main development region (MDR; which consists of the tropical Atlantic and Caribbean Sea south of 21.5°N), and later develop into hurricanes and major hurricanes (Goldenberg and Shapiro 1996). During 2004, nine tropical storms formed in the MDR, with seven subsequently intensifying into hurricanes. These systems accounted for 92% of the total ACE value. Major Hurricane Ivan, the strongest hurricane of the season, which eventually made landfall in Alabama and brought hurricane-force winds to the western Florida Panhandle, produced the largest storm total ACE value ($70.4 \times 10^4 \text{ kt}^2$) in the reliable record dating back to 1944.

The 2004 hurricane season was a continuation of a series of above-normal seasons that began in 1995 (Goldenberg et al. 2001), in response to favorable atmospheric and oceanic conditions in the MDR.

^{4,1} Note that Nicole, which developed in October, was officially categorized as a “subtropical” cyclone by NOAA’s National Hurricane Center (NHC).

During 1995–2004, Atlantic hurricane seasons have averaged 13.6 TSs, 7.8 Hs, and 3.8 MHs, with an ACE value of 169% of the median, and with above-normal activity in every season except for the two El Niño years of 1997 and 2002. In contrast, seasons during the below-normal 24-yr period of 1971–94 averaged only 8.6 TSs, 5.0 Hs, and 1.5 MHs, with an ACE value of 75% of the median, and included only three seasons that were above normal (1980, 1988, 1989).

(iii) *Landfalling U.S. tropical systems and associated rainfall*

During 2004, three of the systems that struck the United States hit as tropical storms (Bonnie, Hermine, and Matthew), three struck as category 1–2 hurricanes (Alex, Gaston, and Frances), and three hit as major hurricanes (Charley, Ivan, and Jeanne). The first eight strikes,^{4,2} including all five in Florida, occurred during August and September. For this 2-month period, rainfall from Florida to Pennsylvania was 200% or more of average, mainly due to the landfalling storms. The total rainfall associated with these systems reached 500 mm or more across Florida, Georgia, and the western Carolinas (not shown), and accounted for 60%–80% of the 2-month total in these regions.

Rainfall totals for each of the nine named storms that struck the United States are summarized in Fig. 4.6. Three of these hurricanes with long tracks over the eastern United States produced the largest precipitation totals. The first of these was H Frances during 5–9 September, which brought more than 175 mm of rain to Florida, Georgia, and the western Carolinas (Fig. 4.6f). The second was MH Ivan during 16–18 September, which produced more than 150 mm

^{4,2} According to NOAA/NHC, a hurricane strike occurs if that location passes within the hurricane’s strike circle, a circle of 125 n mi in diameter, centered 12.5 n mi to the right of the hurricane center (i.e. in the direction of motion). Therefore, a strike is different than a landfall, which is the intersection of the surface center of a tropical cyclone with a coastline.

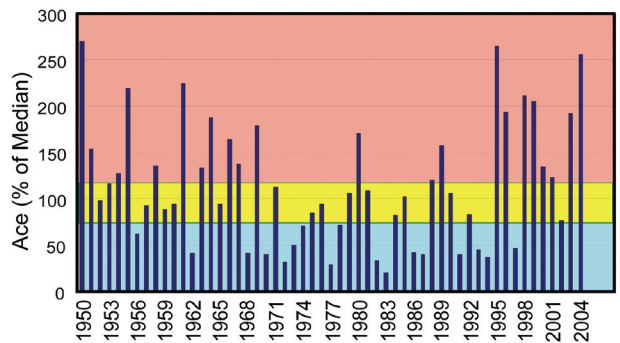


FIG. 4.5. Atlantic hurricane season values of the NOAA ACE Index expressed as percent of the 1951–2000 median value. NOAA definitions of season types are indicated by the background shading, with pink, yellow, and blue indicating above-, near-, and below-normal seasons, respectively.

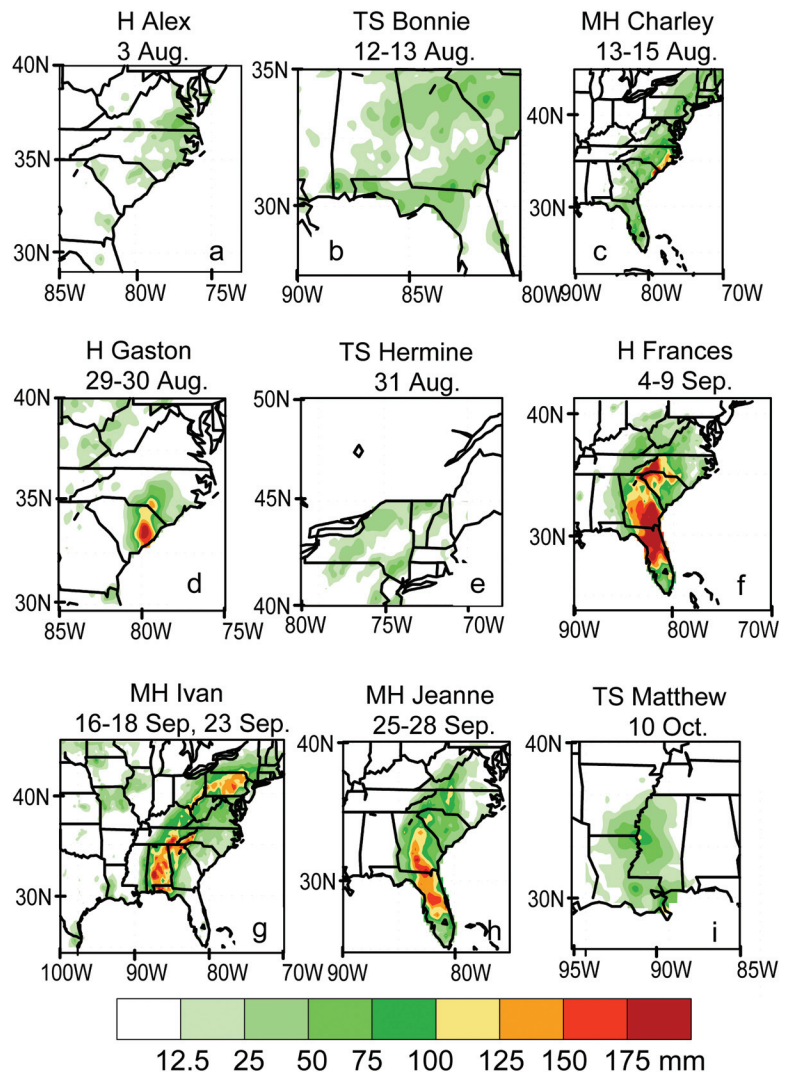


FIG. 4.6. Storm total rainfall amounts (mm) for the nine tropical systems that struck the United States during 2004: (a) Alex, (b) Bonnie, (c) Charley, (d) Gaston, (e) Hermine, (f) Frances, (g) Ivan, (h) Jeanne, and (i) Matthew.

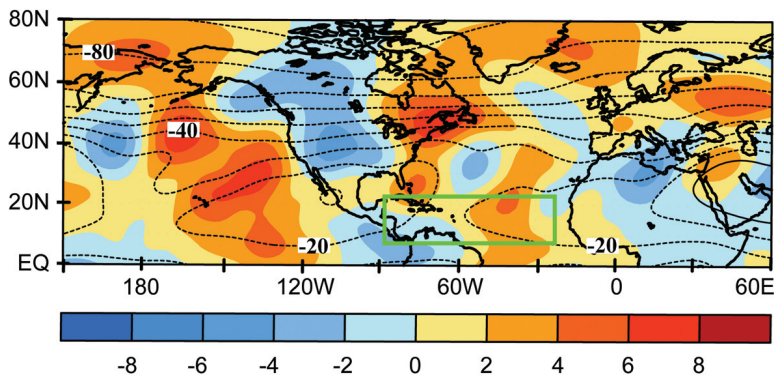


FIG. 4.7. 200-hPa streamfunction (contours, interval is $10 \times 10^6 \text{ m}^2 \text{ s}^{-1}$) and anomalies (shading) during Aug–Sep 2004. Anticyclonic (cyclonic) anomalies are indicated by positive (negative) values. The green box denotes the MDR, with anomalies determined as departures from the 1971–2000 base period monthly means.

of rain from Alabama to Pennsylvania (Fig. 4.6g). Ivan eventually tracked to the southwest, and back into the Gulf of Mexico, where it regained tropical storm status before making a second landfall on 23 September in southeastern Texas. The third was MH Jeanne during 25–28 September, which produced 100+ mm rainfall totals from Florida to the western Carolinas (Fig. 4.6h).

All but one of the nine named storms (Alex) that struck the United States during 2004 officially made landfall. Since 2002, the United States has experienced 19 landfalling named storms, with seven occurring in 2002 and four in 2003 (Bell et al. 2003; Bell et al. 2004; Pasch et al. 2004; Lawrence et al. 2005). Eleven of these 19 systems hit as tropical storms and eight hit as hurricanes. The Gulf Coast region from the southern tip of Texas to the southern tip of Florida has been struck by 12 of these named storms (5 in 2002, 3 in 2003, and 4 in 2004), with 8 hitting as tropical storms and 4 as hurricanes.

(iv) *Atmospheric and oceanic conditions*

Almost all of the 2004 seasonal activity occurred during August and September, and the mean atmospheric and oceanic conditions during this period were characteristic of most above-normal seasons. At middle and upper levels, the subtropical ridge was stronger than average from the Gulf of Mexico to northern Senegal (Fig. 4.7), with large anticyclonic anomalies

that extended northward along the U.S. east coast. South of the mean ridge axis, anomalous upper-level easterly flow covered the entire MDR (not shown). Over the eastern North Atlantic and western Africa, these conditions are consistent with the ongoing active Atlantic multidecadal signal (Bell et al. 2004). Over the western subtropical North Atlantic and eastern United States they were linked to a large-scale pattern of extratropical circulation anomalies that had previously persisted from April through July.

The pronounced westward extent of the enhanced subtropical ridge and anomalous upper-level easterlies contributed to below-average vertical wind shear across the MDR during August–September (Fig. 4.8), which aided in the formation of intense and long-lived hurricanes. The mean steering current during September 2004, characterized by a 500-hPa ridge along the U.S. east coast, caused the systems to track further west than normal, eventually making landfall in Florida and the Gulf Coast region. Several of these systems were then steered over the eastern United States, producing heavy rains and flooding along their paths. These conditions were in marked contrast to the climatological mean (not shown), which features a broad trough across the eastern United States that acts to divert (i.e., recurve) hurricanes out to sea, often well prior to reaching the U.S. east coast.

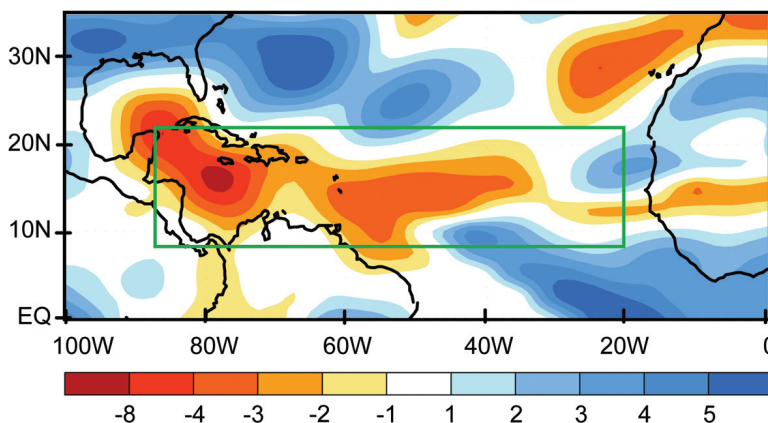


FIG. 4.8. Anomalous magnitude of the 200–850-hPa vertical wind shear (m s^{-1}) during Aug–Sep 2004. Yellow–red and blue shading indicates below-average and above-average wind shear magnitudes, respectively. The green box denotes the MDR, with anomalies determined as departures from the 1971–2000 base period monthly means.

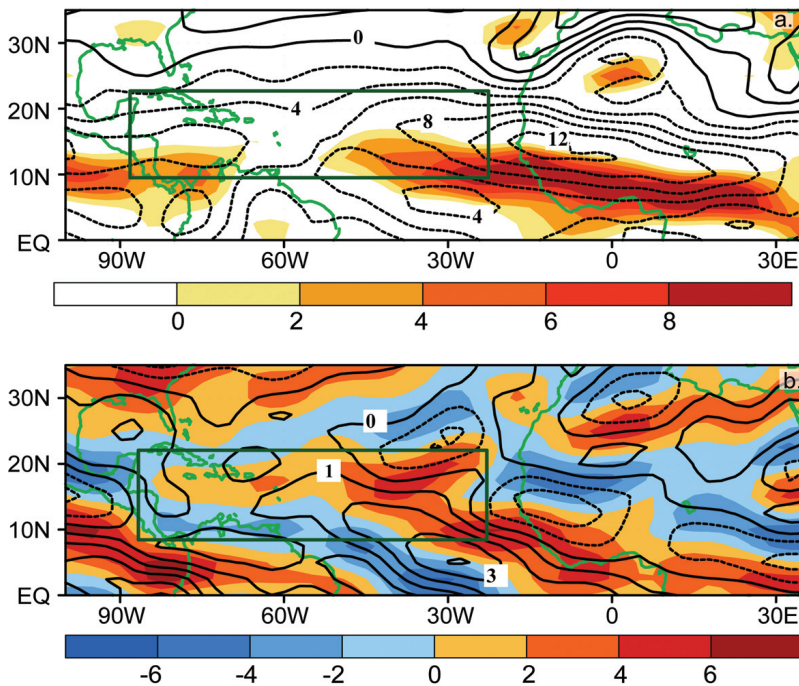


FIG. 4.9. 700-hPa zonal winds (contours) and relative vorticity (shading) during Aug–Sep 2004: (a) mean and (b) anomalies. The contour interval for winds is 1.0 m s^{-1} , and for vorticity is $1 \times 10^{-6} \text{ s}^{-1}$. In (a), only cyclonic relative vorticity values are shaded. In (b), cyclonic anomalies are shaded yellow–red and anticyclonic anomalies are shaded blue. The green box in both panels denotes the MDR, with anomalies determined as departures from the 1971–2000 base period monthly means.

In the lower atmosphere, the 700-hPa African easterly jet (AEJ) was well defined during August–September, and its associated region of strong cyclonic vorticity extended farther west than normal into the central MDR (Fig. 4.9a). These conditions were associated with a below-average strength of the tropical

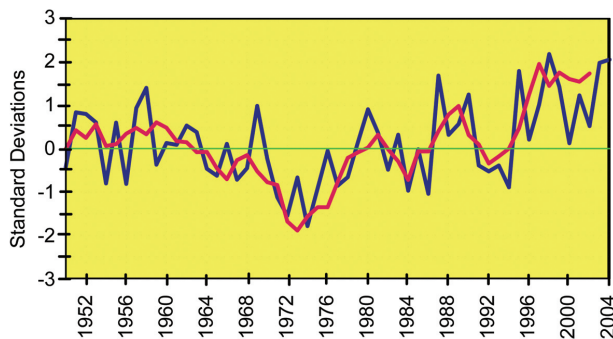


FIG. 4.10. Aug–Sep area-averaged, standardized SST anomalies (blue) in the MDR during 1950–2004. The standardized 5-yr running mean of Aug–Sep anomalies is shown in red. The analysis is based on the extended reconstructed SST dataset of Smith and Reynolds (2004), with anomalies determined as departures from the 1971–2000 base period monthly means.

easterly trade winds, as indicated by westerly anomalies from the eastern Pacific to western Africa (Fig. 4.9b). The 2004 hurricane season also featured exceptionally warm (0.5° – 1.25°C above average) SSTs in the central MDR. For the entire MDR, area-averaged SSTs during August–September were almost two standard deviations above normal—the second warmest since 1950 (Fig. 4.10).

The conditions described above indicate that the African easterly waves during the peak of the season were embedded within an extended region of increased cyclonic vorticity along the equatorward flank of the AEJ as they moved westward over very warm SSTs into the low-shear environment of the central and western MDR. This combination of conditions is known to favor very active hurricane seasons. These conditions are also key ingredients of the active Atlantic multidecadal signal that has prevailed since 1995 (Landsea et al. 1999; Mestas-Núñez and Enfield 1999; Goldenberg et al. 2001; Bell et al. 2004).

II) NORTH PACIFIC TROPICAL STORMS

(i) Western North Pacific typhoon season—S. J. Camargo⁵

The 2004 western North Pacific typhoon season was an active one, with 32 tropical cyclones [tropical depressions (TDs), tropical storms (TSs), and typhoons (TYs)], which was slightly above the 1971–2000 climatological median of 30.5 (JTWC 2005). All but two of the tropical cyclones in 2004 (i.e., TD Malou and TD Haima) reached tropical storm intensity or higher.^{4.3} Figure 4.12a shows the number of tropical cyclones reaching at least tropical storm strength each year since 1945. There were 30 named storms (NSs)^{4.4} in 2004 (9 TSs and 21 TYs),

^{4.3} In contrast to the JTWC data, the Japan Meteorological Agency (JMA) categorized Malou as a tropical storm, with winds ~ 40 kt during landfall at 1300 UTC 4 August 2004.

^{4.4} Named storms include all tropical cyclones that reach at least tropical storm intensity (34 kt or greater), that is, TS and TY.

which was above the climatological median of 26 (75th percentile, 29.5 NSs). The nine tropical storms in 2004 equaled the climatological median, and four of these tropical storms were not officially named (01W, 02W, 05W, 21W). Twenty-one tropical cyclones reached typhoon intensity, which was well above the climatological median of 17.5 (75th percentile, 20 TYs), and the highest number since the El Niño year of 1997, when 23 typhoons developed. Seven of these typhoons became supertyphoons, which was above the 75th percentile of the climatological mean of six (the median is four). During the period 1971–2000, 62% (13%) of the named tropical cyclones reached typhoon (supertyphoon) intensity; while in

2004 the percentage was 70% (23%). The long-term data suggest that more frequent and intense tropical cyclones are characteristic of El Niño years in the western North Pacific basin (Camargo and Sobel 2004), and tropical cyclone–intensity indices are correlated with the Niño-3.4 and Niño-4 indices in the western and central tropical Pacific (Camargo and Sobel 2005). According to both the NOAA and International Research Institute for Climate Prediction (IRI) definitions, a weak El Niño occurred in 2004 with anomalous warming in the central tropical Pacific (see section 4.a), which likely contributed to such an active season in 2004.

Overall, only 50% of the named storms occurred between July and October in 2004, compared to the clima-

“FENOMENO CATARINA:” THE SOUTH ATLANTIC’S FIRST HURRICANE?—M. RUSTICUCCI³⁵ AND M. A. FORTUNE¹⁷

The rapid development on 27 March 2004 of a strong cyclone with hurricane-force winds in the South Atlantic Ocean, and its westward propagation and landfall along the southern coast of Brazil, astonished the meteorological community (Gusso 2004). As such an unusual event, there was widespread disagreement whether the cyclone was tropical, extratropical, or a “hybrid” system. NOAA’s National Hurricane Center (NHC) classified Catarina as a

“category 1” hurricane, while specialists in both Brazil’s national meteorological service [Instituto Nacional de Meteorologia (INMET)] and the Weather Forecasting and Climate Studies Center [Instituto Nacional de Pesquisas Especiais (INPE) Centro de Previsão de Tempo e Estudo Climáticos (CPTEC)] classified it as a “fenomeno” (phenomenon in Portuguese). Initial observations suggested that it appeared to be a hybrid of a tropical and an extratropical cyclone (Silva-Dias et al. 2004). The maximum recorded wind speed and surface pressure during landfall were 147 km h⁻¹ (~79.4 kt) and 993 hPa at Siderópolis, Brazil, respectively, at 0300 (LST) on 28 March.

Atmospheric conditions associated with Catarina at times differed from those of a tropical cyclone, because it developed both barotropic and baroclinic characteristics during its life cycle (Mattos and Satyamurty 2004). Initially, it was observed as a low pressure disturbance that developed along a cold front over the South Atlantic Ocean, but in 2 days it acquired the typi-

cal characteristics of a tropical cyclone, with rain- and cloud bands cyclonically converging into a well-defined eye. Catarina mostly resembled both Mediterranean lows (Reale and Atlas 2001), and hurricane-like vortices that develop between Australia and Tasmania. These are considered “hybrid systems” that originate as extratropical, cold core vortices, but develop a warm core due to latent heating in the convectively active center. Cyclone Catarina developed a clearly visible “eye” and an associated wall cloud of very intense convection where the strongest winds were observed (Fig. 4.11). In the eye region, initializations of two models [NCEP’s Aviation (AVN) model and the Regional Atmospheric Modeling System (RAMS)] exhibited a warm core, surrounded by the extensive cold core air mass (Bonatti et al. 2004; Menezes and Silva-Dias 2004).

As the cyclone intensified over the South Atlantic Ocean, Brazilian authorities were notified and measures were taken to minimize the possible loss of human life. Sampaio-Calearo et al. (2004) considered the results “very satisfactory,” considering the minimal loss of life and the lack of local experience in forecasting an event such as this one. However, damages on the southern coast of Santa Catarina state and the northern coast of Rio Grande do Sul state were extensive, and reached approximately 330 million U.S. dollars.

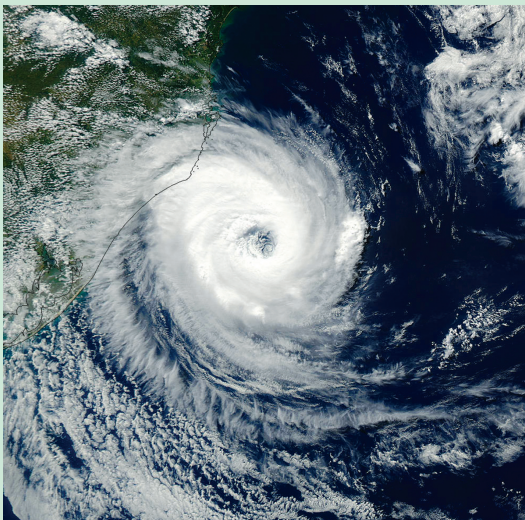


FIG. 4.11. Satellite image at 1630 UTC on 24 Mar 2004 of cyclone “Catarina” over the South Atlantic Ocean, from the afternoon overpass of NASA’s Moderate Resolution Imaging Spectroradiometer (MODIS) on board the *Terra* satellite.

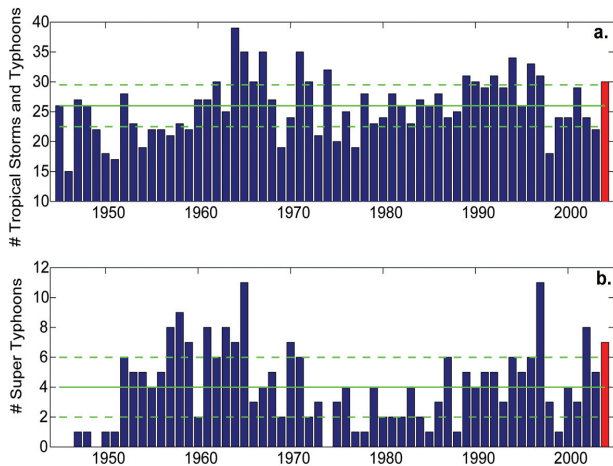


FIG. 4.12. Western North Pacific basin statistics over the period 1945–2004: (a) the number of tropical storms and typhoons per year, and (b) the number of super typhoons per year. The solid green line indicates the median for the 1971–2000 base period, and the dashed green lines show the 25th and 75th percentiles (source: JTWC).

tological average of 70%. Of the 15 NSs that formed during the peak season (July–October), 8 occurred in the month of August, which was close to the historical record of 9 that occurred in both 1960 and 1992. The five NSs in June was a record high since 1945, surpassing the previous record of four that was set in 1963 and 1965. A well-established monsoon trough and an active MJO in June led to the formation of five typhoons, with four of them affecting populated areas (Padgett 2005). In addition, the two NSs in September tied the previous record low for the month.

The yearly and monthly values of the ACE Index (Bell et al. 2000) were elevated in the western North Pacific in 2004. The 2004 yearly ACE Index ($471.4 \times 10^4 \text{ kt}^2$) was 175% of the climatological median ($268.3 \times 10^4 \text{ kt}^2$), corresponding to the third highest value in the historical record (Fig. 4.13a), second only to the El Niño years of 1992 and 1997. The typhoon season (June–November) ACE Index ($361.0 \times 10^4 \text{ kt}^2$) was also well above normal (163% of the climatological median of $220.7 \times 10^4 \text{ kt}^2$), and the 10th highest value of the historical record.

ACE Indices were higher than their climatological median in most months (Fig. 4.13b), especially in April, May, June, and August, all with values above the 75th percentile of the climatology. The anomalously high ACE Index in April (third in the historical record) was due to supertyphoon Sudal (supertyphoons have occurred in April in only five previous years), while the anomalously high May value (6th

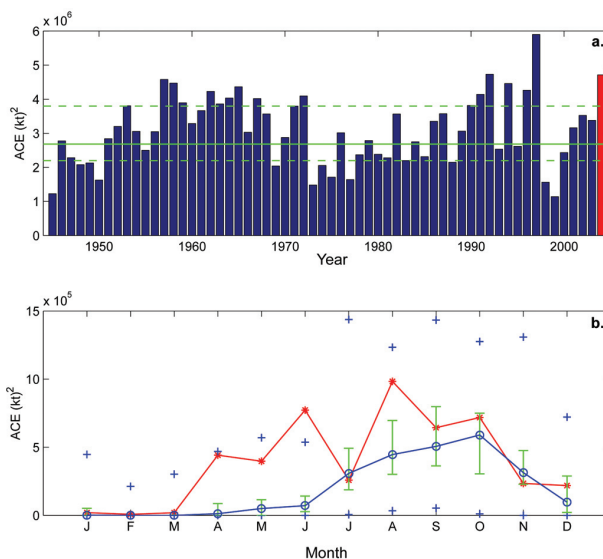


FIG. 4.13. (a) ACE Index for the western North Pacific for the years 1945–2004. The solid green line indicates the median for the 1971–2000 base period, and the dashed green lines show the 25th and 75th percentiles. (b) ACE Index per month in the western North Pacific in 2004 (red line) and the median in the years 1973–2002 (blue line), where the green error bars indicate the 25th and 75th percentiles. In the cases with no error bars, the upper and/or lower percentiles coincided with the median. The blue plus signs (+) denote the maximum and minimum values during the period 1945–2003 (source: JTWC).

in the historical record since 1945) was due to the simultaneous occurrence of three tropical cyclones in the basin, including one supertyphoon (Nida) and one “midget” typhoon (Omais). In June, the ACE Index reached a historical record ($77.22 \times 10^4 \text{ kt}^2$), due to the contributions of supertyphoons Dianmu (48%) and Mindulle (30%). The August ACE Index was the sixth highest in the historical record, with supertyphoon Chaba contributing to 60% of the total monthly value. During 2004, supertyphoons Dianmu and Chaba intensified to wind speeds of $\sim 155 \text{ kt}$; since 1990 only 10 supertyphoons have reached such high winds speeds, with 6 of them in the El Niño years of 1992 and 1997.

The number of days with named storms in 2004 was near normal (163.5 days), compared with the climatological median of 161.5 days. In contrast, the number of days with intense typhoons (number of days with at least one typhoon with wind speeds $> 95 \text{ kt}$) was 45.5—the third highest in the historical record (below only 1958 and 1997), and more than twice the 1945–2000 median value of 19.4 days. The tropical storms and typhoons in 2004 had an

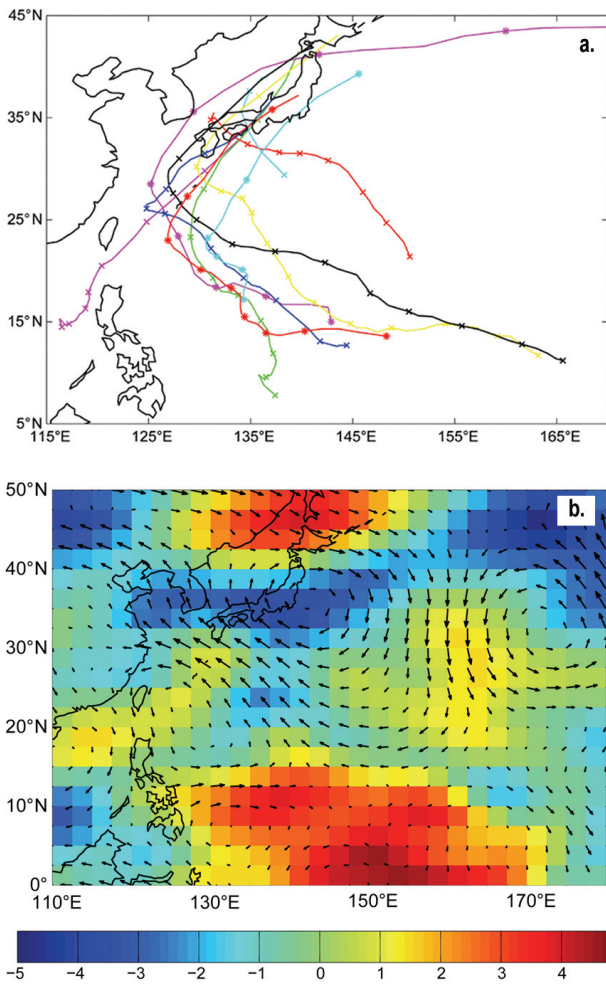


FIG. 4.14. (a) The observed tracks of the 2004 tropical cyclones that made landfall in Japan, and (b) the anomalous 500-hPa winds (vectors) and anomalous vertical wind shear (m s^{-1} ; shading) during Jul–Oct 2004.

average tropical cyclogenesis position of 12.6°N , 144.3°E , which was very near the climatological mean (12.9°N , 143.5°E). The average track position of all named storms in 2004 was at 18.7°N , 135.4°E , and was also close to the climatological average (19.0°N , 134.2°E).

One of the most striking features of this typhoon season in the western North Pacific basin were the 10 landfalls in Japan, which shattered the previous record of 6. Figure 4.14a shows the tracks of the 2004 tropical cyclones that made landfall in Japan. This uncharacteristically large number of landfalls was accompanied by anomalous southeasterly winds and below-normal total wind shear (Fig. 4.14b). This synoptic pattern propagated the tropical cyclones toward the Japanese islands, which generated many impacts. Of these landfalling systems, Ma-On was the strongest typhoon to affect southeastern Japan in

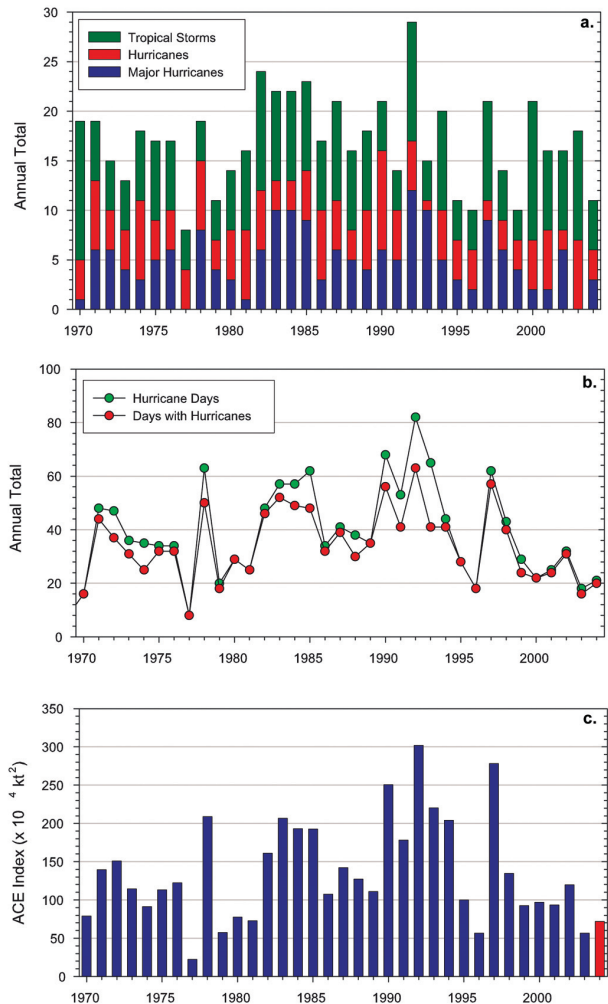


FIG. 4.15. Annual tropical cyclone statistics for the ENP basin over the period 1971–2004: (a) number of tropical storms, hurricanes, and major hurricanes, (b) days with hurricanes (the number of days with winds ≥ 64 kt) and hurricane days (days with winds ≥ 64 kt \times number of storms with winds ≥ 64 kt on those days), and (c) the ACE Index ($\times 10^4 \text{ kt}^2$) with 2004 highlighted in red.

over 10 yr (Padgett 2005). Although typhoon Tokage was not as intense, its impacts were more substantial, causing at least 69 deaths due to the high winds, flooding, and mudslides.

(ii) *Eastern North Pacific hurricane season—*
D. H. Levinson¹⁹

(a) *OVERVIEW OF THE 2004 SEASON*

Hurricane activity was below average during the 2004 season in the eastern North Pacific (ENP) Ocean. A total of 12 NSs, 6 Hs, and 3 MHs occurred in the ENP basin in 2004, which was below NOAA's 1971–2003 climatology of 15.5 NSs, 9 Hs, and 4.3 MHs each year (Table 4.1). In addition, there were

no landfalling systems of either TS or hurricane strength during the entire ENP hurricane season, which typically spans from mid-May through the end of November.

Despite the below-average activity in the ENP, there were several notable aspects of the season. The season started off slowly, because TS Agatha was the only tropical cyclone to form during May, and there was no tropical cyclogenesis during the month of June. Cyclogenesis activity resumed in July as two hurricanes developed—Celia, which was the first tropical cyclone of the season to reach hurricane strength, and Darby, which intensified into the first major hurricane of the season. Major Hurricane Darby was also the first major hurricane to form in the ENP in almost 2 yr. The last tropical cyclone to intensify into a major hurricane was Kenna back in October of 2002, which reached category 4 strength and made landfall on the coast of Mexico with sustained winds of 120 kt (the third strongest landfall on record for the Pacific coast of Mexico).

The majority of the tropical cyclones that developed in 2004 propagated in the typical west-northwest direction away from the Mexican coast, and into environmental conditions that are normally unfavorable for further development (i.e., colder sea surface temperatures and increasing vertical wind shear). The only named storm that recurved toward the Mexican coast during the season was H Javier, which was the strongest tropical cyclone of the ENP season, with sustained winds of 130 kt (category 4 on the Saffir-Simpson scale). Javier dissipated into a tropical storm as it approached the Baja Peninsula, eventually making landfall on the west coast of the peninsula as a TD on 19 September. Not included in the seasonal statistics in Table 4.1 were four tropical depressions that developed in the ENP during 2004, but did not intensify to minimal tropical storm strength (02E, 06E, 09E, and 16E), while an additional depression (01C)

developed southwest of the Hawaiian Islands on 5 July, in the central Pacific part of the ENP basin (defined as west of 140°W to the date line).

(b) COMPARISON OF THE 2004 SEASON WITH CLIMATOLOGY

The variability of tropical cyclone activity in the ENP basin since 1970 is shown in Figs. 4.15a–c. In general, seasonal hurricane activity in the ENP basin has been below average since the mid-1990s based on several widely used statistics. From the standpoint of the annual numbers of hurricanes and major hurricanes, tropical cyclone activity has been below average since 1995. In 2004, the number of named storms, hurricanes, and major hurricanes were all well below the long-term means, and there were no landfalling tropical cyclones in any of these categories during the season (Table 4.1). In terms of *days with hurricanes*, as well as *hurricane days* (Fig. 4.15b), both of these statistics also have shown an obvious downward trend that began in the mid-1990s.

The ACE Index (Bell et al. 2000) for the ENP basin is shown in Fig. 4.15c. The ACE Index value in 2004 of just over $70 \times 10^4 \text{ kt}^2$ was well below both the mean

TABLE 4.1. Comparison of the 2004 east North Pacific hurricane season with climatology. The climatological statistics are from the NOAA National Hurricane Center's 1971–2003 averages, except those statistics with a *, which denotes the 1951–2000 climatology of landfalling tropical storms and hurricanes in Mexico from Jauregui (2003).

	Climatology	2004
Named storms	15.5	12
Hurricanes	9	6
Major hurricanes (category 3–5)	4.3	3
Landfalling tropical storms*	1.34	0
Landfalling hurricanes*	1.3	0
Intense landfalling hurricanes*	0.3	0
ACE Index	Mean = $129.7 \times 10^4 \text{ Kt}^2$ Median = $111 \times 10^4 \text{ Kt}^2$ Near normal = $100\text{--}150 \times 10^4 \text{ kt}^2$	$70.84 \times 10^4 \text{ kt}^2$

and median values, and also below NOAA's definition of a "below normal" season (Table 4.1). A well-defined peak in the seasonal ACE Indices occurred in the early 1990s, with the largest annual value occurring back in 1992. Similar to the other tropical cyclone statistics already discussed, there has been a clear decrease in the ACE Index for the ENP basin that began in 1995. The one exception to the observed decreasing trends in ENP hurricane activity since the mid-1990s was the 1997 hurricane season, which was an El Niño year. Another interesting aspect of the below-normal activity in the ENP since 1995 is that it appears to be inversely related to the observed increase in activity in the North Atlantic basin over the same time period, and the so-called Atlantic multidecadal SST mode (Landsea et al. 1998, 1999; Goldenberg et al. 2001).

One important aspect of the 2004 ENP hurricane season was the near absence of landfalling tropical systems. Reliable long-term records of landfalling tropical storms and hurricanes are available back to 1951, with limited information extending back to the beginning of the twentieth century (Jauregui 2003). Because Mexico has extensive coastlines that are affected by both ENP and North Atlantic tropical cyclones, the Servicio Meteorológico Nacional (SMN; National Meteorological Service) of Mexico typically groups all landfalling tropical cyclones for both basins together. Figure 4.16 shows the number of Mexican landfalling tropical systems (TDs, TSs, and Hs) as well as those that reached at least minimal hurricane strength over the period 1971–2004. For the 2004 season, three systems made landfall in

Mexico along the Pacific coast as tropical depressions (Javier, 16E, and Lester), and there were no landfalls of any tropical cyclones along the Gulf of Mexico and Caribbean coasts of the country. Despite the lack of any official reports of damage or casualties with these landfalling systems, these tropical depressions did generate substantial amounts of precipitation in the Sierra Madre Occidental mountain range and adjacent coastal areas of the country (see section 6a111 for further details). As can be seen in Fig. 4.16, the 2004 hurricane season was one of only five seasons since 1970 with no landfalling hurricanes in Mexico on either coast, and the first since 1991. The 2004 season sharply contrasted with 2003, which had the second most landfalling tropical cyclones and hurricanes over the past 35 yr.

(c) ENVIRONMENTAL INFLUENCES ON THE BELOW-NORMAL EAST NORTH PACIFIC HURRICANE SEASON

Tropical cyclone activity (both frequency and intensity) in the ENP is related to several, large-scale environmental influences, including SSTs, the phase of ENSO, and the phase of the quasi-biennial oscillation (QBO) in the tropical lower stratosphere (Whitney and Hobgood 1997). Obviously, there is a strong relationship between SSTs and the phase of ENSO, so these two factors are well correlated. Note that the influences of ENSO and the QBO on activity in the ENP are somewhat different, and in some cases inverse (Landsea et al. 1998), to those found in the North Atlantic basin by Gray (1984) and Shapiro (1989).

NOAA's National Hurricane Center has identified above-normal tropical cyclone activity during El Niño years in the ENP basin, while seasons with ENSO-neutral conditions tend to have less activity, and seasons with the lowest activity are typically associated with La Niña years. However, using tropical cyclone data from 1963 to 1993, Whitney and Hobgood (1997), found that there was very little difference in the frequencies, maximum intensities, or relative intensities of tropical cyclones over the ENP basin between El Niño and non-El Niño years. It is important to note that this result was possibly due to the timing difference in the ENP between the maximum frequency of hurricanes in September each year, and the peak in the above-average SST anomalies associated with El Niño events during the Northern Hemisphere winter. For example, in 2004 a weak El Niño developed in the central equatorial Pacific region during July–October, but SSTs remained near average or below normal in the ENP during this formative phase of the warm event (not shown).

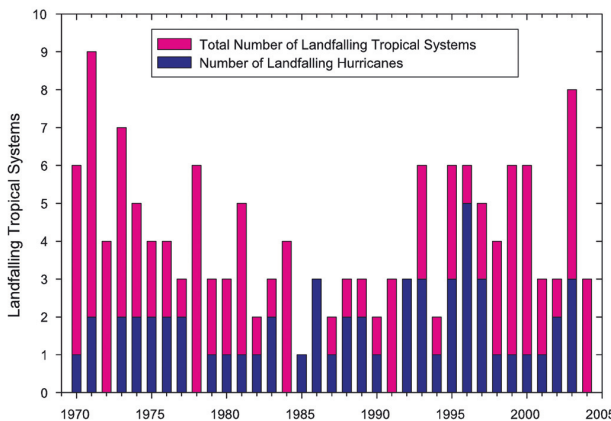


FIG. 4.16. The annual number of landfalling tropical cyclones (tropical depressions, tropical storms, and hurricanes) and hurricanes along the Pacific, Gulf of Mexico, and Caribbean coasts of Mexico over the period of 1970–2004 (data courtesy of the Meteorológico Servicio Nacional, SMN-Mexico).

It is also important to note that ENP tropical cyclones tend to attain a higher intensity when the QBO is in its westerly phase at 30 hPa in the tropical lower stratosphere, but there also appears to be a slight decrease in the observed seasonal frequency as well (Whitney and Hobgood 1997). During the latter half of 2003, the QBO switched from an easterly to a westerly phase at both 50 and 30 hPa, and the phase remained westerly in the lower stratosphere throughout the 2004 hurricane season. Therefore, it is possible that the development of three major hurricanes in 2004 in the ENP basin, as opposed to none in 2003, was affected by enhanced upper-level outflow due to the presence of the westerly phase of the QBO. The below-average frequency in 2004 (i.e., number of NSs, Hs, and MHs) also support the proposed physical link with the QBO's westerly phase. In contrast to the QBO, near- and above-normal vertical wind shear anomalies in the midtroposphere (850–200 hPa) were observed during August and September 2004, in the basin's primary development region in the ENP, west of the Pacific coast of Mexico (see Fig. 4.8). The presence of increased vertical shear in the midtroposphere would inhibit tropical cyclone development and intensification, and was likely another factor in the below-normal activity observed in 2004.

iii) SOUTH PACIFIC AND AUSTRALIA REGION TROPICAL CYCLONES—D. H. Levinson¹⁹ and M. J. Salinger³⁶

The tropical cyclone season in the South Pacific–Australia region typically extends over the period from November through April, with peak activity from December through March corresponding with the austral summer and early autumn. During the 2004 part of the season, there were nine NSs (sustained winds ≥ 34 kt) in the region as a whole (i.e., all areas south of the equator and east of 110°E in the South Indian and South Pacific basins). Of these, four attained cyclone status (CYC; winds ≥ 64 kt) and three reached major cyclone status (MCYC; winds ≥ 95 kt, category 3 or higher on the Saffir–Simpson scale). Four of these systems developed in the South Pacific basin, while five formed along the northern and northwestern coasts of Australia.

(i) South Pacific region tropical cyclones

Figure 4.17 shows the seasonal frequency of tropical cyclones in the South Pacific basin from 1974 to 1975 through the 2003–04 season. A total of four tropical cyclones formed in the South Pacific Ocean during the January through April period (Heta, Ivy, Grace, and 22P), of which Heta and Ivy were classified as major cyclones.

The most destructive of these was MCYC Heta, which devastated Niue on 6 January, and also affected Samoa and Tonga. Heta formed north of Fiji on 28 December 2003, developed into a tropical cyclone on 2 January, and passed west of Samoa on 5 January where strong winds (gusts of 145–160 km h⁻¹; 78–86 kt) and heavy rainfall resulted in extensive damage to property, crops, roads, and bridges. Heta intensified further to a category 5 system (i.e., a super cyclone) as its center passed just west of Niue on 6 January, with estimated wind gusts on the island of 275 km h⁻¹ (~148 kt). According to reports, the capital, Alofi, bore the brunt of the cyclone with half of the commercial area wiped out, while much of the damage to the southern area of Aliluki was from storm surge and high surf. There were two confirmed fatalities, with several others injured, and many people were left homeless. A national disaster resulted from Heta's impacts in Niue, with considerable property damage, closed roads, telecommunications and electrical outages, and severely damaged crops and vegetation.

The other major cyclone in 2004, Ivy, formed west of Fiji on 22 February, bringing damaging winds up to 130 km h⁻¹ (~70 kt) and heavy rainfall to parts of Vanuatu on 25–26 February. In addition, TS Grace originated in the Coral Sea west of New Caledonia on 19 March, but winds only reached gale force and it was rather short lived. However, strong winds and heavy, but not excessive, rainfall affected parts of New Caledonia.

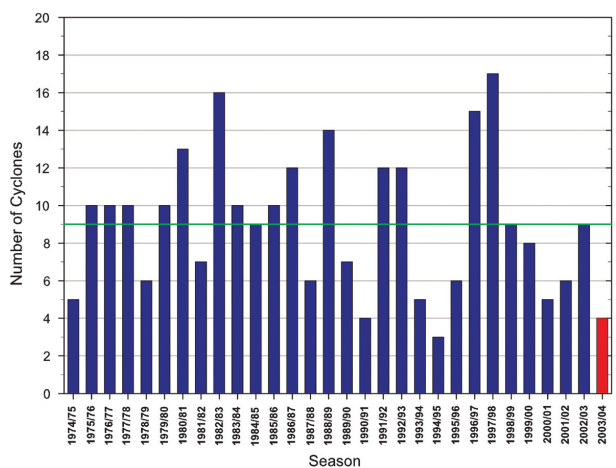


FIG. 4.17. The number of South Pacific tropical cyclones for the 2003–04 season (solid red bar) compared to seasonal frequencies during the past 30 yr (note: all four of the tropical cyclones in the 2003–04 season occurred between Jan and Apr 2004). The horizontal green line indicates the 30-yr average.

(ii) *Australia region tropical cyclones*

In the Australian region, five NSs formed over the period January to April 2004 (Ken, Fritz, Monty, Evan, and Fay). Of these, Monty developed into a cyclone and Fay intensified into a major cyclone during their life cycles.

Four of the five named storms made landfall in western and northern Australia in 2004, with only TS Ken dissipating over the South Indian Ocean west of the North West Cape. CYC Monty made landfall near Mardie in Western Australia with winds of approximately 154 km h^{-1} ($\sim 83 \text{ kt}$; category 2 on the Saffir–Simpson scale) and a maximum gust of 169 km h^{-1} ($\sim 91 \text{ kt}$) on 1 March (Fig. 4.18). The strongest tropical cyclone of the season was MCYC Fay, which formed in the Timor Sea on 16 March and drifted westward, reaching category 4 strength on 21 March with sustained winds of 222 km h^{-1} ($\sim 120 \text{ kt}$) and gusts of 269 km h^{-1} ($\sim 145 \text{ kt}$). However, the Australian Bureau of Meteorology (BoM) estimated gusts of 300 km h^{-1} ($\sim 169 \text{ kt}$) at Fay’s maximum intensity, $\sim 280 \text{ km}$ north-northwest of Cape Leveque. MCYC Fay made landfall along the Pilbara coast between Pardoo and Wallal, Western Australia on 27 March with maximum sustained winds near 175 km h^{-1} ($\sim 95 \text{ kt}$; category 2) and estimated wind gusts of 235 km h^{-1} ($\sim 127 \text{ kt}$). Two weaker systems, TS Evan and TS Fritz, made landfall in the Gulf of Carpentaria region at tropical storm strength, and produced locally heavy rainfall.

(iii) *Comparison with climatology*

Despite the fact that these are two separate regions with distinct areas of cyclogenesis (i.e., the South Pacific basin and the eastern section of the South Indian Ocean), the World Meteorological Organization

(WMO) categorizes the tropical cyclones in these two separate basins as one larger region. Reliable statistics for tropical cyclones in the Australian region extend further back in time. Historical records in Australia go back to the late 1700s, but these obviously have severe limitations (Lourensz 1981). As with most other regions, the introduction of routine satellite coverage in the late 1960s in Australia brought a significant increase in the quality of the tropical cyclone records, especially for accurate position and intensity observations (Holland 1981). The BoM officially uses the 1969–70 season as the beginning of their climatological statistics. Accurate track information is more limited in length for tropical cyclones in the South Pacific, which is why New Zealand’s National Institute of Water and Atmospheric Research (NIWA) uses the 1974–75 season for the start of their seasonal statistics. Therefore, 1975 was used as the beginning

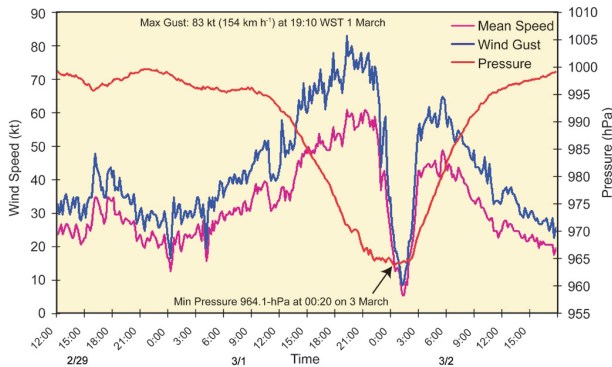


FIG. 4.18. Measurements of surface pressure (hPa), wind speed (kt), and wind gust (kt) during the passage of Cyclone Monty at Mardie station in Western Australia, over the period of 29 Feb to 2 Mar 2004.

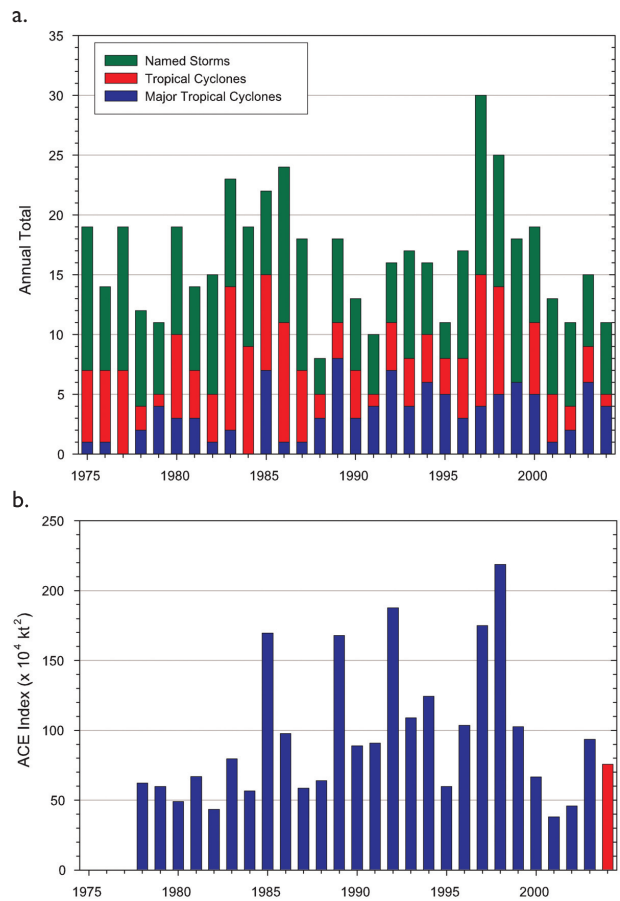


FIG. 4.19. Annual tropical cyclone statistics for the combined South Pacific and Australian basins over the period of 1975–2004: (a) number of tropical storms, cyclones and major cyclones, and (b) the estimated annual ACE Index (in $\text{kt}^2 \times 10^4$; Bell et al. 2000). Note that the ACE Index is estimated due to a lack of consistent 6-h-sustained winds for every storm.

of the combined, regionwide tropical cyclone statistics presented herein.

As shown in Fig. 4.17, four named storms developed during the 2003–04 season (all four in calendar year 2004), which was well below the 30-yr mean of nine NSs and the second lowest number over the period of record. The annual statistics of the combined South Pacific–Australian basin tropical cyclones are shown in Fig. 4.19. The total number of NSs and CYCs (Fig. 4.19a), as well as the estimated annual ACE Index (Fig. 4.19b), have declined in recent years, at least relative to the extremely active years of 1997 and 1998, which had the record number of named storms and the highest ACE Index since 1978 (note: incomplete 6-h sustained wind data in the region prior to 1978 prevented the accurate determination of basinwide ACE Index values).

According to the latest Intergovernmental Panel on Climate Change (IPCC) report (2001), there has been no discernible trend in the annual number of tropical cyclones in the South Pacific and Australian region over the period of reliable data. In contrast to this assessment, tropical cyclone activity in the Australian part of the region (105°–160°E) has declined somewhat over the past decade, according to the official climatology (Australian Bureau of Meteorology 2005). However, this may be partly due to improved analysis and discrimination of weak cyclones that previously were estimated at minimum tropical storm strength. It should also be noted that the period of reliable tropical cyclone data is too short to associate any trends in activity with climate change. However, increased cyclone activity in the Australian region has been associated with La Niña years, while below-normal activity has occurred during El Niño years (McBride 2004; Kuleshov 2003; Kuleshov and de Hoedt 2003). This appears to contrast with the South Pacific part of the region where the opposite signal has been observed, and the most active years have been associated with El Niño events (Fig. 4.17), especially during the strong 1982–83 and 1997–98 El Niños.

IV) INDIAN OCEAN TROPICAL CYCLONES—K. L. Gleason¹⁹

(i) North Indian Ocean

The North Indian Ocean (NIO) tropical cyclone season extends from May to December, with two peaks in activity during May–June and November when the monsoon trough is climatologically positioned over tropical waters in the basin. Tropical cyclones in the NIO basin develop in the Bay of Bengal and the Arabian Sea typically between latitudes of 8°N and 15°N, and are usually short lived

and weak, quickly moving into the subcontinent. However, strong and “severe cyclonic storms,” as illustrated by Neumann et al. (1993), can periodically develop with winds greater than 130 kt. In fact, perhaps the greatest human fatality toll on record due to a tropical cyclone hails from the Bangladesh supercyclone of 1970, where at least 300,000 people died, primarily from the associated storm surge in the low-lying deltas (Holland 1993). According to the Met Office,^{4,5} the NIO is the only area in the world where tropical cyclones are not given names. However, the Joint Typhoon Warning Center (JTWC) in Hawaii provides identifiers for all tropical cyclones in the Indian Ocean (North and South), the South Pacific, and the west North Pacific basins.

Using reliable records from 1981 to 2004, a mean of 4.8 NSs (sustained winds ≥ 34 kt), 1.7 CYCs (sustained winds ≥ 64 kt), and less than one MCYC (sustained winds ≥ 95 kt) form each year in the NIO. The 2004 tropical cyclone season was near normal with one CYC and five NSs forming from May to November (Fig. 4.20a). The estimated ACE Index for the NIO basin in 2004 was approximately 13×10^4 kt², which was slightly below the 1981–2004 mean of 17×10^4 kt² (Fig. 4.20b).

The most intense cyclone during the NIO tropical cyclone season, Agni, developed just west of the Maldives in the Arabian Sea during late November. CYC Agni tracked to the northwest and became a category 1 cyclone for 2 days in November, with sustained winds of 65 kt. Agni weakened to tropical storm strength and maintained this intensity for the first 4 days of December, before dissipating completely near the coast of Somalia.

Two of the four NIO TSs in 2004 made landfall. Tropical storm 03A formed in early October in the Arabian Sea and came ashore in the Kutch region of India near the Pakistan–India border, bringing heavy rains and a peak wind intensity of 40 kt. Tropical storm 02B formed in the Bay of Bengal in mid-May and made landfall on the northern coast of Myanmar with sustained winds of 60 kt. Two additional tropical storms (01A, 04A) developed in the Arabian Sea, but did not affect land (for additional information on the Indian Monsoon and its impacts, see section 6fiv).

(ii) South Indian Ocean

The tropical cyclone season in the SIO is normally active from December through April (note, in this

^{4,5} Information online at the Met Office Web site: www.metoffice.gov.uk/sec2/sec2cyclone/tcbulletins/05b.html.

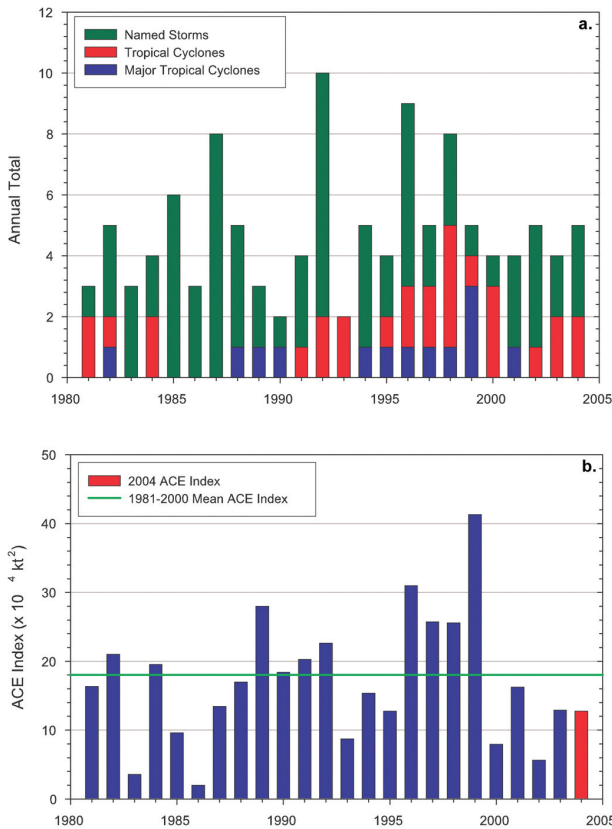


FIG. 4.20. Annual tropical cyclone statistics for the North Indian Ocean over the period of 1981–2004: (a) number of tropical storms, cyclones, and supercyclones, and (b) the estimated annual ACE Index (in $kt^2 \times 10^4$) for all tropical cyclones during which they were at least tropical storm or greater intensities (Bell et al. 2000). Note that the ACE Index is estimated due to a lack of consistent 6-h-sustained winds for every storm.

section, the SIO tropical cyclone data are summarized by calendar year, rather than by season). The South Indian Ocean tropical cyclone basin extends from the African coastline to 110°E and from the equator southward, although most cyclones develop south of 10°S latitude (tropical cyclones that form in the SIO east of 110°E are included in the Australian summary, see section 4b11). The vast majority of SIO landfalling cyclones impact Madagascar, Mozambique, and the Mascarene Islands, including Mauritius. Due to a lack of historical record keeping by individual countries, and no centralized monitoring agency, the SIO is probably the least understood of all tropical cyclone basins (Atkinson 1971; Neumann et al. 1993).

Using reliable data from 1981 to 2004, the SIO averages 14 NSs, nearly 8 CYCs, and approximately 4 MCYCs each year. In 2004, the SIO tropical cyclone occurrences were slightly above average, with 15 NSs, 10 CYCs, and 5 MCYCs (Fig. 4.21a). The estimated

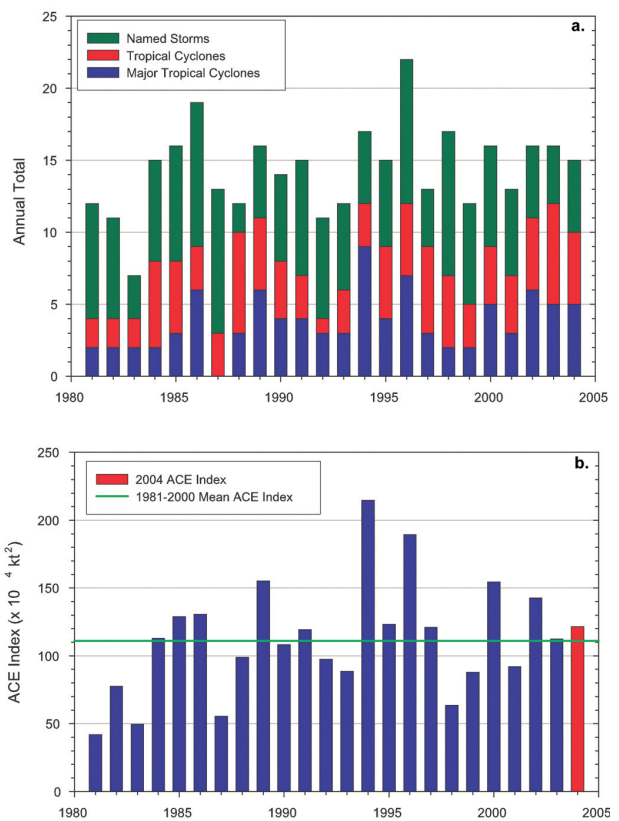


FIG. 4.21. Same as in Fig. 4.20, but for tropical cyclones in the South Indian Ocean.

ACE Index for the SIO during 2004 was almost $110 \times 10^4 kt^2$ (Fig. 4.21b), which is near the 1981–2004 average of $112 \times 10^4 kt^2$. In fact, the estimated ACE Index for four of the last five years has been close to or above average. During 2004, the strongest tropical cyclones in the SIO, and the largest contributors to the annual ACE Index value, were cyclones Gafilo and Bento, both with sustained winds of 140 kt at their peak intensities.

Madagascar was struck by the only two landfalling tropical cyclones in the SIO basin during 2004. Elita formed in late January in the Mozambique Channel and struck Morondava, Madagascar, as a weak category 1 storm with peak sustained winds of 65 kt. CYC Elita traveled quickly across the island, which minimized flooding, and proceeded out to sea where the cyclone dissipated in early February. Gafilo developed in the SIO northeast of the Mascarene Islands early in March and proceeded westward. Within 3 days, Gafilo intensified into a category 5 cyclone (a supercyclone; sustained winds ≥ 135 kt) and impacted northern Madagascar on 7 March. Supercyclone Gafilo made landfall near Antalaha, Madagascar, at category 5 intensity, which destroyed most structures

in the region. Extensive flooding was also prevalent throughout northern Madagascar as a result of the intense rainfall and storm surge. Gafilo moved westward across the island and into the Mozambique Channel before turning south and making landfall a second time in the southwest part of Madagascar as a tropical storm. According to local reports, Gafilo was one of the strongest cyclones to hit Madagascar in the last 50 yr.

5. POLAR CLIMATE

a. Arctic

i) TEMPERATURE—A. M. Waple⁹

Analysis using NCDC's GHCN extended reconstructed SST (ERSST) combined dataset of surface temperature observations (Smith and Reynolds 2005); land surface temperatures north of 60°N for 2004 were the 21st warmest year since 1900 in the Arctic region, and followed the record warm year of 2003 (Fig. 5.1). Annual temperatures were especially warm over Alaska and Greenland, with negative temperature anomalies over much of the Canadian Arctic and east-central Siberia (Fig. 2.3).

Seasonal temperature extremes were especially notable for north-central Siberia and the Canadian Archipelago in spring (March–May; Fig. 7.3), with negative anomalies of more than 2°C west of Hudson Bay, while above-average temperatures were present in western Alaska and eastern Russia. The pattern of temperature anomalies in the summer (Fig. 7.5) was similar to spring, but with more extensive cold anomalies in North America, and with larger positive anomalies in western Alaska (> 3°C) that were accompanied by much drier-than-average conditions. These anomalously warm and dry conditions contributed to a record-breaking wildfire season in the state [see section 6a(ii)(iv)(b)]. Summer temperatures for Alaska were also the warmest since reliable statewide records began in 1918 (see Fig. 6.9). September–November temperatures (Fig. 7.7) reflected a diminished area of negative anomalies across northern Canada and north-central Siberia, with above-average temperatures in central and northern Russia, while warmth persisted for Alaska and Scandinavia.

According to the Arctic Climate Impact Assessment (ACIA), released in 2004, temperatures across many Arctic regions have warmed at almost twice the rate of global temperatures over the past few decades (see section 2a), and consequences of this warming are likely to be experienced worldwide (ACIA 2004). Annual warming trends across land and ocean surfaces from 65° to 85°N since 1880 (from NCDC's GHCN ERSST dataset; Smith and Reynolds

2005) have increased markedly over the last several decades. Since 1880, the Arctic region has warmed at a rate of 0.05°C decade⁻¹; however, since 1979 (the period over which we can compare in situ data to satellite observations), the rate is 0.32°C decade⁻¹. Satellite-based observations since 1979 reveal a 0.38°C decade⁻¹ warming trend (see section 2b). The slightly larger trend in satellite data is reasonable, based on limited in situ stations north of around 70°N, whereas satellites can measure temperature across a greater expanse of the Arctic region. Even more notable warming has occurred since the early 1990s in both the satellite and in situ station measurements.

ii) SEA ICE—R. S. Stone,³⁷ D. C. Douglas,¹³ G. I. Belchansky,³ and S. D. Drobot¹⁴

Recent decreases in snow and sea ice cover in the high northern latitudes are among the most notable indicators of climate change. Northern Hemisphere sea ice extent for the year as a whole was the third lowest on record dating back to 1973, behind 1995 (lowest) and 1990 (second lowest; Hadley Center–NCEP). September sea ice extent, which is at the end of the summer melt season and is typically the month with the lowest sea ice extent of the year, has decreased by about 19% since the late 1970s (Fig. 5.2), with a record minimum observed in 2002 (Serreze et al. 2003). A record low extent also occurred in spring (Chapman 2005, personal communication), and 2004 marked the third consecutive year of anomalously extreme sea ice retreat in the Arctic (Stroeve et al. 2005). Some model simulations indicate that ice-free summers will occur in the Arctic by the year 2070 (ACIA 2004).

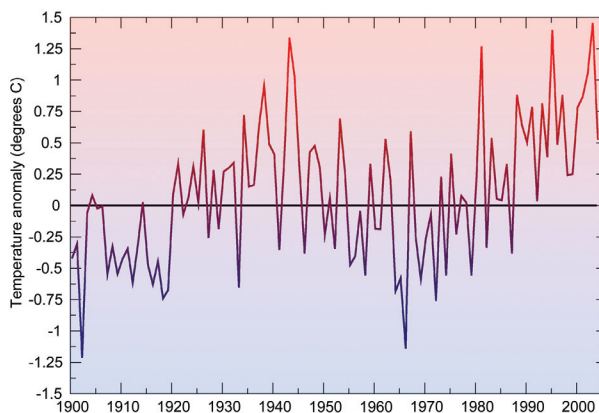


FIG. 5.1. Annual temperature anomalies (in °C) for land areas north of 60°N over the period of 1900–2004 from the NOAA/NCDC GHCN ERSST blended dataset of surface temperature observations (Smith and Reynolds 2005). Anomalies were determined with respect to the 1961–90 base period means.

Following the 1989 positive shift in the Arctic Oscillation (AO) index (Thompson and Wallace 1998), significant declines in multiyear ice (MYI) occurred in the region of the Chukchi–Beaufort Seas (Belchansky et al. 2004a). Since 1979, MYI has decreased by more than 60% in the western Arctic (Fig. 5.3). The most pronounced decline began in 1989 in the east Siberian region, followed a few years later in the Beaufort–Chukchi region. After rebounding in 1997, the downward trend resumed. These dramatic declines in the western Arctic dominate the trend for the entire basin.

Both dynamic and thermodynamic processes have contributed to decreases in sea ice concentration and overall thinning of the Arctic ice pack (Rothrock and Zhang 2005). Drobot and Maslanik (2003) hypothesized that during positive AO index winters, the Beaufort gyre (a large region of converging ice) weakens, favoring transport of MYI along the transpolar drift stream rather than recirculating it within the Beaufort Sea. Rigor and Wallace (2004) further demonstrated that during positive phases of the AO, a weakened Beaufort gyre tends to entrain younger, thinner ice that is more vulnerable to summer melt. In recent years, during which the AO index has been neutral or negative, there have been further declines in ice volume, especially in the western Arctic, which suggests that factors other than the phase of the AO influenced the observed declines in sea ice.

One plausible explanation relates to anomalous atmospheric circulation patterns that have occurred in the western Arctic in recent years. To illustrate, analyses are presented for contrasting years of relatively extreme ice retreat. Figure 5.4 compares average environmental conditions for 4 yr of large ice

retreat (1998, 2002–04) with a period during which ice retreat was minimal (1985–88). Mean fields of 850-hPa geopotential heights represent synoptic patterns for spring, a critical transition period in the annual cycles of snow and sea ice (Stone et al. 2005). Figure 5.4a illustrates typical climatological conditions during March, April, and May in the western Arctic. A well-defined high pressure system north of Alaska, referred to as the Beaufort Sea anticyclone (BSA), is coupled with the Aleutian low (AL). The BSA effectively blocks Pacific air from flowing into the Arctic basin, keeping northern regions cold and relatively dry. Also, the persistence of the BSA maintains the Beaufort gyre, which forces recirculation and convergence of ice in this region.

Climatologically, in late May, the North Slope of Alaska and eastern Siberia remain snow covered, as indicated by Normalized Difference Vegetation Index (NDVI) imagery (Fig. 5.4a). Melt onset over sea ice typically does not commence until the first week in June north of Alaska, and not until late June north of Siberia, as indicated by the passive microwave analysis. During these years of late snowmelt and late onset of melting over sea ice, the pack does not retreat very far north of the coastlines in September.

In contrast, Fig. 5.4b shows the composites of four recent years in which minimal ice extents have been observed. During spring of these years, the BSA was poorly defined. Instead, a ridge of high pressure persisted over eastern Alaska and the AL shifted westward—a pattern that favors the intrusion of warm, Pacific air into the Arctic basin (Stone et al. 2002). This synoptic pattern was corroborated using wind fields computed from the National Centers for Environmental Prediction (NCEP)–National Center for Atmospheric Research (NCAR) reanalyses

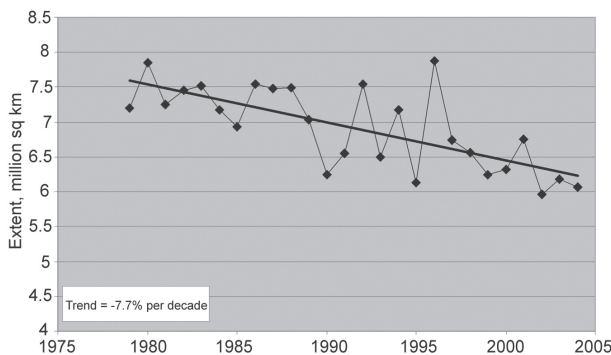


FIG. 5.2. Time series and linear trend in Sep Arctic sea ice extent, 1979–2004. The calculation was made for areas having > 15% ice concentration. The regression yielded a $7.7\% \pm 3.0\%$ decrease decade⁻¹ at a 99% confidence interval (courtesy of J. Stroeve, NSIDC; Stroeve et al. 2005).

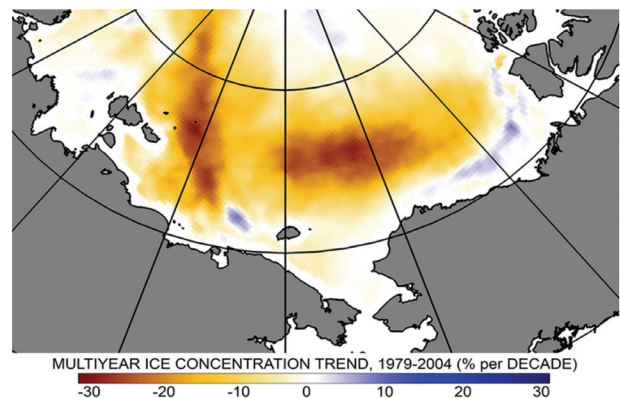


FIG. 5.3. The 26-yr (1979–2004) linear trend in Jan MYI concentrations within the western Arctic (updated from Belchansky et al. 2004a).

(not shown). This warm, southerly flow accelerates snowmelt over Alaska and eastern Siberia, and ice melt in the Bering Sea and Sea of Okhotsk. By late May, Pacific air warmed further as it advected over high-latitude tundra that was continuously exposed to intense solar radiation, which lead to an early onset of melt. Therefore, an early and prolonged melt season amplifies late summer sea ice retreat, especially in the western Arctic where the ice pack has become younger and thinner (Rigor and Wallace 2004).

III) GREENLAND—J. E. Box⁷

Coastal station temperature records around Greenland indicate warming trends since the early 1980s that are large in the context of longer-term records (1873–2004). This recent warming has brought once anomalously cold Greenland regional temperatures in phase with the global warming pattern. Considering the last 55-yr period (1950–2004) when data are available from a collection of stations around the circumference of the ice sheet, the years of 2003 and 2004 were among the warmest, and were possibly the warmest, years on record (Table 5.1). The 1930s and 1940s also represent an exceptionally warm period in the long-term record. However, since 1895 at Tasiilaq (Nuuk), 2003 was the warmest (warmest) and 2004

the 9th warmest (20th warmest) of this 110-yr record. Therefore, regional variability in warming over the annual time frame is apparently large. Despite this variability, these recent increases in temperature are coherent among the entire collection of more than 15 Greenland climate stations. The observed warming has certainly contributed to increased rates of melting, and placed the Greenland ice sheet as a significant contributor to global sea level rise (Box et al. 2004).

Seasonally, the majority of warming has been observed during the winter and spring. Summer and autumn trends have been smaller, owing to the

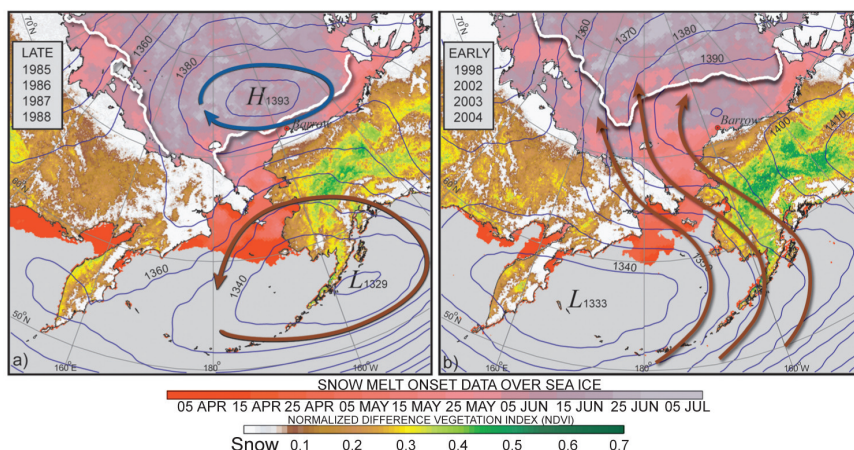


Fig. 5.4. Environmental conditions over the western Arctic averaged for years with (a) minimum and (b) maximum sea ice retreat. The extent of late summer ice retreat, defined as the southern limit of >50% mean ice concentration during 16–30 September, is shown as a bold white line. Thin blue lines depict 10-m contours of mean Mar–May 850-hPa geopotential heights from the NCEP–NCAR 40-yr reanalysis project. Generalized circulation patterns are shown with bold vectors. Mean melt onset dates over sea ice (Belchansky et al. 2004b) are color shaded for areas where ice concentrations averaged > 50% during the period 16–31 May. Vegetation greenness is depicted during 16–31 May by the mean maximum NDVI [derived from Global Inventory Modelling and Mapping Studies (GIMMS) NDVI-d and NDVI-n16 datasets].

TABLE 5.1. The observed ranking of 2004 and 2003 as anomalously warm years around Greenland for stations over the 1950–2004 period.

Station	Latitude, longitude	Region	Year and ranking as warmest
Prins Christian Sund	60.0°N, 43.2°W	South	2004 (1), 2003 (2)
Egedesminde	68.7°N, 52.8°W	Central west	2004 (2), 2003 (1)
Tasiilaq	65.6°N, 37.6°W	Southeast	2004 (2), 2003 (1)
Nuuk	64.2°N, 51.8°W	Southwest	2004 (5), 2003 (7)
Danmarkshavn	76.8°N, 18.7°W	Northeast	2004 (9), 2003 (3)

suppression of positive trends from latent heat sinks during snow- and ice-melt periods. Nonetheless, winter warming trends affect the intensity of summer melting owing to changes in the cold content of seasonal snow, which must be melted off before ablation of underlying ice takes place.

The Polar version of the fifth generation Pennsylvania State University (PSU)–NCAR Mesoscale Model (MM5) (Bromwich et al. 2001; Cassano et al. 2001), run in data assimilation mode, provides climate information for the ice-covered interior of Greenland over a longer time period and with a broader spatial coverage than that available from automated weather stations. Annual reconstructions of 2-m air temperature are compared within 1-K root-mean-square error (rmse) of observations from an independent network of automatic weather stations on the inland ice (Steffen and Box 2001). Therefore, a 17-yr set (1988–2004) of Polar MM5 output provides a means for assessing ice sheet melt rates, meltwater discharge, and sea level contributions.

A trend of warming temperatures around Greenland that began in the early 1980s has continued through 2004. In terms of annual mean temperatures for the ice sheet as a whole, the warming in 2004 was the second highest, ranking behind only 1998.

Spatially, the warming signal has been concentrated along the western margin and the topographic divide of the ice sheet (Fig. 5.5a), where the maximum change in temperature exceeded 6 K. The annual mean anomalies in 2004 indicate that temperatures were up to 3.6 K above the 17-yr average, with no grid points over the ice sheet with a negative temperature anomaly for 2004. In concert with this warming was a widespread increase in the duration of melting (Fig. 5.5b). In light of the observations that demonstrate ice sheet dynamical flow increases when melt water is available to lubricate the bed (Zwally et al. 2002), the ice sheet flow rate likely continued to increase in 2004, and the ice sheet remains in a state of net mass loss with significant ($\sim 0.2 \text{ mm yr}^{-1}$) global, eustatic sea level contributions (Box et al. 2004).

b. Antarctic

i) SURFACE CLIMATE—A. M. Waple¹⁹ and E. Rignot³²

Surface air temperatures across the majority of stations on the Antarctic continent were above average in 2004, with the largest temperature trends over the last several decades measured along the Antarctic Peninsula (Fig. 5.6). The observed trends across the rest of the continent have been mixed, with interior stations such as Amundsen–Scott (South Pole) and Vostok showing small, insignificant trends in surface temperature. It is, perhaps, Antarctica’s apparent continent-wide temperature stability that is remarkable in the context of global warming. It is only the Antarctic Peninsula (4% of the continental area) that shows a significant warming trend. The peninsula is also the warmest area of the continent on average, rising above freezing for 2 months yr^{-1} on its warmest coast (BAS 2004). Due to the sparsity of stations on Antarctica, the lack of long-term stations, and the high interannual temperature variability, it is impossible to state with certainty, whether the Antarctic continent is warming or cooling overall.

Trends in sea ice in the Southern Hemisphere have generally increased since the late 1970s (Fig. 5.7), with above-average values of sea ice extent in 2004. However, the seasonal and spatial variability have been extreme in the Southern Hemisphere, with ice shelf and sea ice retreat occurring in

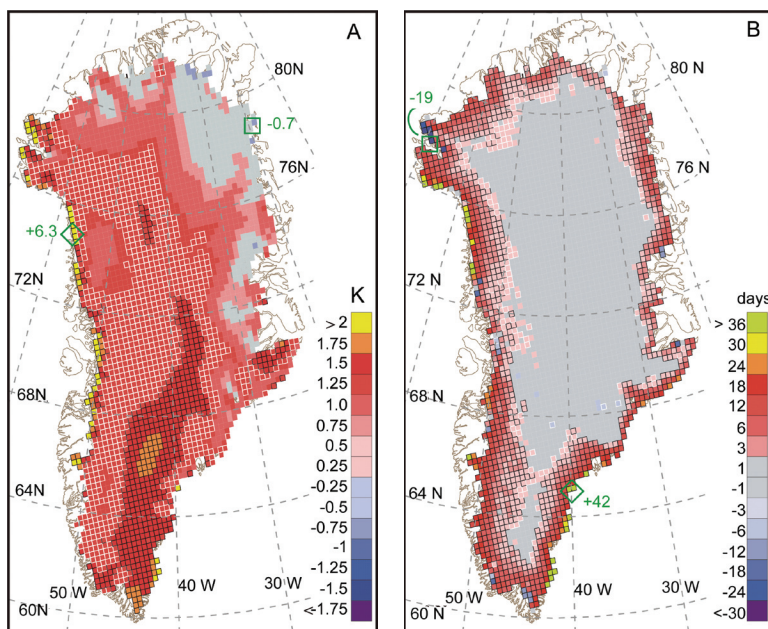


FIG. 5.5. The spatial pattern of change over the Greenland ice sheet (1988–2004) from the Polar MM5 data assimilation output: (a) annual temperature and (b) number of melt days. Student’s *t* test statistical significance above the 85% (95%) confidence interval is indicated by white (black) outlined grid cells, respectively. Locations of maximum and minimum trend values are indicated by green symbols.

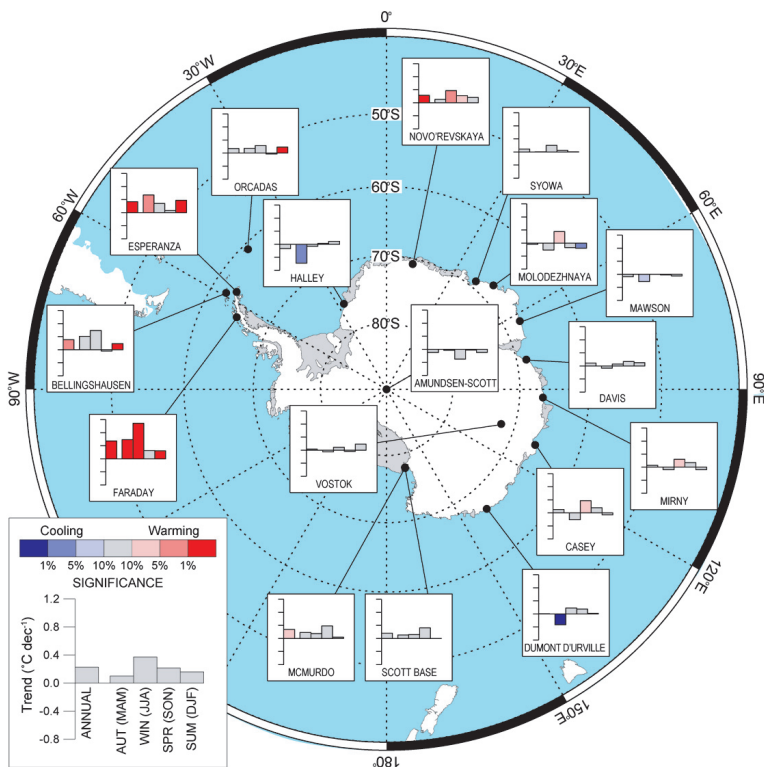


FIG. 5.6. Decadal temperature trends (°C) for selected Antarctic stations (courtesy of Gareth Marshall, British Antarctic Survey).

those areas that have shown a warming trend over the last 50 yr, such as around the Antarctic Peninsula and Bellingshausen Sea (i.e., Vaughan and Doake 1996). The collapse of the Larsen A ice shelf in 1995 in the Antarctic Peninsula, and Larsen B ice shelf in 2002, were both caused by pronounced regional warming. They also provided a unique opportunity to address the question of whether ice shelf removal leads to the acceleration of glaciers and ice sheet collapse, which, if it occurred, would lead to increasing freshwater melting into the ocean and, ultimately, to sea level rise.

Using radar interferometry observations from the European Space Agency (ESA) Remote Sensing Satellites (ERS) 1 and 2, and the Canadian Radarsat-1 satellite, it was found that the Antarctic Peninsula glaciers accelerated significantly in response to ice shelf collapse. Several glaciers accelerated up to 8 times following the collapse, while others in the vicinity that are still buttressed by an ice shelf did not accelerate. Glacier thinning was recorded at several tens of meters per year, and is still ongoing at present. The magnitude of these changes illustrates the fundamental importance of ice shelves on ice sheet mass balance. This evolution is relevant to an area far broader than the Antarctic Peninsula, extending to some of the

largest glaciers in Antarctica. Aircraft surveys, combined with satellite radar interferometry, showed that the Pine Island–Thwaites basin of west Antarctica is thinning rapidly, $\sim 1 \text{ m yr}^{-1}$. Ice shelf thinning rates are increasing with time, and the overall mass loss from this region alone is sufficient to raise the global sea level by $\sim 0.25 \text{ mm yr}^{-1}$. The favored interpretation of the evolution of this region is a weakening of its buttressing floating ice shelves by a warmer surrounding ocean, which, in turn, allowed the glaciers to accelerate. While some parts of west Antarctica are thickening at present, due to ice stream slow down independent of climate changes, the west Antarctic ice sheet as a whole is losing mass at present. The current evolution of the east Antarctic ice sheet is less well known, primarily due to uncertainties in the evolution of snow precipitation in its vast interior regions, and the need to complete the survey of its outlet glaciers.

ii) STRATOSPHERIC OZONE—
R. C. SCHNELL³⁷

Figures 5.8a–d show the development of the 2004 ozone hole over the South Pole station from balloon-borne ozonesonde measurements. The total column ozone showed a typical decline during September,

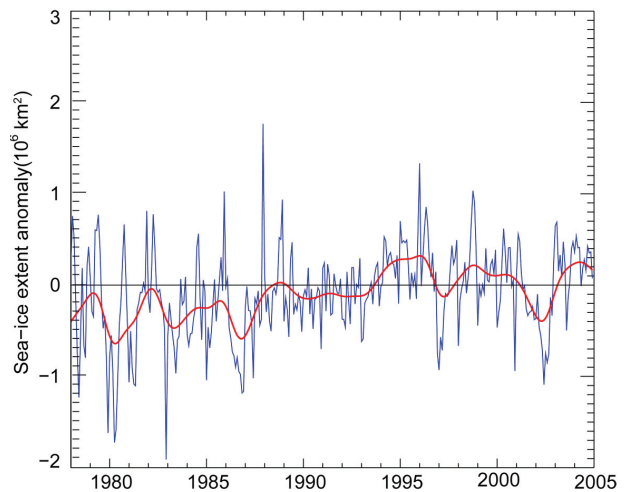


FIG. 5.7. Monthly sea ice extent anomalies ($\text{km}^2 \times 10^6$) for the Southern Hemisphere over the period of 1978–2004 (courtesy of NCEP/Hadley Centre).

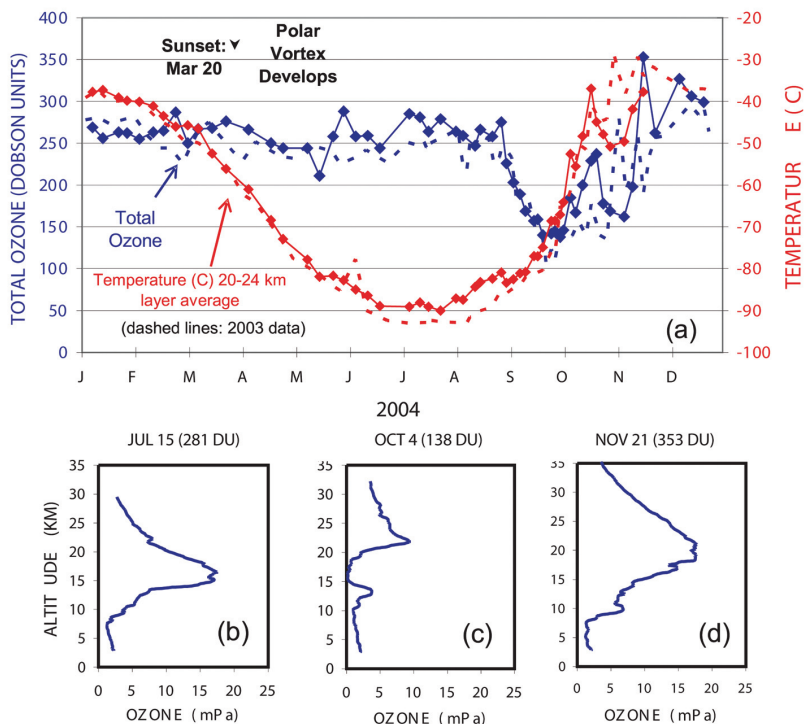


FIG. 5.8. (a) Summary of South Pole total ozone (DU) and stratospheric temperatures measured by ozonesondes during 2004. Three selected profiles of altitude vs ozone partial pressure (mPa) are shown in the lower panels: (b) 15 Jul prior to the 2004 ozone hole, (c) 4 Oct minimum total ozone, and (d) 21 Nov post-ozone hole (courtesy of B. Johnson and S. Oltmans, NOAA/CMDL).

nearly identical to 2003. However, the minimum ozone concentration of 138 DU, measured on 4 October, was above the 1986–2004 average minimum of 117 ± 26 DU. Years with less expansive Antarctic ozone holes are closely correlated with warmer stratospheric temperatures over the continent, partly due to less favorable conditions for the formation of polar stratospheric clouds (PSCs). PSC surfaces enable the transformation of chlorine and bromine compounds into species that destroy ozone when sunlight returns to the Antarctic stratosphere.

The 20–24-km average temperatures in 2004 were relatively warm (Fig. 5.8a), never falling below 183 K (-90°C) during the coldest month (July) when temperatures are typically about 179–181 K. Stratospheric temperatures remained about 2–4 K above average throughout September. By the end of the month, ozone

was nearly completely depleted in the 15–19-km layer (Fig. 5.9c), but high levels of ozone in the 22–25-km layer indicated that the upper-altitude layers of the polar vortex had already begun to show signs of weakening. This was consistent with the WMO’s ozone bulletins, which noted that the circumpolar vortex had begun to change in character due to strong stratospheric wave activity in mid-September, and fewer PSCs were observed. Analysis of NOAA-16 and NOAA-17 data showed the ozone hole reached a maximum size of 19.5 million km^2 twice, on 16 and 22 September (not shown). Ozone hole conditions (< 220 DU) remained over the South Pole until a rapid increase to 353 DU was observed on 21 November 2004 (Fig. 5.8d).

6. REGIONAL CLIMATE

a. North America

i) CANADA—C. Kocot,²² D. Phillips,²² and R. Whitewood²²

(i) Temperature

The average national temperature measured across Canada in 2004 was 0.1°C above normal (with respect to 1951–80 base period mean), and marked the 12th consecutive year of at-

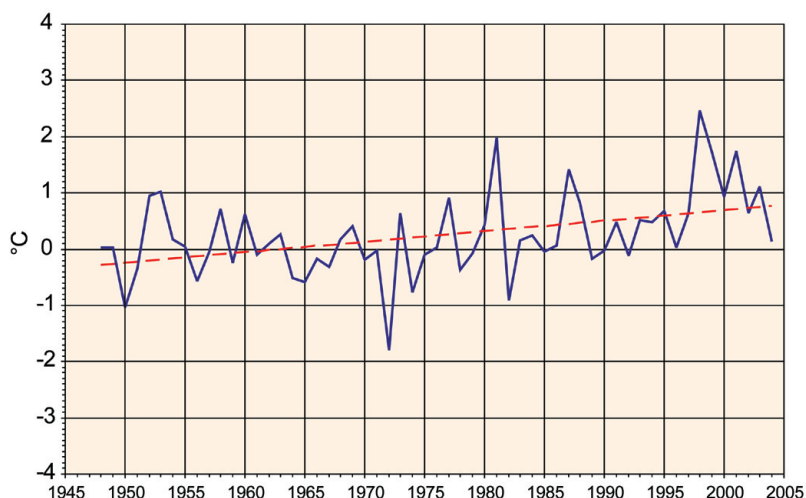


FIG. 6.1. Canadian nationwide annual temperature departures ($^{\circ}\text{C}$, blue line) and long-term temperature trend (red line) for the period of 1948–2004. Departures were determined with respect to the 1951–80 base period, and a linear trend of 1.1°C was determined over the period of record.

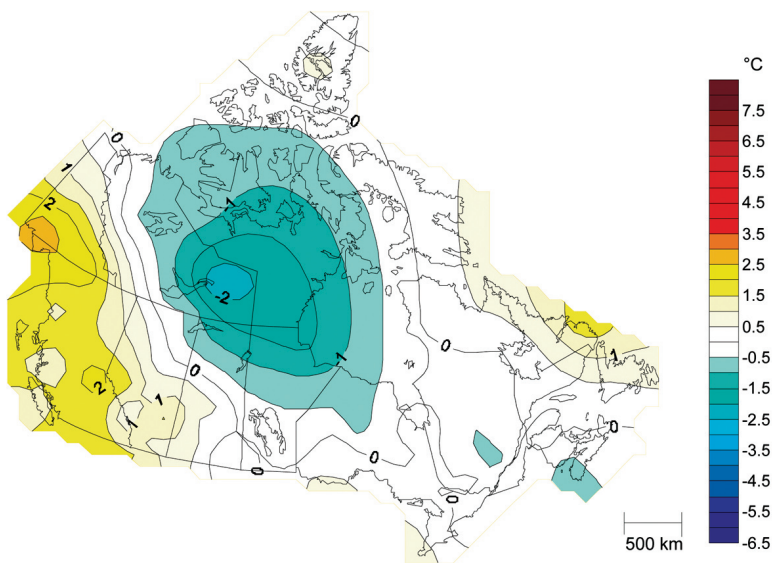


FIG. 6.2. Annual temperature departures from normal (°C) across Canada in 2004. Temperature departures were determined with respect to the 1951–80 base period.

or above-normal nationwide temperatures (Fig. 6.1). Overall, 2004 ranked as the 28th warmest (or 30th coolest) year since nationwide records began in 1948. From a spatial perspective, the warmer-than-normal west and east coasts contrasted with the cooler-than-normal north-central parts of the country (Fig. 6.2). Temperatures in northern Manitoba, Saskatchewan, the eastern part of the Northwest Territories, and most of Nunavut were 1°C below normal in 2004, while departures of 2°C below normal were observed in the lower part of the Northwest Territories. In contrast, temperatures of 1°C or more above normal occurred in Newfoundland and Labrador, as well as from western Alberta westward, with departures of greater than 2°C in parts of British Columbia and southern Yukon. The remainder of the country, however, experienced very close to normal temperatures over the past year.

Three of the 11 climate regions delineated by Environment Canada (EC) had annual mean temperatures in 2004 that were among the 10 warmest on record (not shown). The warmest regions were in western Canada: the Pacific Coast region had its second warmest year (+1.5°C), while the south British Columbia mountains (+1.6°C) and the north

British Columbia mountains/Yukon (+2.2°C) regions both had their fourth warmest year. The coolest regions in 2004 were in the north-central parts of the country: the Mackenzie District (−0.7°C) and the Arctic Tundra (−0.5°C) regions both had their 12th coolest years on record. Of the 11 Canadian climate regions, only the Atlantic region (which is comprised of the provinces of New Brunswick, Nova Scotia, Prince Edward Island, and Newfoundland, excluding Labrador) has shown no increasing linear temperature trend over the 57-yr period of record (not shown). However, the Atlantic region did have a slight cooling trend from 1948 until the early 1990s, with temperatures warming since then. The north British Columbia mountains/Yukon region has had the largest observed increase

in temperatures; 2.0°C over the 1948–2004 period.

(ii) *Precipitation*

Nationally averaged precipitation was near normal in 2004, approximately 0.4% above the 1951–80 base period mean, which placed the year as the 33rd wettest (or the 25th driest) for the 57-yr record (not shown). The areas with precipitation accumulations greater than 20% above normal in 2004 were the

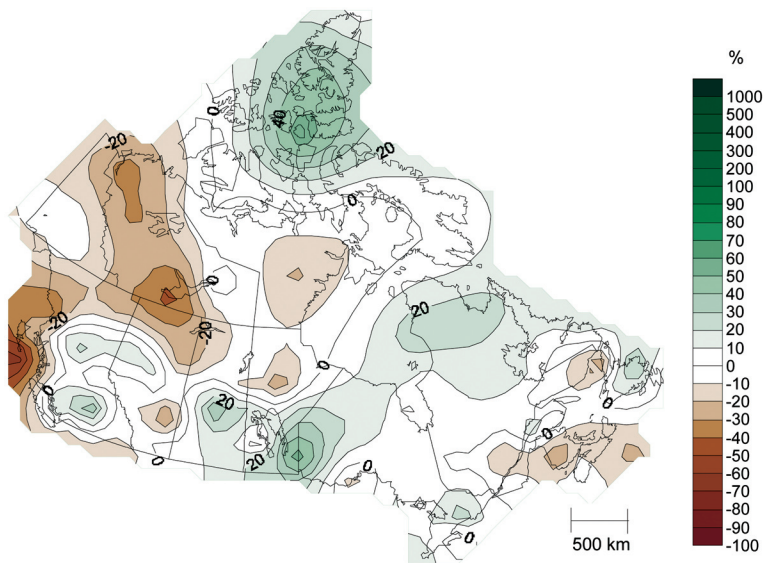


FIG. 6.3. Annual precipitation departures from normal (%) across Canada in 2004. Precipitation departures were determined with respect to the 1951–80 base period.

Arctic Islands, southern Manitoba, and northern Quebec, while the areas with precipitation amounts of at least 20% below normal were the west coast of British Columbia and most of the Northwest Territories (Fig. 6.3). The annual mean precipitation was close to normal over the remainder of the country.

On the regional scale, it was the driest year on record for the Mackenzie District in 2004, approximately 28.3% below normal, or 4.1% drier than 1995, which was the second driest year on record for the region. In addition, ranked among the 10 driest years were the Pacific Coast (fifth, -17.3%) and Atlantic Canada (seventh, -9.0%) regions. Only one region, the Northeast Forest (sixth, +7.3%), was ranked as one of 10 wettest years in 2004. The Arctic Tundra region was wetter than normal (32nd, +4.2%), and the last time this region had a drier-than-normal year was back in 1978 (40th driest, -1.7%).

(iii) *Significant events*

The sea ice extent in 2004 across Canadian Arctic waters remained well below the long-term average. In September, the month usually with the lowest average extent, sea ice was ~13% below the 1973–2003

average. The ice in the Canadian Beaufort Sea was much less extensive and thinner than normal. In fact, according to observations by the Canadian Coast Guard icebreaker *Louis S. Saint-Laurent* 500 km off the Yukon coast, only weak melting first-year ice was found where in the past there typically has been only thick, hard ice several years old. Much further south, in winter/spring, the Labrador coast had the least amount of sea ice since the beginning of records in 1969 (source: Canadian Ice Service). There was less than half the average amount of ice, due, in part, to above-normal air temperatures, as well as persistent onshore winds that prevented the sea ice from expanding eastward (for further details see section 5a11).

The Canadian International Forest Fire Centre (CIFFC) reported a below-average fire year across Canada in terms of the number of fires (6,328 by mid-September; ~83% of normal), but with slightly more hectares of forest burned (3.1 million ha; ~7.7 million ac), which was more than 10% above normal when compared with a recent 10-yr average. However, the east-to-west contrast in the 2004 wild-fire season was dramatic. A large area from Saskatch-

APRIL–JULY 2004: HOT IN ALASKA AND YUKON, COOL IN CENTRAL NORTH AMERICA—G. D. BELL⁴

Introduction

The period of April–July 2004 featured exceptionally warm and dry conditions over western North America, and below-normal temperatures across the eastern half of Canada and the central United States. For much of Alaska and western Canada, April–July mean tem-

peratures were 2°–5°C above average, making this one of the warmest such periods in the 1950–2004 record.

For Alaska as a whole, area-averaged temperature departures reached 1.8°C, exceeding the previous record departure of 1.5°C observed in 1993. In contrast, the April–July 2004 season

had below-average temperatures across central North America and the Midwest (Fig. 6.7b). The largest negative temperature departures were observed across central Canada (2°–3°C below normal), where many locations experienced their coldest April–July in the 1950–2004 record.

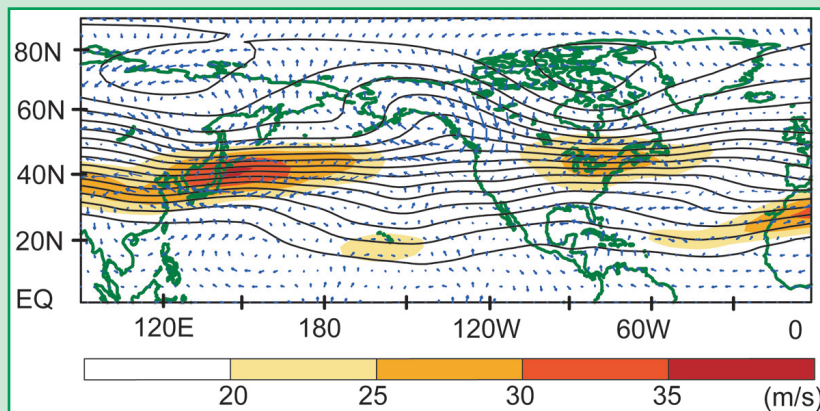


FIG. 6.4. Apr–Jul 2004 mean 200-hPa heights (contour interval is 60 m), wind speeds (shading, $m s^{-1}$) and vector winds.

Atmospheric circulation

The mean upper-level circulation over North America during April–July 2004 featured a persistent ridge over Alaska and northwestern Canada, an amplified trough over Hudson Bay, and above-average upper-tropospheric heights over the southwestern North Atlantic (Fig. 6.4). Each of these features remained nearly stationary, with the associated 500-hPa height anomalies evident during 65%–80% of the 4-month period (not shown). The warm and dry conditions from Alaska to southern California coincided with the anomalous upper-level ridge, while the cool conditions over central North

ewan to Quebec had little or no fire activity, while Ontario set a new record low for the number of fires across the province. Between April and October, the province recorded 426 fires—110 less than the previous lowest year in 1928. In contrast, across British Columbia, Alberta, and the Yukon Territory the fire season began early and was extremely active. In British Columbia there were 2,311 wildfires that burned 227,339 ha (561,765 ac). Alberta wildfires consumed 20% more area than the 10-yr average, and in the Yukon Territory the number of wildfires more than doubled the 10-yr average, with a record 273 fires that burned more than 18,000 km² (1.8 million ha or over 4.4 million ac; ~60% of the national total).

ii) UNITED STATES OF AMERICA—K. L. Gleason¹⁹ and G. D. Bell⁴

(i) Overview

Reliable monthly, seasonal, and annual weather records for the United States exist from 1895 to the present, enabling the climate of 2004 to be placed in a 110-yr context for the contiguous United States. The nationally averaged temperature in 2004 was the 24th warmest in the last 110 yr, with an annual mean of

11.9°C (0.4°C above the 1895–2003 mean). The linear temperature trend for the contiguous United States was 0.1°F decade⁻¹ since 1895, with an increase to 0.6°F decade⁻¹ since 1976. The five most recent 5-yr periods (pentads: 2000–04, 1999–2003, 1998–2002, 1997–2001, 1996–2000), were the warmest pentads in the last 110 yr of national records, illustrating the anomalous warmth of the past 10 yr (Fig. 6.6).

Aided by an active United States landfalling hurricane season, precipitation totals averaged over the contiguous United States ranked sixth wettest in 2004, which was the wettest year nationally since 1998. Pennsylvania had its second wettest year, surpassing 2003 as the previous second wettest year, and the 2-yr period over 2003–04 calendar years, was the wettest such 24-month period on record for the state. Texas and West Virginia also had near-record wetness, each reporting the third wettest year on record.

(ii) Temperature

Temperatures were near average across the contiguous United States during winter (December–February), although warmer-than-average conditions persisted across the central third of the

America were associated with anomalous northwesterly flow between the ridge and downstream trough axes (Figs. 6.5a–d).

This circulation was linked to a persistent hemispheric-scale pattern of height anomalies characterized by an anomalous zonal wave-3 pattern at high latitudes, and by above-average heights near Japan (see Fig. 7.6a). The positive height anomalies over the Gulf of Alaska, the polar region, and near Japan, were the most persistent of these circulation features and were evident for 75%–80% of the period.

While it is not possible to attribute this circulation to a specific cause or causes, three factors that contributed to its longevity have been identified. The first is the anomalous jet and wave structure over the western North Pacific. The east Asian jet core extended only to 155°E during the period, which is approximately 40° longitude shorter than its normal length. This significantly reduced eastward extent of the jet core

was associated with anomalous upper-level diffluent flow throughout the Pacific basin. These conditions are known to favor a westward shift in the positions of the mean ridge and trough axes farther downstream over North America. The second and third likely contributing factors are the hemispheric scale of the circulation anomalies (Fig. 7.6.a), and their deep penetration into the lower and middle stratosphere.

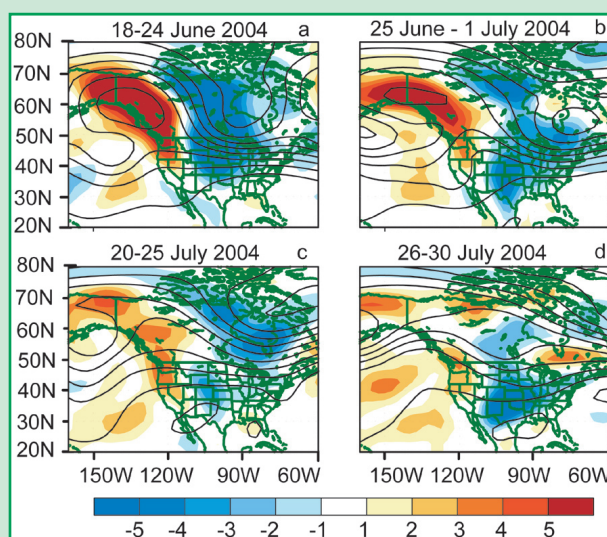


FIG. 6.5. 300-hPa heights (contour interval is 60 m) and 1000-hPa temperature departures during selected cold air outbreaks over the central United States, and central and eastern Canada, from mid-June through July 2004. Anomalies were determined as departures from the 1971–2000 base period daily means.

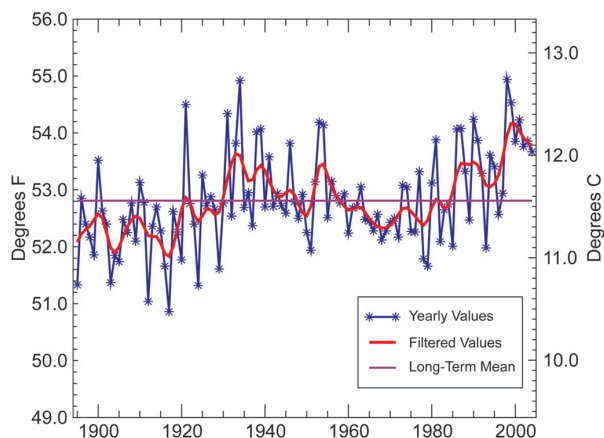


FIG. 6.6. Annual temperature (°F and °C) averaged across the contiguous United States from 1895 to 2004 (data courtesy of the U.S. Historical Climate Network; Karl et. al 1990).

nation, with cooler-than-average temperatures in parts of the Southeast and mid-Atlantic states. Spring (March–May) was exceedingly warm for much of the United States with every state but Florida reporting above-average to much-above-average^{6.1} temperatures (Fig. 6.7a). March was extremely warm in the western half of the United States with Arizona, Colorado, and Utah experiencing their warmest March over the past 110 yr, while Maryland and Delaware

^{6.1} Much above/much below normal (i.e., average or mean) refer to the upper/lower decile of a distribution, above/below normal refer to the upper and lower tercile of a distribution, and near normal refers to the midtercile of a distribution.

had their warmest May on record. In contrast, near-record cold occurred across a wide swath of the central United States during the summer months (June–August), with above- to much-above-average temperatures along the West Coast (Fig. 6.7b).

Several significant cold air outbreaks occurred in the central United States during June and July due to an upper-level pattern with an amplified ridge over western North America and a deep trough over the central and eastern United States. These conditions reflected a complete disappearance of the mean summertime ridge that normally extends from Texas northward to south-central Canada (see the sidebar on p. S46). Minnesota reported its coldest August on record, with 20 additional states in the top 10 coldest for the month.

The cooler-than-average summer temperatures in the East contrasted with record or near-record warm temperatures in the West, as a persistent upper-level ridge dominated the weather pattern during the summer months over eastern Alaska and the Rocky Mountains. Above-average heat occurred west of the Rocky Mountains during the summer months, with both Idaho and Utah having their warmest summer on record. July was extremely warm in the West, with Idaho, Wyoming, Utah, Colorado, Arizona, and New Mexico each reporting their warmest July in the past 110 yr. Idaho and Wyoming also broke records the following month with their warmest August on record for each state. Temperatures during the fall (September–November) of 2004 were much above average in the central portion of the United States, with warmer-than-average temperatures extending through the Ohio Valley to the East Coast, while no state was significantly cooler than average.

Of note was the exceptionally warm and dry summer across Alaska, which was the result of an anomalous

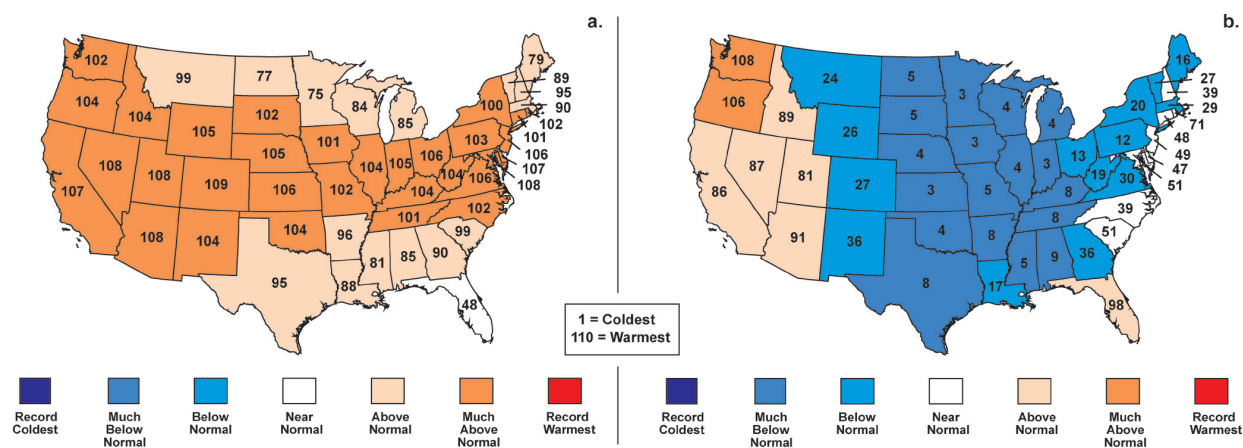


FIG. 6.7. Statewide rankings of temperature as measured across the contiguous United States in 2004: (a) spring (Mar–May) and (b) summer (Jun–Aug). A rank of 110 (1) in the USHCN record represents the warmest (coldest) season since 1895.

blocking ridge of high pressure in the vicinity of the Gulf of Alaska. The summer-averaged statewide temperature was the warmest summer since reliable records began in 1918, with a departure of 2.6°C above the 1971–2000 mean (Fig. 6.9). The previous record summer in 1997 was nearly 1°C cooler than 2004. In addition, the individual months during the May through August period were also the record warmest for Alaska. For the year, 2004 was the fifth warmest on record for the state.

(iii) Precipitation and drought

Precipitation across the United States in 2004 was characterized by persistent moderate wetness in the southern, central, and eastern portions of the country, with continued below-average precipitation in some parts of the West. The average precipitation for the contiguous United States in 2004 was 834 mm, which was above the long-term mean (1895–2004) of 740 mm. Four of the lower 48 states were drier than normal for the year, with 34 of the remaining

TREE RINGS AND WESTERN DROUGHT—C. M. EAKIN,¹⁵ C. WOODHOUSE,¹⁵ AND E. R. COOK¹⁰

A major contribution of paleoclimatology over the last decade has been the development of large-scale gridded datasets that have synthesized widely distributed records of past climatic conditions into unique products. One of these has been the development of gridded reconstructions of past drought conditions from tree-ring data. Cook et al. (1999) developed the first gridded reconstruction of the PDSI from tree rings. The original reconstruction used a network of 388 tree-ring chronologies to develop a 155-point, 2° × 3° grid covering the coterminous United States from 1700 to 1978. The new network used 602 tree-ring chronologies to expand this record in time and space (Cook et al. 2004). The new grid provides 286 points on a 2.5° × 2.5° grid covering most of North America for at least 600, and as much as 2000 yr, combined with instrumental datasets up through 2003.

The extended network of reconstructed drought was recently analyzed for drought patterns in the western United States from 1380 to 2004. Cook et al. (2004) used a drought area index (DAI), calculated as the number of gridpoint reconstructions that exceeded a given threshold of PDSI in each year, with the number of grid points exceeding the threshold divided by the total number of grid points, to provide an estimate of the percent area affected by drought. Figure 6.8 shows that the four driest epochs were before 1300 A.D., whereas the four wettest epochs occurred after that date. The difference between the means of the 900–1300 and 1900–2004 A.D. periods

translates into a statistically significant ($P < 0.001$) average drought area increase of 41.3% in the West during the earlier period. Numerous independent paleoclimatic records that reveal multidecadal droughts during that time period corroborate this record.

The four “megadroughts” seen during the 900 to 1300 A.D. period correspond with the time generally known as the medieval warm period (MWP), which is apparent in globally averaged temperature records, especially those from the Northern Hemisphere (Mann and Jones 2003). Compared to these earlier megadroughts, the drought observed in the western United States since 1999 does not stand out as an extreme event (Fig. 6.8). This finding illustrates that the West can experience far more severe droughts than any found in the twentieth-century instrumental climate record, including the current one. Additionally, if elevated tem-

peratures have been associated with increased aridity in western North America, as during the MWP, this suggests that the projected warming climate over the next century (IPCC 2001) may lead to increases in drought occurrence in the western United States.

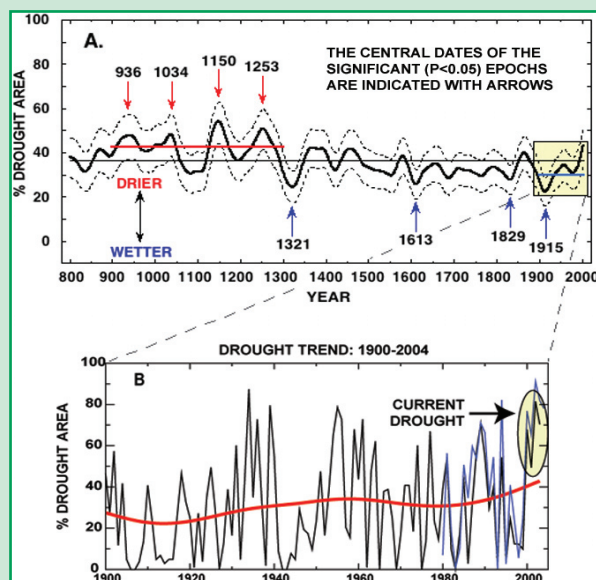


FIG. 6.8. (a) The smoothed DAI reconstruction (solid black curve) for the West, showing two-tailed, 95% bootstrap, confidence intervals (dashed black curves), and the long-term mean (thin horizontal black line). The DAI was calculated as areas with a PDSI less than -1 . Sixty-year smoothing was applied to highlight the multidecadal to centennial changes in aridity across the area (figure from Cook et al. 2004). (b) The enlarged (unsmoothed) DAI reconstruction from 1900 through 2003 (black line) plotted against PDSI from instrumental records (blue line; NCDC's climate division dataset) through 2004. Red line denoted 60-yr smoothing, as in panel (a).

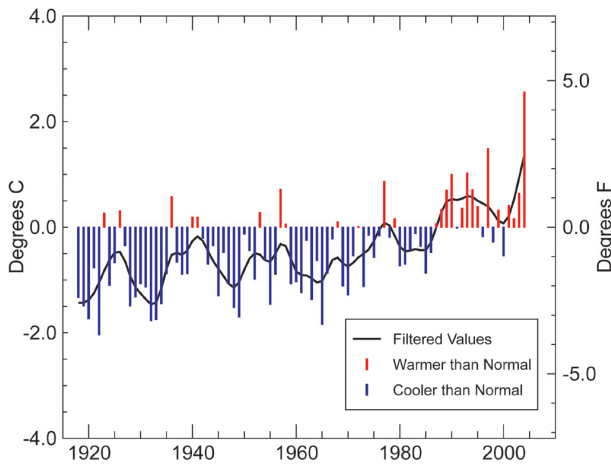


FIG. 6.9. The summer (Jun–Aug) averaged statewide temperature anomaly (°F and °C) for Alaska from 1918 to 2004. Departures were determined with respect to the 1971–2000 base period.

44 states having above-normal to near-record precipitation totals (Fig. 6.10). The observed increase in rainfall and snowfall for the southwestern United States during the fall and early winter can be attributed to a weaker-than-average jet stream across the central and eastern Pacific, along with a persistent high-latitude blocking ridge near the Gulf of Alaska, and an associated trough along the West Coast.

Drought conditions across the United States improved as the year progressed, yet remained a concern

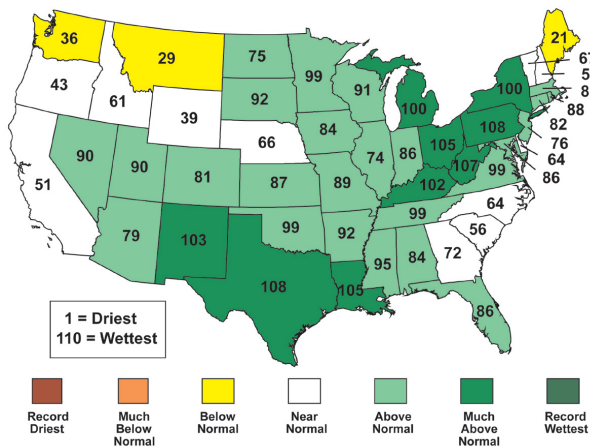


FIG. 6.10. Annual (Jan–Dec) statewide rankings of precipitation as measured across the contiguous United States in 2004. A rank of 110 (1) in the USHCN record represents the wettest (driest) year since 1895. Much above (below)-normal precipitation is defined as occurring in the top (bottom) 10th percentile of the distribution. An above-normal (below normal) designation is defined as occurring in the wettest (driest) third of the distribution.

at the end of 2004, especially in the Pacific Northwest and Northern Rockies. At the beginning of the year, nearly a third (~32%) of the contiguous United States was in moderate to extreme drought, as defined by the Palmer Hydrological Drought Index (PHDI; Palmer 1965; Heim 2002), including much of the West and parts of the Central Plains and upper Mississippi Valley. Precipitation during the subsequent 8 months resulted in the reduction of drought-plagued areas east of the Rockies. During this same period, long-term drought conditions over much of the West persisted. At the peak of the 2004 drought in March, ~69% of the area from the Rocky Mountains to the West Coast was in moderate-to-extreme drought.

March was an exceptionally dry month across the West and Southeast while above-average precipitation fell throughout the central United States. For this month, Montana, Wyoming, Georgia, and South Carolina were each record dry. The extremely dry and warm March across the western United States set the stage for the persistence of long-term drought conditions throughout the summer months. The 4–6 yr of drought in the western United States has had a significant negative impact on a number of hydrological measures. Reservoirs across much of the region remained depleted, streamflow continued to be well below normal, and soil moisture, pastures, and rangeland dried out during June through August. Both in March and in July, two-thirds of the United States from the Rocky Mountains westward was classified as being in moderate-to-extreme drought according to the PHDI.

A generally wetter synoptic pattern from August through December improved conditions throughout much of the Great Basin and Southwest, and especially in California, which brought a remarkable decrease in drought area by the end of December to 4% nationwide, and 10% in the West. Figure 6.11 illustrates the changes in the PHDI from March to December 2004. Improvements in long-term drought conditions are evident across much of the Southwest, the Deep South, and the Northern High Plains over this period.

The primary reason for the drought relief was a pronounced shift in the synoptic pattern from September to November. Below-average 500-hPa heights and an associated increase in Pacific storm activity developed over the western United States in October, which brought above-average precipitation across the southwestern and central United States. Drought conditions in the Southwest improved significantly as a result, with well above average rainfall accumulations during the fall and winter months.

In October, precipitation totals in the Great Plains, the Pacific Northwest, southern California, and the Intermountain Region were significantly above average. Nevada had its wettest October over the past 110 yr, while California had its second wettest. At the end of the month, the percent of the western United States in moderate-to-extreme drought fell to below 20% for the first time in the last 5 yr.

During the last few weeks of December 2004, several strong Pacific storm systems moved into the western United States and provided significant rainfall and snowfall throughout many of the drought-affected locations, and helped increase the winter snowpack across California and the Southwest. However, long-term hydrologic drought remained entrenched in the interior Northwest and Northern Rockies at the end of 2004, due to multiyear precipitation deficits that have persisted for as much as 6 yr throughout portions of these regions.

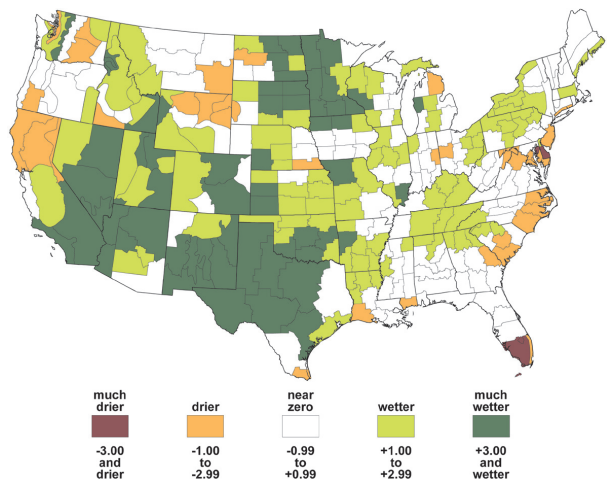


Fig. 6.11. The difference between the 1 Mar and 31 Dec 2004 values of the PHDI, shown by U.S. climate division.

U.S. TORNADO RECORDS—K. L. GLEASON¹⁹

Reports of tornadoes in the United States reached record numbers in 2004, surpassing the previous record by nearly 300. Several severe weather outbreaks in May added to the preliminary annual total of 1722 reported tornadoes. In addition, the record number of reports this past year were significantly affected by the large number of tornadoes associated with landfalling tropical systems, as one tropical storm and five hurricanes affected the U.S. coastline from Florida to the Mid-Atlantic states in August and September. Reliable tornado records began in 1950, and indicate that the previous record was 1424 tornadoes established in 1998. However, the dramatic increase in the number of tornadoes reported in recent years is likely due to improvements in detection technology as well as reporting practices.

The record number of tornadoes for 2004 was largely the result of an active Atlantic hurricane season during August and September (see section 4b)

for details), when individual monthly tornado records were also broken. In August, 173 tornadoes were reported across the contiguous United States. Tropical Storm Bonnie spawned 30 tornadoes, and preliminary reports from Hurricane Charley totaled 25 tornadoes. The previous August record was 120 tornadoes in 1994. Preliminary tornado reports for the month of September 2004 totaled 247, which broke

the previous record of 139 tornadoes set back in 1967. The three landfalling hurricanes in September (Frances, Ivan, and Jeanne) each generated a large number of tornadoes after moving onshore. Hurricane Frances produced the most tornadoes ever reported from one hurricane with 117, while 104 and 16 tornadoes were reported after the landfall of Hurricanes Ivan and Jeanne, respectively.

A more reliable measure of tornado frequency and trend may be found in the number of strong-to-severe tornadoes (F3–F5 on the Fujita scale^{6.2}) that occur each year. A total of 28 F3–F5 tornadoes occurred in 2004, which was slightly below average over the 50 yr of reliable records (Fig. 6.12).

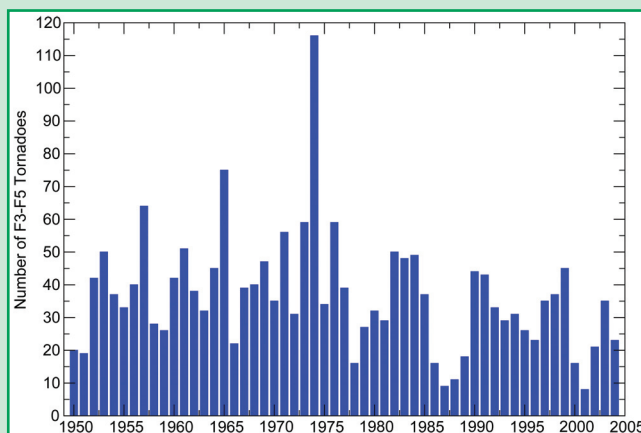


Fig. 6.12. The number of F3–F5 tornadoes between Mar and Aug for the contiguous United States from 1950–2004. A total of 23 occurred during the Mar–Aug time period in 2004. Two additional F3 occurred in Sep, two in Nov, and one in Dec in the Southeast.

^{6.2}The Fujita scale classifies tornadoes based on wind strength, estimated by associated damage (Fujita 1971). The F scale gives each tornado a numerical rating from F0 (weak) to F5 (violent).

(iv) *Snowpack and wildfires*

(a) *SNOW*

Snowpack was generally below average across much of the western United States as the 2003–04 snow season came to an end. Early in the season, snow amounts were near or above normal in many locations. However, rising temperatures and rapid snowmelt in early spring contributed to the below-normal seasonal totals.

In February, Charlotte, North Carolina, reported its third largest snowstorm on record, with accumulations up to 51 cm reported. In addition, an unusual late-season snowstorm affected Tennessee, Indiana, and Kentucky on 13 April, with the latest measurable snowfall on record reported in Jackson, Tennessee.

The first major snowfall of the 2004–05 season occurred during October, when two large storms impacted the West Coast. By the end of December, snowpack was above average in California, the Southwest, and parts of the southern and central Rockies. Much of the the Northwest and Northern Rockies remained below average at the end of the year.

(b) *WILDFIRES*

The United States wildfire season had an early start in 2004 across parts of the Midwest, High Plains, and southern California. Record warm temperatures combined with below-average precipitation during spring increased fire danger across much of the West, which persisted through the summer. Even though it appeared early on in the season that fire activity in the West would be above average, activity remained well below average. At the end of the season in October, several Pacific storm systems moved into the western United States and significantly diminished the remaining fire activity. The season came to a close being characterized as below average for the contiguous United States, with just over 567,000 ha (1.4 million ac) burned.

In contrast to the below-average fire season in the lower 48 states, Alaska had its worst fire season on record in 2004. After a wet spring, the summer months in Alaska were characterized by extremely dry conditions and anomalously warm temperatures, which led to many large wildland fires across the eastern and central interior regions of the state. The persistent heat and lack of rainfall, both in Alaska and the adjacent Yukon Territory of Canada, contributed to

a rapid increase in fire activity in June, which was sustained into August. The effects of the Alaskan and Yukon fires were felt well outside the region, as smoke emissions spread across Canada and eastward to the northeast coast of the United States, and as far south as Louisiana and the Gulf of Mexico coast.

For the 2004 fire season, over 2.7 million ha (6.6 million ac) were consumed in Alaska alone [~1.8 million ha; ~4.5 million ac in the Yukon Territory; see section 6aI(iii) for details], yet there were nearly 300 fewer fires during the 2004 season as compared with 1990, which was the year with the record number of fires (the previous record year for area burned in Alaska was 1957, with ~2 million ha; ~5 million ac). This suggests that many of the fires in 2004 were classified as “large fires” (> 80 ha; > 200 ac), and, in fact, the four largest wildfires in Alaska comprised more than 25% of all of the area consumed in the state during the 2004 season.

Including the record area burned in Alaska, just over 3.2 million ha (8 million ac) were consumed across the United States in 2004, which was well above the latest 10-yr average of ~2.2 million ha (5.5 million ac), and second only to the record year of 2000 when over ~3.4 million ha (8.4 million ac) burned across the United States.

III) MEXICO—M. Cortez Vázquez¹¹

In 2004, the regional climate of Mexico had a number of notable precipitation anomalies. Based on preliminary data, the total precipitation for the summer rainy season (May–October) was 11% above average, which ranked the 2004 monsoon season as the ninth wettest over the 54-yr period of record (1941–2004). The year as a whole was the eighth wettest on record, with the national rainfall index approximately 13% above normal. As shown in Fig. 6.13, 2004 was also the wettest year over the last 10 yr.

Despite the overall wet conditions, 2004 was a year of contrast between northern and southeastern Mexico. In the southeast, regional precipitation totals were near 60% of normal, with a large area of drier-

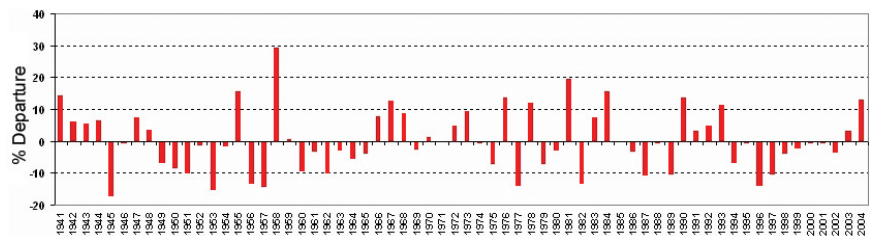


FIG. 6.13. The annual percent departure from normal precipitation across Mexico over the period of 1941–2004. Departures were determined with respect to the period of record mean.

than-normal conditions extending from the southern Gulf of Mexico states of Veracruz and Tabasco, along with portions of the Yucatan Peninsula, to the southern Pacific coast states of Oaxaca and Chiapas. On average, these are the wettest regions in Mexico (Fig. 6.14). Rainfall deficits in the southeast were related to the lack of tropical cyclone activity across the western Gulf of Mexico and the tendency for Pacific tropical cyclones to form farther west and south of normal, which was a typical response to developing El Niño conditions [see section 4bii(ii)].

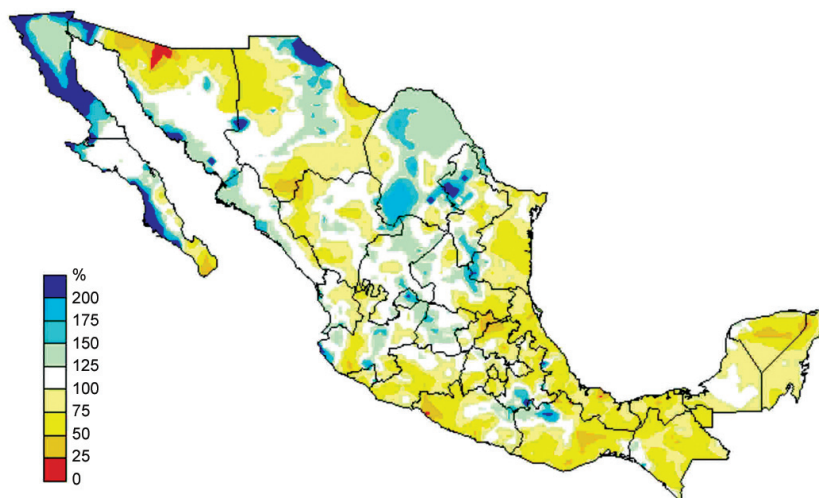


FIG. 6.14. Percent of normal precipitation during the rainy season (May–Oct) for Mexico in 2004. Anomalies were determined with respect to the 1941–2004 period of record means.

The national rainfall index for Mexico was the second wettest on record over the period of January–June. The primary focus for rainfall was in the northeast, where an active convective season occurred during March–June. For example, a series of mesoscale convective systems (MCSs) during the night of 5 April produced over 200 mm of precipitation in northern Coahuila state, which generated severe flooding and more than 30 deaths. During the period of March–June, large sections of Coahuila and the adjacent state of Nuevo Leon reported precipitation totals that exceed the normal annual precipitation in this region of Mexico.

A pronounced wet regime was also observed in northwestern Mexico in association with a very active end to the summer rainy season. On 19 September, Hurricane Javier made landfall as a tropical depression in central Baja California and then tracked northeast across the Gulf of California into Sonora, depositing 100–150 mm of rain along its path in Sonora state as it dissipated [see section 4bii(ii) for further details]. In addition, Baja California and the west coast states from Sonora to Nayarit were very wet during October and early November. These wet conditions were associated with a series of cut-off low pressure systems that interacted with the ITCZ. The anomalously wet end to the summer monsoon caused the warm season (May–October) rainfall totals to exceed 200% of normal across large sections of Baja California. In fact, many locations in northern Baja California reported their wettest October on record. Regional flooding was also reported with tropical depression 16E, which crossed the Gulf of California and made landfall in Sinaloa state on 26 October.

This system produced 100–200 mm of rainfall across northern Sinaloa. For the year as a whole, there were only three tropical cyclones that made landfall in Mexico in 2004, and all of these along the Pacific coast [see section 4bii(ii)]. Therefore, the surplus of precipitation observed in northern and northeastern Mexico in 2004 was primarily due to localized convective storms, rather than a result of a significant contribution from tropical cyclone activity.

b. Central America—E. K. Grover-Kopec⁵

Precipitation across Central America and the Caribbean region during 2004 was largely characterized by below-normal accumulations (Fig. 6.15), which brought dry conditions to some areas for a fourth consecutive year. The largest standardized precipitation departures from their climatological means occurred across an area covering most of El Salvador, Honduras, and Nicaragua. This pattern was similar to the annual precipitation anomalies in 2003 (see Fig. 6.12 in Levinson and Waple 2004), while in 2004 the annual accumulations were about 25%–35% of normal across this region. Significant precipitation deficits were also observed in the southern half of the Central American isthmus, where Costa Rica and Panama received approximately 35% and 50% of their normal annual accumulations, respectively, based on national area-weighted averages. Most of Central America and the Caribbean typically experience a bimodal distribution of precipitation, with relative maxima in May–July and September–October, and the largest monthly deficits across the region were generally observed during these two climatological peak periods.

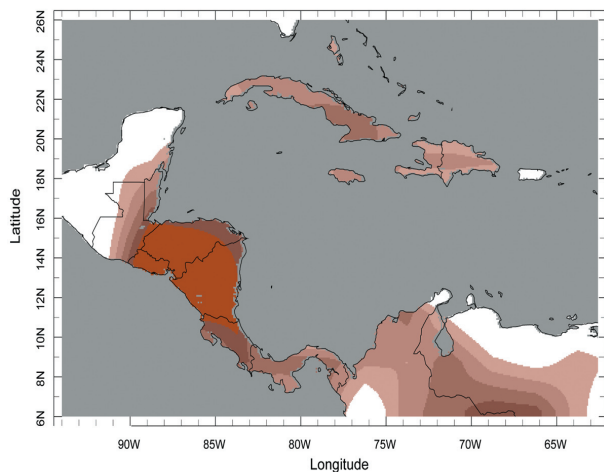


FIG. 6.15. Average of the standardized monthly precipitation anomalies for 2004. Data are from the CAMS_OPI analysis (courtesy of NOAA/CPC), with anomalies determined from the 1979–2000 base period. The Weighted Anomaly Standardized Precipitation (WASP) Index is based on monthly precipitation and is computed using monthly precipitation anomalies, which are standardized by dividing by the standard deviation of the precipitation. The standardized monthly anomalies are then weighted by the fraction of the average annual precipitation for the given month. These weighted anomalies are then summed over particular time periods, in this case 12 months. The value of the WASP is also standardized (Lyon 2004, 2005).

Drought in eastern Cuba, which started to develop in mid-2003, was among the most notable climatic events in the region during 2004. Water resources, already well below normal after a year of below-average rainfall, were significantly impacted by precipitation deficits during the spring. Rainfall across most of central and eastern Cuba was below the 20th percentile of the climatological distribution during April and May. In central Cuba, precipitation accumulations during May, which typically coincides with the start of seasonal rains, were less than 60% of average; 105 mm of rainfall was observed, compared to the average accumulation of 180 mm. As a result, the national reservoir level fell to only 39% of capacity, and drought conditions began to significantly impact agricultural activities. By midyear, the drought was affecting 85% of the population in the eastern provinces (source: World Food Program).

Each year a short lull in seasonal rains during either July or August is relatively common across most of the region, but the break in the 2004 rainy season in Guatemala and Honduras lasted twice as long as usual. Precipitation accumulations were between the

10th and 20th percentiles of the climatological distribution across both countries during July–August. In Honduras, the 2-month precipitation totals ranged between 60% and 20% of normal, with the driest areas in the eastern portion of the country.

Below-normal precipitation from May through July in Nicaragua contributed to anomalously low annual accumulations. The accumulated precipitation in the country’s northern and northwestern provinces in May and June was approximately 50% and 33% below normal, respectively. In contrast, wet conditions were observed across eastern Nicaragua during late June and early July, as a series of tropical waves brought heavy rainfall and mudslides to the region.

Destructive rains also fell at the end of May near the border between Haiti and the Dominican Republic on the island of Hispaniola. Moisture-laden southerly winds associated with a tropical low pressure system brought approximately 550 mm of rain to the area during 18–25 May. The resulting floods and mudslides reportedly caused approximately 2000 deaths, and was one of the most significant climatic events of the region in 2004.

Average surface temperatures for 2004 were near or slightly above normal across the region (Fig. 6.16). The primary exception was Guatemala, where the annual average exceeded 1°C across most of the country. Above-average temperatures were observed in the northern half of the Central American isthmus during February and July–October, with monthly averaged departures ~1°C above normal.

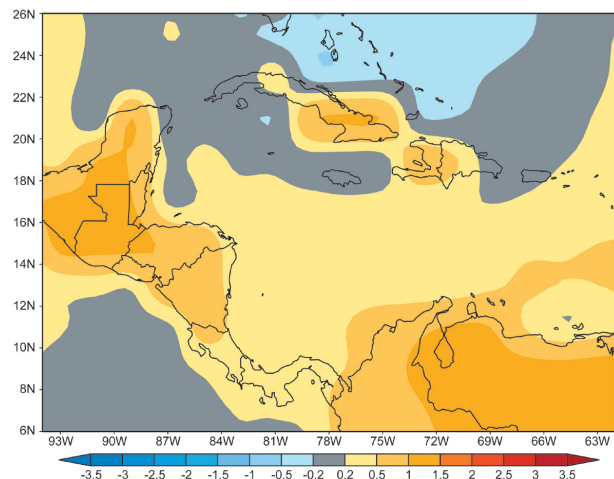


FIG. 6.16. Annual temperature anomalies (°C) across Central America and the Caribbean region in 2004 from the CAMS (courtesy of NOAA/CPC). Anomalies were determined with respect to the 1961–90 base period.

c. South America—M. Rusticucci³⁵

i) TEMPERATURE

South America experienced warmer-than-normal conditions across much of the continent in 2004. Preliminary values calculated from the GHCN-gridded dataset (Peterson and Vose 1997) indicated that the South American continent-wide annual mean temperature for 2004 was 0.53°C above the 1961–90 base period average. As shown in Fig. 6.17, the southern part of the continent had the warmest annual temperature anomalies for the year. Every month, with the exception of May, resulted in positive regional-scale temperature anomalies.

May was an anomalously cold month over most of South America, with the largest cold anomalies covering a large region on the southern end of the continent. According to the daily temperatures in many of the stations monitored by NOAA's Climate Prediction Center (CPC), the cold outbreak in May was the most intense and extensive of the year. This cold wave, which is typical of the eastern side of the Andes in winter, occurred earlier than normal and was observed simultaneously in the western hillside region in Chile. The monthly temperature anomalies reached -5°C , based on the gridded temperature values in GHCN. The associated atmospheric circulation showed the usual characteristics of previous cold waves in the region, with persistent high pressure

systems over the southwestern and southern parts of the continent. This surface synoptic pattern has been known to generate successive cold air outbreaks on the eastern side of the anticyclones (Rusticucci and Vargas 1995). Cold advection during May propagated anomalously northward into the tropical areas of the continent, and cold anomalies were observed as far north as 10°S .

ii) PRECIPITATION

The annual precipitation anomalies for South America are shown in Fig. 6.18. Rainfall was highly variable in 2004, although above-average precipitation was measured across the majority of the continent. The largest positive anomalies were measured along the Andes Mountains, especially in northeast Bolivia and parts of Chile, as well as in parts of northeast Brazil.

The year began in northeastern Brazil with excessive precipitation that resulted in floods in January and February, followed by precipitation deficits from April to June. In Colombia, heavy rains that began in October continued into November, generating floods and/or landslides that occurred in 24 out of country's 33 departments. In the south, the drought that developed in 2003 continued until early 2004. By the end of the year, precipitation surpluses were observed across the majority of the drought-affected regions,

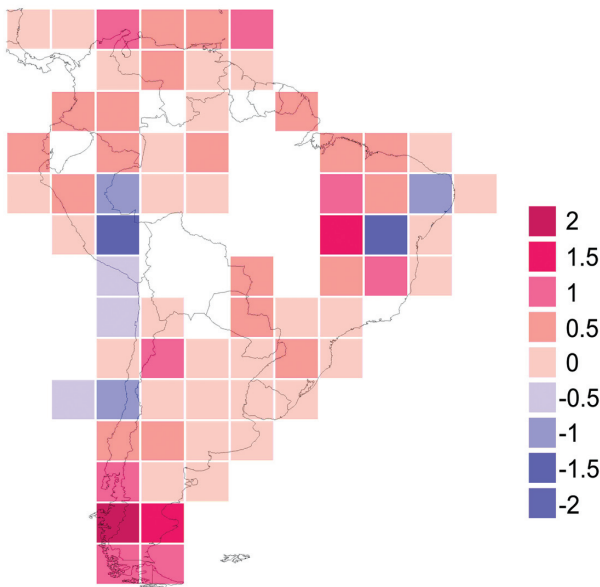


FIG. 6.17. Annual 2004 temperature anomalies ($^{\circ}\text{C}$), with departures from the 1961–90 base period mean values (source: GHCN global gridded products; Peterson and Vose 1997). The lower limits of intervals are indicated.

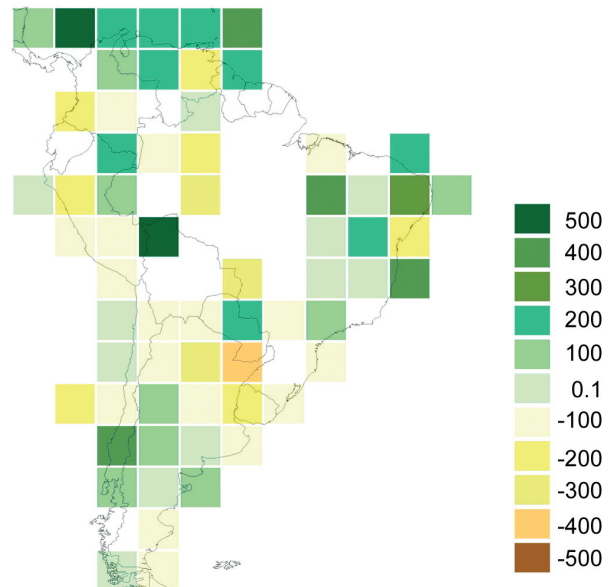


FIG. 6.18. Annual precipitation anomalies (mm), with departures from the 1961–90 base period mean values (source: GHCN global gridded products; Vose et al. 1992).

although deficits remained in the most agriculturally productive regions of Argentina and Uruguay.

d. Europe—J. Kennedy²¹

The annual mean temperature across Europe as a whole in 2004 was 0.98°C above the 1961–90 base period average (based on Jones et al. 2001). Annual temperature anomalies in excess of 1°C occurred across parts of northwest Europe and Scandinavia (see Fig. 2.3). Observed temperature anomalies over much of the rest of Europe were between 0.5° and 1°C, apart from the southeast, where temperatures were between 0.2° and 0.5°C above average. A limited area of the Black Sea had cooler-than-average temperatures for the year.

i) WINTER (2003–04)

Seasonal mean temperatures were above average over most of Europe during the 2003–04 winter (December–February; Fig. 6.19a). The only exceptions were parts of Greece, Turkey, and Norway, which had below-average temperatures for the season.

Warmer-than-average SSTs in the North Atlantic in January, combined with general westerly flow, brought above-average temperatures and precipitation to Western Europe (GPCC 2004; Rudolf et al. 1994, 2003).

Precipitation accumulations above the 70th percentile extended into Eastern Europe, as temperatures during the month were generally below average in this region. For example, between 9 and 12 January, anomalously cold temperatures and significant snowfall in parts of Turkey isolated around 2000 villages.

In February, temperatures were above average in Europe, except for the Adriatic region and northern parts of Norway. Precipitation levels were significantly above average in Eastern Europe, where accumulations over a large area exceeded the 90th percentile. In Western Europe, most of the region experienced below-average precipitation, as a persistent and relatively stationary high pressure system brought subsidence and dry conditions for much of the month.

ii) SPRING

Spring (March–May), temperatures were above average over much of Europe, with seasonal means exceeding the 90th percentile in many areas of the northwest (Fig. 6.19b), while temperatures were near average across southern Europe. Precipitation was significantly below average over much of Sweden and Finland in spring, as well as in the south of the Ukraine, where accumulations were below the 10th percentile.

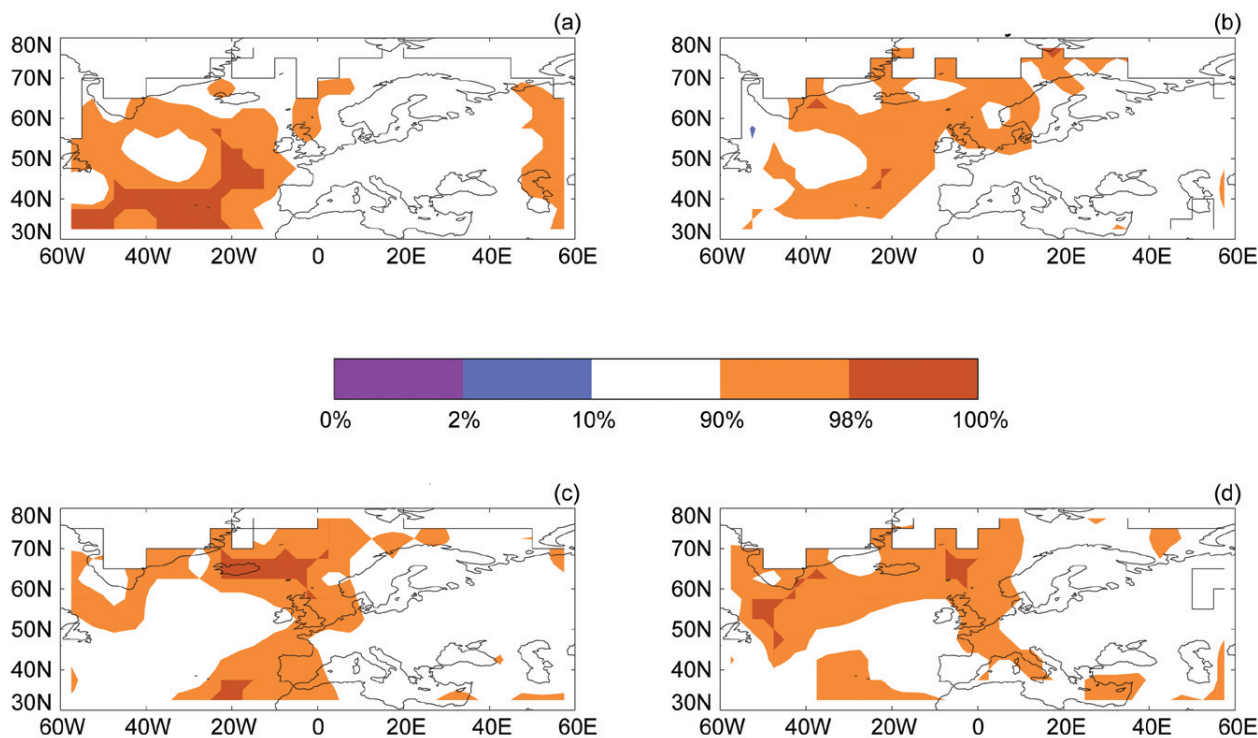


FIG. 6.19. Surface temperatures across Europe in 2004, expressed as percentiles of 1961–90 modified two-parameter gamma distribution for (a) winter (Dec–Feb) 2003–04, (b) spring (Mar–May), (c) summer (Jun–Aug), and (d) autumn (Sep–Nov) 2004 (Jones et al. 2001; Jones and Moberg 2003; Horton et al. 2001).

March was warmer than average, with only a few isolated areas in the Mediterranean region with below-normal monthly mean temperatures. Precipitation surpluses were measured over much of Spain, with monthly accumulations as high as 186 mm recorded in the south of the country, which was nearly 300% of the average monthly total.

In April, temperatures in northwest Europe rose above the 90th percentile, with parts of Norway exceeding the 98th percentile. These warmer-than-average conditions at the surface were consistent with 500-hPa height anomalies that extended over Scandinavia (not shown).

Temperature anomalies formed a dipole pattern across Europe in May, with positive anomalies north and west of a line running from the southwest tip of Portugal to the southern tip of Finland, and negative anomalies south and east of this line. The North Sea and adjoining regions experienced monthly average temperatures above the 90th percentile. In contrast, monthly mean temperatures in Estonia and Latvia were colder than average, with values below the 10th percentile. Precipitation during May was near average over much of central Europe, although significant surpluses were measured in the Ukraine, where precipitation levels exceeded the 90th percentile in the southern part of the country.

III) SUMMER

Above-average temperatures occurred across most of Europe during the summer (June–August), with seasonally averaged temperatures above the 90th percentile in several countries in the northwest (Fig. 6.19c).

In June, the temperatures in Europe approached both high and low extremes (Fig. 6.20). Temperature anomalies in western Europe exceeded the 90th percentile, while large areas of Spain and Portugal exceeded the 98th percentile for the month. Toward the end of June, maximum temperatures in many areas of Spain exceeded 40°C. Further east, anomalously low 500-hPa heights in June were associated with surface air temperatures below the 10th percentile in Finland, with below-average temperatures in northeastern Europe. Precipitation was below average in Iberian Peninsula, as well as much of France, where deficits dropped totals below the 10th percentile. Rainfall exceeded the 70th percentile east of the Baltic and in the former Yugoslav republic of Macedonia. The rainfall in the latter case generated extensive flooding, which affected approximately 100,000 people and 50% of the agricultural land in the region.

Long-term rainfall deficits on the Iberian Peninsula were exacerbated in July, which was the sixth consecutive month of below-average rainfall in the northwestern portion of the region. The hot, dry weather worsened the fire danger over most of Spain and Portugal, as forest and bush fires burned around 27,000 ha of land during the month. Temperatures elsewhere in Europe were mostly above average in July, with below-average temperatures observed only in southern Sweden and areas of the Black Sea and Ukraine. The mean temperature in central England for July was 0.3°C below the 1961–90 average (Parker et al. 1992), but above-average SSTs in the adjacent seas brought the area-averaged temperature to above normal.

August temperatures were above the 90th percentile over large areas of central and western Europe. West of 30°E, the only countries with temperatures below the 90th percentile were France, northern Spain, and Ireland. A series of low pressure systems, including the remnants of two tropical systems, brought above-average precipitation to Portugal, Spain, Belgium, the Netherlands, and countries bordering the Black Sea (Fig. 6.21). In France and England, precipitation accumulations exceeded the 90th percentile, and the England and Wales precipitation series was the wettest August since 1956 (Jones and Conway 1997; Alexander and Jones 2001).

IV) AUTUMN

Autumn (September–November) temperatures were above average in Europe during 2004, with sea-

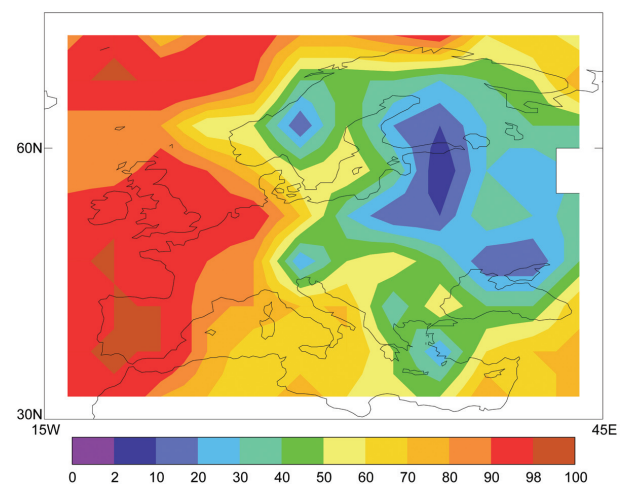


FIG. 6.20. Surface temperatures across Europe during Jun 2004 expressed as percentiles of the 1961–90 base period—modified two-parameter gamma distributions (Jones et al. 2001; Jones and Moberg 2003; Horton et al. 2001).

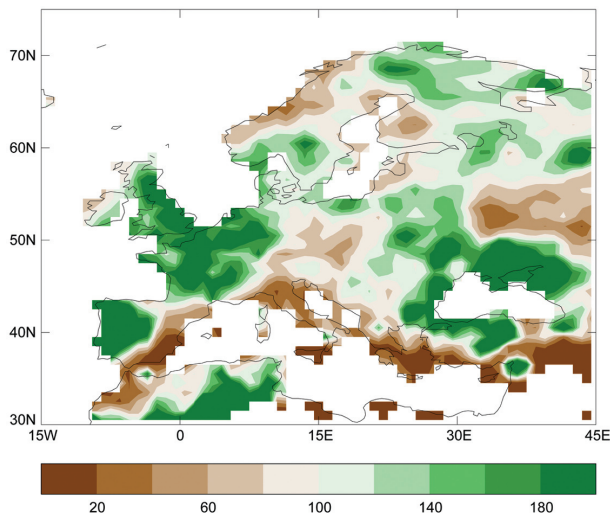


FIG. 6.21. Precipitation anomalies in Aug 2004 for the European region, expressed as percentages of the 1961–90 base period mean (GPCC 2004; Rudolf et al. 1994, 2003).

sonal means exceeding the 90th percentile in Turkey, and across a large region from Scotland to the south of Italy (Fig. 6.19d).

With the exception of Romania and Hungary, temperatures were generally above average in September, with monthly mean values above the 90th percentile measured over a swath extending from England to Finland. The anomalously warm temperatures were accompanied by dry conditions, as monthly averaged precipitation was below the 30th percentile in France, southern Spain, Poland, and Belarus. The worst deficits occurred in parts of southeastern Turkey, which received little or no rain at all during the month.

October temperatures were above average everywhere, except for Ireland and eastern Finland. Monthly mean temperatures above the 90th percentile were observed in the western Mediterranean, and the south and east of Turkey. Precipitation was above average in coastal areas of the North Atlantic Ocean, while above-average precipitation was evident across a broad area from the southern tip of Sweden eastward into Russia. Conditions remained dry in Turkey, along with Bulgaria, Romania, and most of Scandinavia, which had some precipitation accumulations below the 10th percentile for the month.

Temperatures were below average in November across northern Scandinavia and the Baltic states, as well as in southwest Europe. Elsewhere, conditions were warmer than average, with monthly mean temperatures across much of the United Kingdom and the eastern Mediterranean above the 90th percentile.

Severe storms in the Mediterranean during the month brought precipitation surpluses to Italy, along with heavy snowfall to the eastern sections of Turkey. In contrast, precipitation was below average in the Iberian Peninsula and western France.

e. Africa

- 1) NORTH AFRICA—M. A. Bell,⁵ O. Baddour,² and M. A. Fortune¹⁷

The Mediterranean coast of North Africa receives most of its rainfall during October–April, largely from midlatitude cyclones and associated cold fronts. In the Atlas Mountains of northern Morocco, Algeria, and Tunisia, cold frontal passages can bring sub-freezing temperatures and heavy rain, occasionally causing floods and landslides.

There were pronounced seasonal changes in 2004 in North Africa. Wet and dry conditions alternated from one season to another in most parts of the region. At the end of 2003, the 3-month (October–December) precipitation in North Africa was generally above normal, particularly in parts of northern Morocco, northeastern Algeria, and Tunisia, where precipitation was as much as 150% of normal in the first half of the 2003–04 rainy season. However, the winter (December–February) was characterized by below-normal rainfall, with many stations in Morocco reporting no precipitation at all in January. From late December 2003 through February 2004 most of the region was extremely dry, with monthly precipitation deficits between 25 and 50 mm (Fig. 6.22). Rainfall in late February and mid- to late March helped to avoid the development of drought across most of Morocco and northern Algeria, although seasonal precipitation deficits remained along the central coast of Algeria and in southern Morocco.

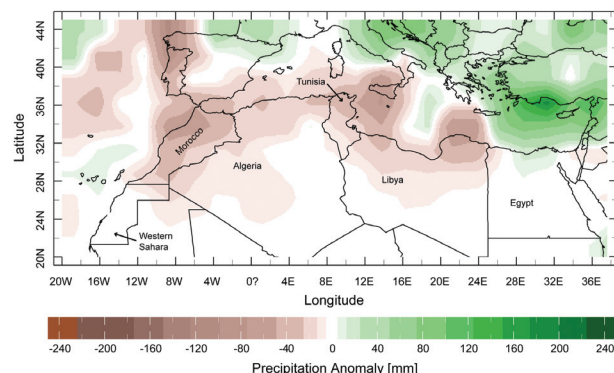


FIG. 6.22. Jan–Feb 2004 precipitation anomalies (mm) for North Africa. Anomalies were determined with respect to the 1979–2000 base period means (CAMS_OPI data courtesy of NOAA/CPC).

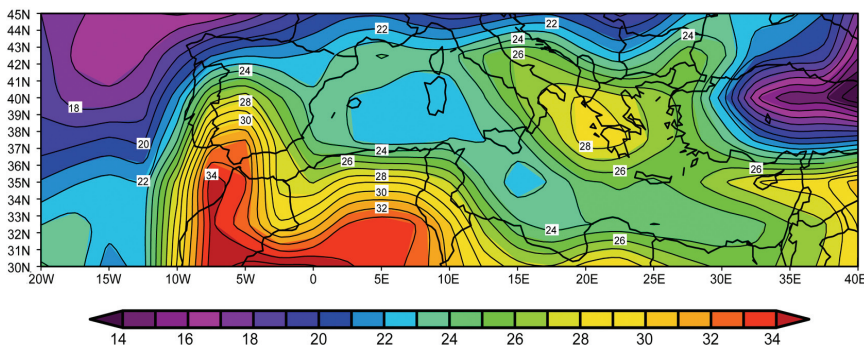


FIG. 6.23. The average surface air temperature ($^{\circ}\text{C}$) across North Africa during Jun–Jul 2004 (courtesy of the NOAA-CIRES Climate Diagnostics Center).

The spring was exceptionally wet, cold, and windy, with some locations reporting monthly rainfall values of 50% above normal. Heavy rainfall affected central Algeria in late March and in mid-April, as over 40 mm of precipitation fell during 14–16 April in the arid Adrar region of central Algeria, which receives little more than 20 mm of precipitation per year, on average. The resulting flooding extensively damaged homes and infrastructure, caused three deaths, and affected about 5500 people in the area of Timimoun (source: the Algerian Directorate-General of Civil Protection).

The summer began early and unusually warm as soon as the spring ended. Both June and July were very hot in Morocco (Fig. 6.23), with several records broken during a persistent heat wave. The peak of the heat wave occurred on 29 June, as the temperature in Sidi-Slimane, Morocco, climbed to a record high of 47°C .

Beginning in September, and through the first half of the 2004–05 winter rainy season, northern Algeria and Tunisia received plentiful rainfall. Although the rainy season started late in northern Morocco, heavy precipitation at the end of October helped to bring rainfall totals to near-normal amounts by the end of the year. During November, colder-than-normal conditions and snow covered a vast domain from Morocco to Tunisia. Temperatures as low as -15°C were recorded at high elevations above 1000 m, and snowfall reached low-lying areas to as low as a 300-m elevation.

ii) WEST AFRICA—W. M. Thiaw,⁴ G. D. Bell,⁴ M. A. Bell,⁵ and M. A. Fortune¹⁷

(i) Rainfall

West Africa can be divided into two quasi-homogeneous rainfall regions: the Sahel and the Gulf of Guinea. The Sahel (10° – 20°N , 18°W – 20°E) receives approximately 90% of its mean annual rainfall dur-

ing June–September. The monsoonal rainfall is closely related to the north–south movement of the ITCZ, which begins moving northward in March and typically reaches its northernmost position in August. This produces a unimodal rainy season from June to September in the Sahel, where moisture originating south of the ITCZ is able to support westward-propagating

mesoscale convective systems. Further south, along the central Gulf of Guinea coast, the rainy season is bimodal and runs from about April to October, but with less rainfall in midsummer. The movement and configuration of the ITCZ also produces a pronounced strong north–south gradient in annual precipitation totals across the region, with average totals exceeding 600 mm in the south and only 100 mm in the north.

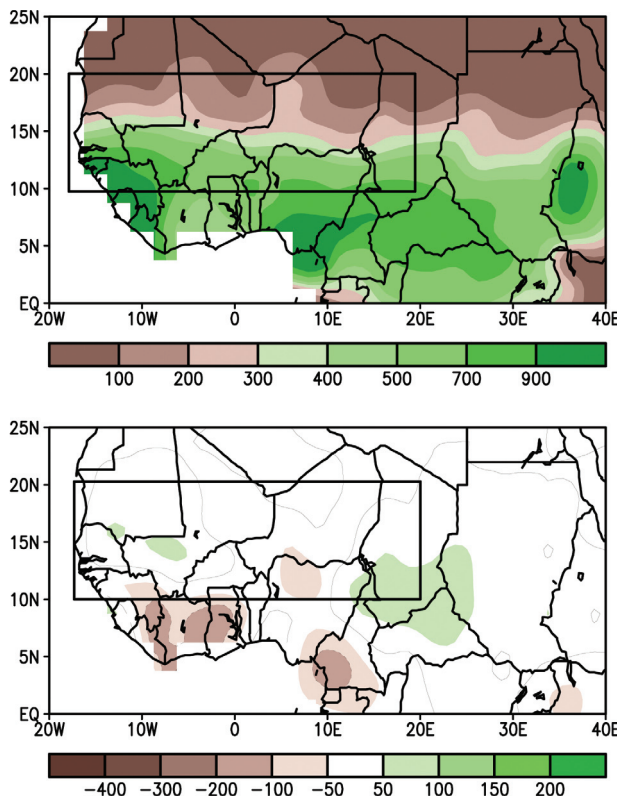


FIG. 6.24. Jun–Sep 2004 (a) total precipitation (mm), and (b) precipitation anomalies (mm) for West Africa (anomalies determined with respect to the 1979–2000 base period; CAMS_OPI data courtesy of NOAA/CPC). The box denotes the approximate boundaries of the Sahel region (10° – 20°N and 18°W – 20°E).

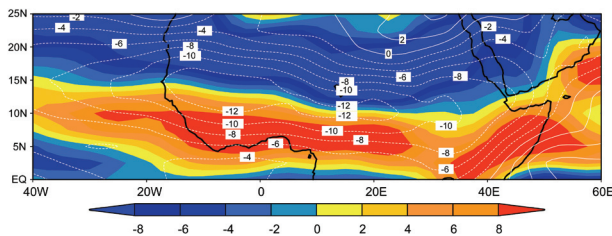


FIG. 6.25. Aug–Sep 2004 mean 600-hPa zonal wind (contours, m s^{-1}) and relative vorticity (shaded, $2 \times 10^{-6} \text{ s}^{-1}$) across West Africa, the Sahara, and the northern sector of the Greater Horn of Africa.

Precipitation for the region as a whole was below the long-term mean (1979–2000) in 2004, and it was highly variable. The rainy season featured near-normal rainfall across most of the Sahel (Fig. 6.24). Rainfall amounts ranged between 700 and 900 mm in the southwestern corner of the Sahel and 100–200 mm in the extreme northern areas (see box in Fig. 6.24a). The exceptions were local areas in southwestern Mauritania, western Mali, and southern Chad, where rainfall amounts were between 50 and 100 mm above

average (Fig. 6.24b). However, rainfall was below normal in some areas of the Gulf of Guinea region. While the Nigeria–Cameroon border experienced heavy rainfall several times during the monsoon, precipitation was below average for most locations along the Guinea Coast. Rainfall deficits ranged from 100 to 300 mm below normal from eastern Guinea to Ghana, and less over northern Nigeria.

(ii) *Atmospheric circulation*

Sahel rainfall is primarily controlled by the depth and northward penetration of the West African monsoon system, which, in turn, is related to the position of the mid- and upper-level jets. These larger-scale circulation features are fairly sensitive to changes in the global monsoon circulation on both interannual and interdecadal time scales. The near-average 2004 rainy season was associated with a near-normal West African monsoon. At 925 hPa, strong southwesterly winds averaging $6\text{--}9 \text{ m s}^{-1}$, which originated in the South Atlantic trade wind zone, extended well north into the Gulf of Guinea region (not shown). However, in contrast to the 2003 rainy season, the presence of

THE 2004 DESERT LOCUST OUTBREAK—M. BELL⁵

Favorable rainy seasons in West and North Africa in 2003 and 2004 were responsible for fostering the largest desert locust outbreak that affected the region since the destructive locust plague of 1987–89 (FAO 2004). The above-average June–September 2003 rains in the Sahel, which helped to produce a bumper harvest, also favored locust breeding, increased locust densities, and aided swarm formation in the summer breeding areas of the northern Sahel in 2003. By the middle of October 2003, desert locust swarms had formed in Mauritania, Sudan, and Niger.

Over the next several months, the swarms migrated north to their winter breeding areas on the south side of the Altas Mountains in Morocco, Algeria, and Tunisia (Fig. 6.26a), where they continued to breed and increase in number with the help of well-timed precipitation. The swarms took advantage of good rains and soil moisture

conditions in March, April, and May 2004 to breed and increase their populations. Before the locusts migrated south again in the summer, they caused localized damage to crops in Morocco and Algeria.

The cycle continued during the summer of 2004 as the swarms migrated southward at the onset of the rainy season in the Sahel, where precipitation was again plentiful enough to sustain the outbreak, particularly in Mauritania (Fig. 6.26b). Although limited, targeted control efforts prevented massive crop damage on a regional scale. Despite these efforts, crops and pasture in Mauritania were heavily damaged, as were crops in localized areas of Mali and Burkina Faso. While cereal production in the Sahel was estimated at 11.6 million metric tons (near the recent 5-yr average), in Mauritania where the locust infestation was heaviest, as much as 50% of the cereal harvest was lost.

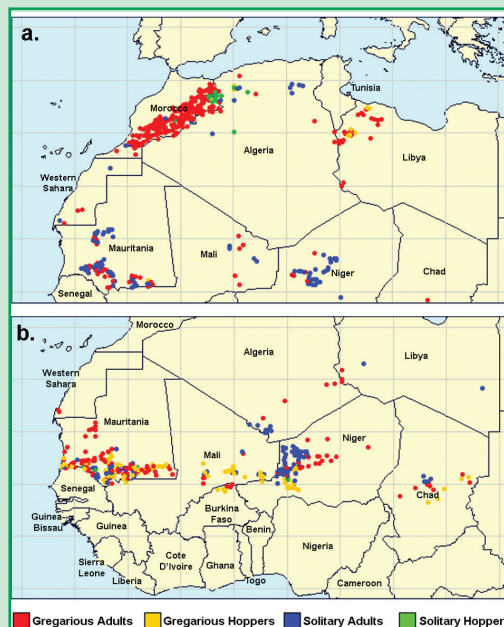


FIG. 6.26. Locations of desert locusts and the type of swarm during 2004 in North Africa and the Sahel: (a) Jul and (b) Sep (source: Desert Locust Information Service of the Migratory Pests Group, Food and Agricultural Organization of the United Nations).

an anomalous north-to-south anticyclonic–cyclonic circulation couplet across West Africa favored the intrusion of strong northeasterly flow into the Sahel and contributed to less African wave disturbance activity. This monsoon pattern was also evident at 850 hPa (not shown), and contributed to the limited penetration of moist, unstable air into the Sahel.

This anomalous cyclonic circulation reflected a weakening of the cyclonic shear along the equatorward flank of the AEJ at 600 hPa, and a southward shift of the mean AEJ axis to 15°N across the western Sahel (Fig. 6.25). Note that the mean position of the AEJ axis over the western Sahel was at about 17.5°N during both the wet 1999 and 2003 seasons. At upper levels, the monsoonal circulation was associated with a slightly enhanced divergent flow at 200 hPa (not shown). This divergent flow was weaker than in the wet 1999 and 2003 seasons, but stronger than that of the 1997 season when the Sahel was dry. Consistent with this flow pattern, the amplitudes of the subtropical ridges across both hemispheres (not shown) were near average, resulting in a tropical easterly jet (TEJ) in the upper troposphere at 200 hPa close to the climatological mean.

It should be noted that warm ENSO episodes (i.e., El Niños) typically lead to rainfall deficits in the Sahel (Ropelewski and Halpert 1987, 1989, 1996). However, the effects of the weak El Niño episode in 2004 on rainfall in the Sahel were mitigated by anomalous warmth in the tropical North Atlantic Ocean (see section 2eii). Therefore, the anomalously warm SSTs in the North Atlantic, combined with a near-average West Africa monsoon circulation, resulted in near-average rainfall across the Sahel.

iii) EAST AFRICA AND THE GREATER HORN—M. A. Bell,⁵
P. G. Ambenje,¹ A. K. Njogu,²⁸ and M. A. Fortune¹⁷

Climatologically, the timing of the rainy seasons in the Greater Horn of Africa (GHA) is governed by the north–south migration of the ITCZ through the course of the year. Climate extremes in the GHA are influenced by SST anomalies in the Indian and Atlantic Oceans, as well as the general atmospheric circulation. Extreme climatic events are often linked to large-scale anomalies, such as the ENSO, tropical cyclone activity in the Indian Ocean, and the variability of the monsoon.

Regionally, rainfall exhibits pronounced variability, both spatially and temporally, as well as strong seasonality. Although the complex orography and presence of the East African lakes makes the climate of the region quite complicated, three general subregions can be delineated according to their rainfall

regime: the southern, equatorial, and northern sectors. In the southern sector, central and southern Tanzania has a unimodal rainfall regime, with precipitation primarily between December and April. Northern Tanzania, Kenya, and southern Ethiopia and Somalia comprise the equatorial sector, and generally exhibit a bimodal rainfall regime, with the “long rains” during March–May, and the “short rains” during October–December. However, both western and coastal areas also receive significant rainfall during the months of July and August. In the northern sector, the major rainy season in northern Ethiopia, Eritrea, Djibouti, and eastern Sudan occurs during the months of June–September, but a few areas receive a secondary peak from March to May.

(i) *Southern sector*

At the end of 2003, drought conditions across most of Tanzania were responsible for shortages of food for about 2 million people. During January–April 2004, moderate rainfall was observed over the southern sector. In the southernmost areas, abundant rainfall totals as high as 150–200 mm were recorded from January to April. The rains were unusually heavy in parts of eastern Tanzania, but deficient elsewhere. In fact, distinct areas of the country experienced both their wettest and driest conditions on record since 1961. Fortunately, the first half of the 2004–05 rainy season in southern Tanzania began well, with above-normal precipitation in December 2004.

(ii) *Equatorial sector*

In the equatorial sector, both January and February 2004 were unseasonably wet, and in March much of the subregion received normal to above-normal rainfall. This enhancement of rainfall appeared to signal the onset of the long rains season, but an unprecedented dry spell in the first half of April disrupted the establishment of the season. Then, intense rainfall in the second half of April heralded the true onset of the long rains. Consequently, rainfall was poorly distributed in April: the eastern parts of Uganda and much of Kenya received rainfall in excess of 200 mm, while coastal areas and the eastern subregion recorded amounts below 50 mm. In the Coast, Eastern, North Eastern, and Rift Valley provinces of Kenya, precipitation ended early and accumulations were well below normal in most areas; many stations recorded March–May totals that were no more than 50% of normal (Fig. 6.27).

The largest deficits of the season were in May, when abnormally dry conditions were found throughout the GHA region. Western and central Kenya and

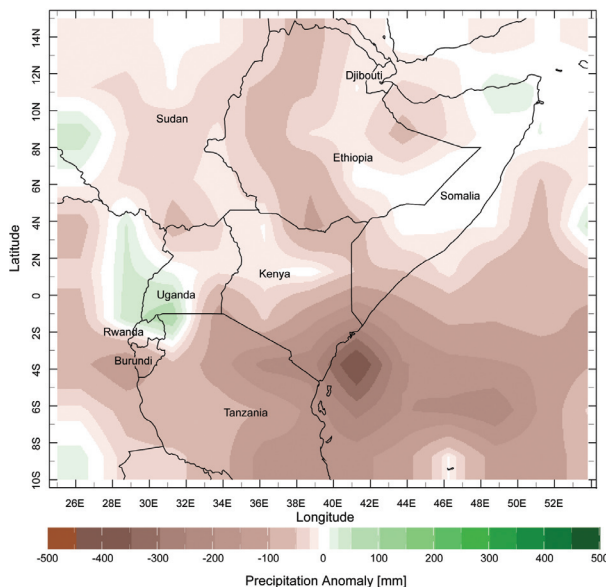


FIG. 6.27. Mar–May 2004 precipitation anomalies (mm) during the long rains season for the Greater Horn of Africa. Anomalies were determined with respect to the 1979–2000 base period means (CAM5_OPI data courtesy of NOAA/CPC).

parts of Uganda had normal-to-wet conditions by the first half of May, but the long rains ended by the second half of the month. In fact, coastal Kenya and isolated areas of Uganda reported the driest conditions on record since 1961. The government of Kenya declared the drought situation a “national disaster,” and the World Food Programme (WFP) made plans to feed the about 1.8 million affected people. In spite of the anomalously dry long rains season, heavy rainfall events during April in Kenya were responsible for floods and landslides, especially in southern and western sections of the country.

As expected, dry conditions persisted through the summer over most parts of the equatorial sector. Rainfall was also suppressed in areas bordering Lake Victoria, where significant rainfall is normally expected from June to August; these locations reported rainfall below 75% of the long-term means. Longer-term dry conditions allowed water levels in the lake to fall to 10-yr lows in 2004. Below-average rainfall in river basins that serve southern Sudan also resulted in lower-than-normal seasonal flood levels in 2004.

The short rains of October–December 2004 brought much-needed precipitation to sections of southern Ethiopia, southern Somalia, and northern and eastern Kenya (not shown). The eastern equatorial areas had above-normal rainfall during the short rains season, with flood damage occurring in much of the equatorial subregion.

(iii) Northern sector

The rainy season began later than usual in May for the northern sector, which resulted in abnormally dry conditions. For example, isolated areas in northern and southern Ethiopia experienced their driest conditions on record for the month since 1961. The rest of the season was generally wetter than normal in the southwest, but was characteristically dry in the eastern and northern parts of the subregion. Overall, the June through August rainfall totals (not shown) indicated that the subregion had slightly below average summer rainfall.

A most notable development in the northern GHA was the improved rainfall in the last half of 2004 in northern Somalia, where 4 yr of drought has devastated the region. Improved June–September rains in some areas of the Ethiopian Highlands in 2004 contributed to an estimated 24% increase in food production in Ethiopia, compared to 2003 (FAO 2004). In Eritrea, however, poor June–September precipitation was blamed for a cereal harvest that was expected to be only about half of normal and 20% below the previous year’s harvest.

IV) SOUTHERN AFRICA—W. M. Thiaw,⁴ B. Garanganga,¹⁸ W. Landman,²⁴ and M. A. Fortune¹⁷

The rainy season in southern Africa extends from October to April, with the largest amounts typically observed from December to March. During the austral winter, from mid-April to September, the region experiences generally dry weather. Southern Africa rainfall tends to be deficient during El Niños, and abundant during La Niñas (Ropelewski and Halpert 1987, 1989, 1996; Hastenrath 1995; Dai et al. 1997; Thiaw et al. 1999). Despite neutral ENSO conditions during the latter half of 2003 and the first half of 2004, rainfall was below normal across most of the eastern half of southern Africa, and strong intraseasonal variability played a significant role in the 2003–04 rainfall season in southern Africa.

(i) 2003–04 rainy season

The 2003–04 rainy season in southern Africa was characterized by below-normal rainfall in the climatologically wet areas, including portions of northeastern South Africa, southern and central Mozambique, and most of Zimbabwe. The seasonal rainfall was in the 10th–30th percentile in northeastern South Africa and the western half of Zimbabwe (Fig. 6.28). The climatologically dry areas of the region registered normal to above-normal rainfall amounts in the 60th–90th percentile across southern Namibia and western Botswana. Near-normal conditions prevailed

elsewhere. Overall, the onset of the 2003–04 rainy season was once again delayed in October 2003, as in the previous year. The dryness persisted through December 2003. However, above-normal rainfall prevailed across the region in the remainder of the season, with the March 2004 rains above the 90th percentile in the historical record.

After a generally dry first half of the season (October–December 2003), the second half (January–March 2004) was characterized by normal to above-normal rainfall (not shown). Amounts exceeding 500 mm occurred across northern Zimbabwe through Zambia to southern Tanzania, Malawi, and northeast and northwest sections of the Democratic Republic of Congo. Much of Mozambique had rains in excess of 400 mm, and the Indian Ocean islands of Mauritius and Seychelles also registered rainfall surpluses, with amounts exceeding 600 mm. In March, tropical cyclones were contributing to the above-normal seasonal precipitation along the east coast. Even the traditionally drier southwest had unusually wetter-than-normal conditions during this period. However, for agricultural activities the rains came too late, especially in southern Malawi and northern Mozambique.

In South Africa, the 2003–04 rainfall season ended on a high note, with widespread rains over the summer rainfall regions, so that the larger part of the country received between 75% and 125% of the January–March 2003 seasonal rainfall, and some areas over the northeastern interior received more than 175% of the January–March mean. Although above-average rainfall was observed over the northeastern parts of South Africa, the southwestern cape areas, though predominantly a region of winter rainfall, continued to experience drought conditions.

The dry conditions in South Africa prevailed through the winter, but relief came during the spring. However, most of the rainfall in the spring and early summer in the southwestern cape fell in a few isolated events. Although these events contributed significantly to the season’s rainfall, they did not occur over the primary reservoir drainage basins, and, thus, water levels in the areas reservoirs began to drop. Below-normal rainfall during the following winter resulted in reservoir water levels not being replenished.

(ii) *Atmospheric circulation*

The low-level atmospheric circulation for the 2003–04 rainy season featured easterly winds that averaged about 4 m s^{-1} (not shown) from the Indian Ocean westward into Madagascar and interior southern Africa. This flow was very close to the climatological mean wind in the region for this season.

The significant rainfall deficits in November–December 2003 were associated with weak anomalous westerly flow (less than 2 m s^{-1}) from the southern Atlantic into southern Africa (not shown), and near-average surface high pressure in the South Indian Ocean. Moreover, a blocking pattern with intense subsidence and above-normal heights across the southern Atlantic and Indian Oceans prevented a strong mid-latitude trough south of the Cape of Good Hope from entering the continent. This pattern suppressed convection over southern Africa during this period.

In contrast, during January and March of 2004 rainfall was abundant in the 75th and 95th percentiles in these 2 months, due to an anomalous trough at 500 hPa that was centered just off of the west coast of South Africa (Fig. 6.29). There was also an associated low-level cyclonic circulation (not shown), which favored the intrusion of midlatitude disturbances into the region. All of these factors contributed to intense rainfall across southern Africa. Note that Tropical Cyclone Elita (see section 4brv), which made landfall along the west shores of Madagascar in late January 2004, contributed to the enhanced rainfall along the east coast of southern Africa.

(iii) *2004–05 rainy season*

The first half of the 2004–05 rainy season (October–December 2004) was characterized by a late start and significant rainfall deficits across the southern half of the region. The dry conditions persisted from

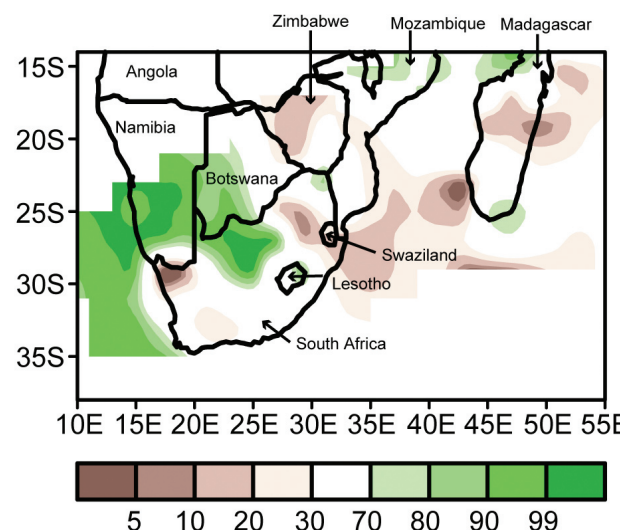


FIG. 6.28. Percent of normal precipitation during the Oct 2003–Apr 2004 rainy season across southern Africa (CAM5_OPI data courtesy of NOAA/CPC).

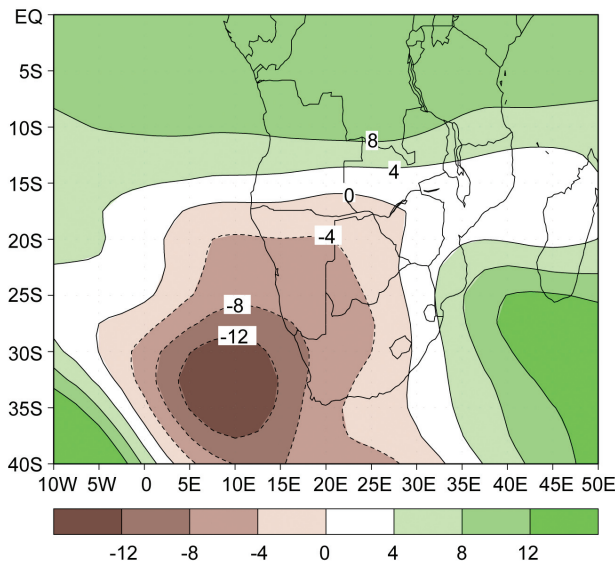


FIG. 6.29. The 500-hPa geopotential height anomalies (dam) in Jan–Mar 2004 over southern Africa (courtesy of NOAA/CPC).

October through mid-November, followed by a brief recovery.

The rains in the north began in earnest in November, with this region recording rainfall in excess of 90 mm in the last 10 days. In contrast, the whole southern half of the region had below-normal rains in November. Overall, the southern half of the region experienced below-normal rainfall during October–December 2004, while the northern half had above-normal rains (Fig. 6.30). Rainfall amounts ranged between 100 and 200 mm in the south, to between 100 and 400 mm in the central sector, and from 400 to over 600 mm in the northern sectors. Less than 65% of normal rainfall was received over much of the central and southern sectors. Normal to above-normal rainfall fell over the northern and northeastern tier of the region, as Malawi and northern Mozambique were once again wetter than normal, with rainfall totals above 600 mm—over 200 mm more than the 1961–90 mean.

The start of the 2004–05 austral summer coincided with the start of a weak El Niño event, which caused dry conditions during the first few months of the normal rainy season over most of the summer rainfall regions. Rainfall increased toward the end of the year in South Africa, as much of the summer rainfall region received from 75% to 125% of the seasonal mean during October–December. The high rainfall at the end of 2004 can be partially attributed to warm SST anomalies over the southwestern Indian Ocean. Nevertheless, in the South

African areas of the Free State, the Northern Cape, and some low-lying areas of the northeastern interior still received less than 75% of the October–December mean rainfall.

f. Asia

i) CHINA—P. Zhai⁴² and X. Zou⁴²

(i) Temperature

The majority of China had near-normal or above-normal temperatures in 2004. For the country as a whole in 2004, the annual mean temperature anomaly was 0.8°C above the 1971–2000 base period mean (Fig. 6.31), which was the eighth consecutive year of warmer-than-normal temperatures that began in 1997. In addition, the annual mean temperature in 2004 was among the four highest over the 1951–2004 period, but was below the record warmest year of 1998.

Regionally, annual temperatures were 1°–2°C above normal in 2004 in northeast China, the lower reaches of the Yangtze River, and the western part of northwest China. Near-normal annual temperatures were observed across the other regions of the country (Fig. 6.32). Warmer-than-normal temperatures were observed in all four seasons, especially during the 2003/04 winter (December–February). In fact, the 2003/04 winter in China was the third warmest on

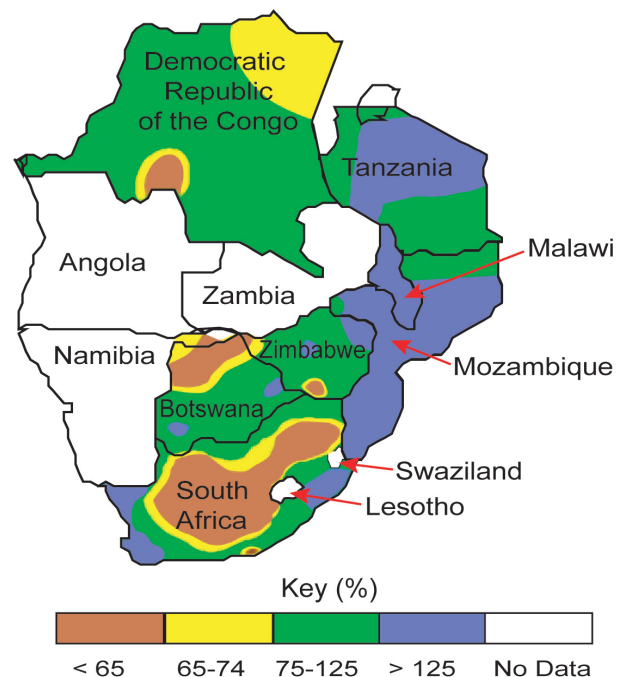


FIG. 6.30. The percent of normal precipitation during the first half of the 2004–05 rainy season (Oct–Dec) across southern Africa [courtesy of the Drought Monitoring Centre (DMC) Harare].

record, and the fourth consecutive warmer-than-normal winter since 2000/01.

(ii) Precipitation and droughts

It was an anomalously dry year across China as a whole in 2004, with a deficit of 22 mm below the 1971–2000 base period mean (Fig. 6.33). The central parts of northeast China, the southern sections of south China, and southeastern Xinjiang Province were particularly dry, having received only 50%–70% of their mean annual rainfall.

Spring droughts developed quickly and expanded across much of northern China from March to mid-April. Persistent rainfall deficits, along with warmer-than-average temperatures, significantly impeded the growth of crops in the region. Excessive precipitation in late April alleviated the drought conditions across much of northern China, while a severe-to-extreme drought continued across the central and western part of northeast China—widely regarded as the worst drought since 1951. These regions in northeast China had their driest January to mid-June period on record. The impacts of the spring drought in northeast China were so severe that over 6.5 million ha (> 16 million ac) were affected (source: Ministry of Civil Affairs of China).

At the beginning of autumn, an extended period of dry weather brought drought conditions to southern China. In October, the situation became more serious, with less than 10 mm of rainfall averaged across the region. Drought conditions quickly expanded and intensified across much of the middle and lower reaches of the Yangtze River and south China. The accumulated precipitation in most of these regions was 30%–80% below normal during the period from September to early November. In early and mid-November, from 50 to over 150 mm of precipitation brought some drought relief to the middle and lower reaches of the Yangtze River, as well as the northern part of south China, although severe drought conditions persisted in the central and southern sections of south China.

(iii) Floods and heavy rainstorms

Although there was no widespread flood event on China’s main rivers in 2004, regional heavy rains and storm-triggered landslides and mudflows still brought serious damage to some territories. For example, heavy downpours pounded central China and Guangxi Province (in south China) during the period of 14–21 July, which swelled rivers and generated flooding, killing at least 95 people during this event. During 3–6 September, a total of 187 people lost their

lives due to heavy rains and landslides in Sichuan Province and Chongqing. On 9–10 November, torrential rains fell on the cities of Wenzhou and Taizhou in the Chinese eastern border province of Zhejiang. In Wenling station, 253.1 mm of precipitation fell within 24 h, which broke the November record for the province. According to official statistics, 1477 people lost their lives due to rainstorms, floods, rain-related landslides, and mudflows during 2004 (source: Ministry of Civil Affairs of China).

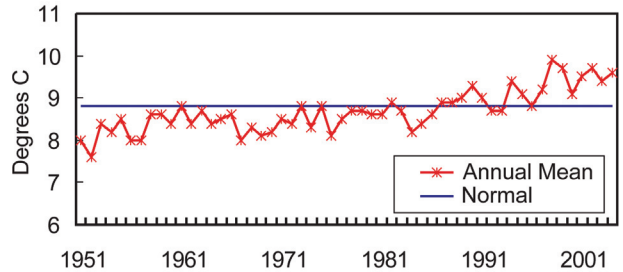


FIG. 6.31. The mean annual temperature (°C) averaged over China from 1951 through 2004. The black line denotes the 1971–2000 base period mean temperature.

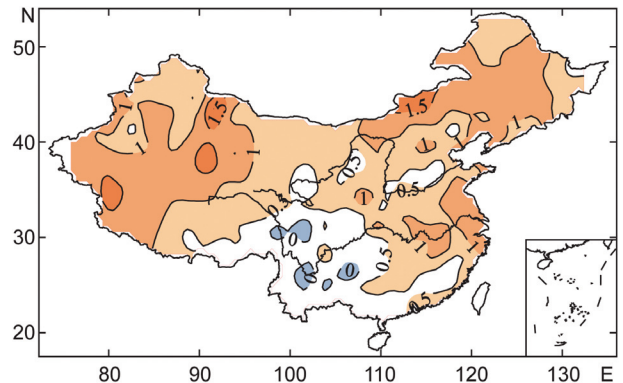


FIG. 6.32. The annual surface air temperature departures (°C) across China in 2004. The annual departures were determined with respect to the 1971–2000 base period means.

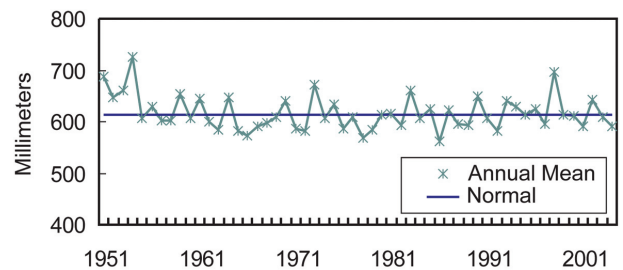


FIG. 6.33. The annual mean precipitation totals (mm) across China from 1951 through 2004. The black line denotes the 1971–2000 base period mean precipitation.

(iv) Typhoons

There were eight landfalling typhoons and tropical storms along the southeastern coast of China in 2004. During the period of 12–14 August 2004, Typhoon Ranim ravaged Zhejiang Province, with a maximum wind speed about 45 m s^{-1} when it made landfall at Wenling on 12 August. Ranim was the worst typhoon to hit Zhejiang since 1957 (second only to the unnamed typhoon that landed on the Xiangshan county of Zhejiang on 1 August 1956), and also was the worst to hit China since 1997. It brought heavy rains to Zhejiang, Fujian, Jiangxi, Anhui, and Hubei Provinces. At least 169 people lost their lives, and millions of people were evacuated from their homes. The accompanying strong winds, torrential rainfall, and significant flooding caused more than 2.4 billion U.S. dollars in direct economic losses, of which Zhejiang suffered the most damage (source: Ministry of Civil Affairs of China).

(v) Dust storms

A total of 19 dust storms occurred in China during 2004, which were more frequent than in 2003. Of particular note was the period of 26–28 March 2004, when an unusually strong dust storm swept over most of northern China, especially impacting the central Inner Mongolia region. This event increased the difficulty of the disaster relief efforts associated with an earthquake that occurred in the region on 25 March, in the areas of the northern autonomous region.

ii) SOUTHWEST ASIA—F. Rahimzadeh,²⁹ A. Taghipour,³⁹ and E. K. Grover-Kopec⁵

Most of the landscape of Southwest Asia is semi-arid steppe, and generally receives the majority of its annual precipitation from extratropical disturbances traveling eastward from the Mediterranean Sea between November and April (Barlow et al. 2002). Precipitation during February–April is especially important to the annual accumulations in the central portion of the region. From July through August, the South Asian monsoon typically brings precipitation to southeastern portions of Afghanistan, but tends to suppress convective precipitation across areas farther north and west.

Precipitation totals were not uniformly distributed in 2004, but moderate precipitation predominated across large parts of Southwest Asia. As a weak El Niño developed in the central Pacific Ocean during mid-2004 (see section 4a), the entire region began to receive more rainfall, and both the annual and seasonal accumulations were near or above their long-term means. For the year as a whole, annual

precipitation accumulations were near normal for most of the region, with a few notable exceptions in Afghanistan and Iran [see sections 6fii(ii) and (iii) below, respectively]. In Tajikistan, despite annual precipitation accumulations that were primarily near average, parts of the country received nearly 300% of their normal precipitation during the spring (source: Tajik Meteorological Service).

As a result of the generally above-average annual precipitation in 2004, drought conditions dissipated over most of Southwest Asia. However, drought persisted in the southeast of Iran and western sections of Afghanistan and Pakistan for the seventh consecutive year. Coincidentally, floods were a constant threat across parts of Southwest Asia. The annual flooding, fed by heavy rainfall, left millions of people in dire need, as flood waters washed away homes, roads, and crops.

All of Southwest Asia experienced above-normal surface temperatures during 2004. Annual temperatures were 1° – 2.5°C above average across the region, with the largest departures observed in Uzbekistan and western Kazakhstan (Fig. 6.34). Most of the anomalously warm conditions occurred during both the January–March and August–November periods. Cooler-than-normal conditions (i.e., temperatures $\leq 1^{\circ}\text{C}$ below normal) were observed in Turkmenistan and Uzbekistan during April and July.

(i) Afghanistan

Climate conditions during the spring (March–May) adversely affected snowpack in the mountains

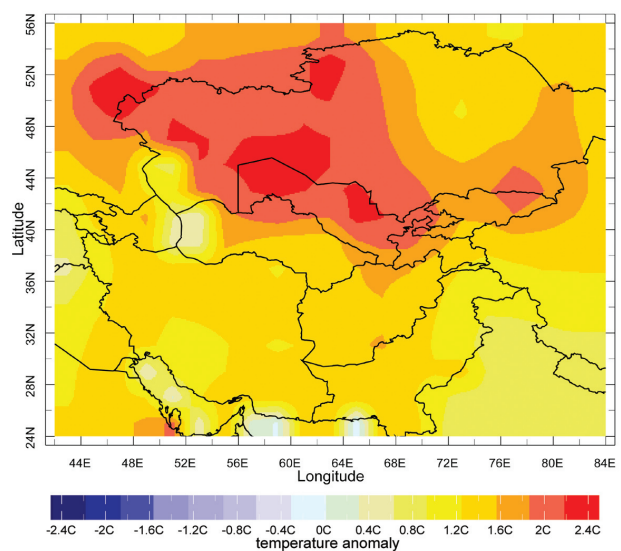


FIG. 6.34. The annual mean surface temperature anomalies ($^{\circ}\text{C}$) in 2004 across southwest Asia (CAM5 data courtesy of NOAA/CPC).

of Afghanistan, which provides most of the region's water supply. Temperatures in the mountainous northeast area averaged $\sim 4^{\circ}\text{C}$ above normal from January through March. In addition, precipitation during March and April, typically the wettest months of the year, was $\sim 80\%$ below normal in the northeast. These conditions combined to hasten the melting of the remaining snowpack from the winter of 2003/04, and hampered the buildup of new snowpack, thus, rendering poor water supplies for later in the year. The impacts of below-normal water resources were particularly severe in southern and northwestern Afghanistan—regions still recovering from the long-term drought of the late 1990s and early 2000s. Crop failures and dried-up rivers and wells were commonly reported in these areas (source: *New York Times*).

In contrast to the dry conditions that dominated the first half of 2004, the October–December period brought above-average precipitation to northern and western sections of Afghanistan (Fig. 6.35). Precipitation accumulations during these months exceeded the 90th percentile of the climatological mean, suggesting an early start to the 2004–05 rainy season across the country. For example, over 50 mm of precipitation fell in portions of the northeast during October, while nearly 100 mm of precipitation was observed in the extreme western part of the country during December.

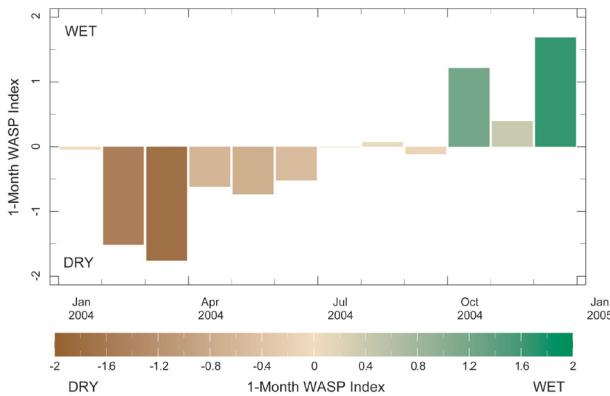


FIG. 6.35. National area-weighted average 1-month WASP Index for Afghanistan during 2004. Precipitation anomalies were determined from the 1979–2000 base period means (CAMS_OPI data courtesy of NOAA/CPC). The WASP Index is based on monthly precipitation and is computed using monthly anomalies, which were standardized by dividing by the standard deviation of the precipitation. The standardized monthly anomalies were then weighted by the fraction of the average annual precipitation for the given month. The value of the WASP Index is also standardized (Lyon 2004, 2005).

(ii) Iran

Anomalous warm temperatures were observed across Iran in 2004, with departures between 1° and 4°C above normal. Overall, the country was abnormally dry for the year, as some areas received only 20% of their normal annual precipitation. In addition, below-normal precipitation accumulations were recorded in northwestern Iran during February, March, and October. Climatologically, the northwestern region is the wettest part of the country, and receives on average approximately 500 mm of precipitation per year.

In contrast to the northwestern portion of the country, southwest Iran experienced abnormally wet conditions for much of 2004. Above-normal precipitation in January, April, June, July, and December contributed to annual accumulations that were about 125 mm above average, or 200% of normal levels. Monthly precipitation accumulations in southwestern Iran during December were in the 90th percentile of the climatological distribution. The resulting flooding caused approximately 4000 people to be displaced and 54 deaths (source: Dartmouth Flood Observatory).

From a seasonal perspective, mean temperatures were warmer than average across large parts of Iran during the 2003/04 winter (December–February; not shown), while an area from the southwest to northeast of the country received from 300%–800% of their long-term average precipitation (Fig. 6.36). In contrast, precipitation totals across the southeast of Iran were within 0%–20% of normal, where prolonged

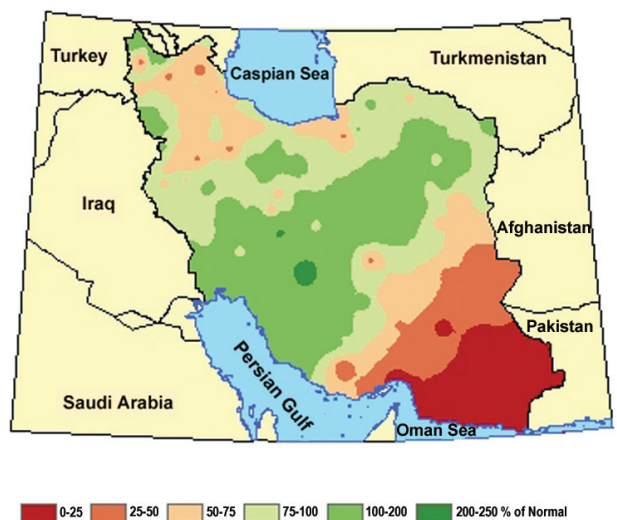


FIG. 6.36. The observed precipitation during winter for Iran, expressed as a percentage of the long-term mean [source: I.R. of the Iran Meteorological Organization (IRIMO)].

warm and dry conditions persisted for the seventh consecutive year.

In spring, temperatures were 4°C below the long-term mean in the western half of Iran, and up to 4°C above average in the eastern half of the country. For the season, most of Iran received more precipitation than the long-term mean (up to 224% of normal). However, a few stations in the southeast of the country had no measurable precipitation at all during spring, and, on average, the entire region received only 10 mm (3%–10% of normal). On an annual basis, precipitation decreased 27% with respect to 2003, and 3% compared to the long-term mean.

In summer, temperatures were 1°–2°C above normal over most parts of Iran, and the summer was also wetter than average. Figure 6.37 shows the summer precipitation anomalies across Iran. In general, conditions were wetter than normal during the summer, except over parts of the southeast and southwest.

Similar to the summer, autumn temperatures in 2004 were warmer than average across most of Iran. In addition, a majority of the country received above-average annual precipitation, except areas in the southeast. For example, the precipitation totals in Lorestan Province were ~300% of normal, while only 25%–50% of the average in the southeast and parts of central Iran

III) RUSSIA—O. N. Bulygina,⁸ N. N. Korshunova,⁸ and V. N. Razuvaev⁸

Surface temperatures across Russia were generally warmer than average in 2004. The mean annual air

temperature anomaly, averaged over the territory of Russia, was 0.9°C above the long-term mean, which was slightly less than the annual anomaly of 1.2°C measured in 2003. Since 1950, the annual trend in temperature across Russia has increased at approximately 0.3°C decade⁻¹. The following is a seasonal overview of the Russian climate during 2004 (see Fig. 6.38 for a map of the seven designated climatic regions in Russia).

(i) Winter

Most of Russia was warmer than usual in January 2004, with temperature anomalies varying from 2° to 5°C above average. The warmer-than-average temperature conditions were caused by frequent intrusions of Atlantic cyclones, which transported marine air masses inland as far as eastern Siberia and the republic of Yakutia-Sakha. These intrusions also brought moisture and abundant precipitation throughout European Russia in January, as well as to parts of the Far East (Fig. 6.39). In the Orlov region, monthly precipitation was 250% of normal, while the eastern section of Kamchatka received 338% of the average monthly precipitation. In Moscow, the largest amount of January precipitation was reported since records began in 1891 (Fig. 6.39)—88 mm of monthly precipitation (~210% of normal).

In February, abundant precipitation was measured throughout European Russia, western and eastern Siberia (except for the far northern section), the Maritime Territory, and the Amur region (Fig. 6.39). In the Voronezh and Belgorod regions, and the Kras-

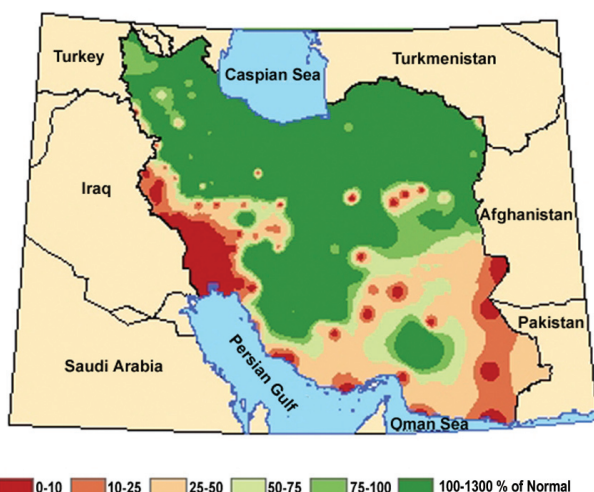


FIG. 6.37. The observed precipitation during summer for Iran, expressed as a percentage of the long-term mean (source: IRIMO).



FIG. 6.38. Map of the seven quasi-homogeneous climatic regions within Russia: (I) the northern part of European Russia and western Siberia, (II) the northern part of eastern Siberia and Yakutia, (III) Chukotka and Kamchatka, (IV) the central and southern parts of European Russia, (V) the central and southern parts of western Siberia, (VI) the central and southern parts of eastern Siberia, and (VII) the Far East.

nodar Territory, monthly precipitation was nearly 2.5 times above the long-term average, while the Rostov region received almost 3 times their monthly normal precipitation (282%). As for temperature, the highest positive anomalies were observed in western Siberia and in the south of eastern Siberia. In contrast, in the north of eastern Siberia temperature anomalies were 8°C below normal.

(ii) *Spring*

Colder-than-average conditions persisted in northern sections of western Siberia during March, as monthly air temperature anomalies were below the long-term average. In European Russia, the southern section of eastern Siberia, and the Far East, temperatures were 2°–4°C warmer than normal. Against the background of positive temperature anomalies in Kamchatka, monthly precipitation was 2.5 times above normal in March, while approximately 3 times the average monthly precipitation fell in the Krasnodar Territory (280%) and the Amur region (320%).

April was cold over most of European Russia and in western Siberia (except for Kemerovo region and Altai Territory). Anomalously cold temperatures developed over western regions of the Khanty-Mansi Autonomous Area, where temperature anomalies exceeded –6°C. In the Altai Territory and Kemerovo region, rain showers persisted for up to 3 days (13–15 April), as some locations received 200%–300% of their normal precipitation. As a result, flooding occurred on the Upper Ob and Tom Rivers, with rising water levels of up to 2.6 m day⁻¹ reported.

Very warm conditions were observed in the Ural region during May. In the Sverdlovsk and Kurgan regions, mean monthly temperatures were 4°–5°C above normal. In both the cities of Omsk and Krasnoyarsk, the highest air temperature in the last 100 yr was recorded during the month. Temperatures were also very warm across most of western Siberia, with daily maximum temperatures of 32°–38°C across southern sections of the region. In many of the cities in the Novosibirsk region and Altai Territory, monthly mean temperatures were the highest since records began. The anomalously warm weather was accompanied by precipitation deficits across these areas (10%–40% of the monthly means), which increased the fire hazard to extreme levels and helped trigger forest fires. Wildland fires were recorded in the Sverdlovsk and Chelyabinsk regions, while the worst fire conditions were reported in the Kurgan region. Forest fires were also reported in the Novosibirsk region, Altai Territory, and Republic of Altai during May.

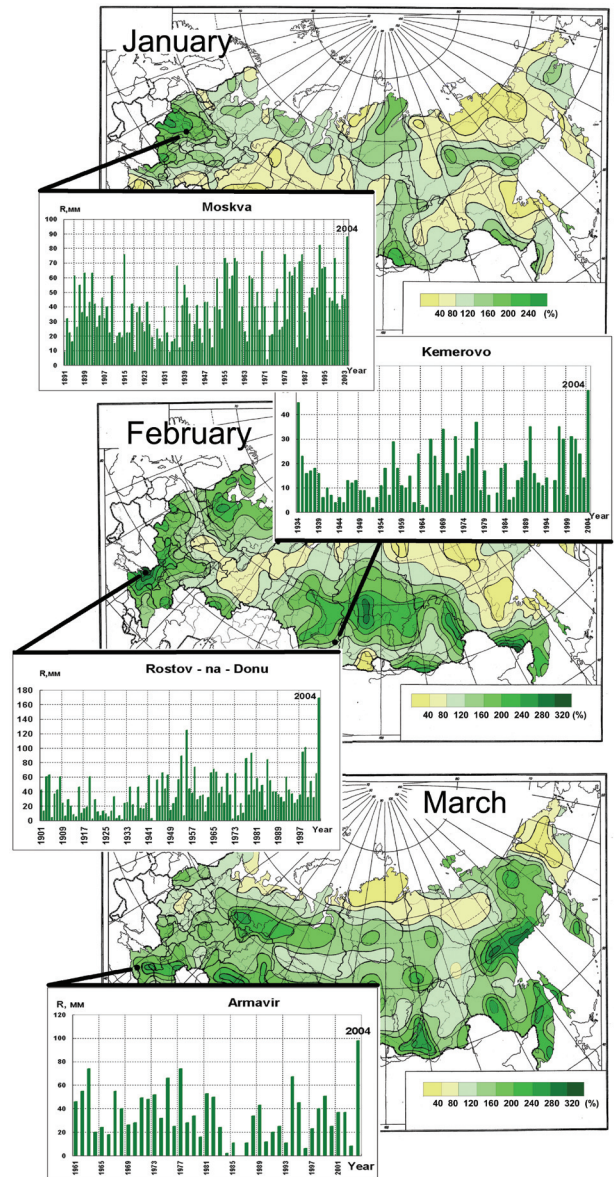


Fig. 6.39. Percent of monthly precipitation in 2004: (top) Jan, (middle) Feb, and (bottom) Mar. Inset graphs: the record wet conditions at specific sites (Moskva, Kemerovo, Rostov-na-Donu, and Armavir).

(iii) *Summer*

Severe weather affected European Russia and the Far East during the summer months. For example, during the first 10-day period of June, heavy rain with 30 mm of hail was recorded in the Northern Caucasus. Frequent and intense rainfall during the month brought flooding to the rivers of the Northern Caucasus, along with debris and mudflows to the mountains. In July, unusual thunderstorm activity was reported in European Russia, accompanied by showers, squalls, and hail. On 5–6 July, Typhoon Mindulle struck the Maritime Territory on the Pa-

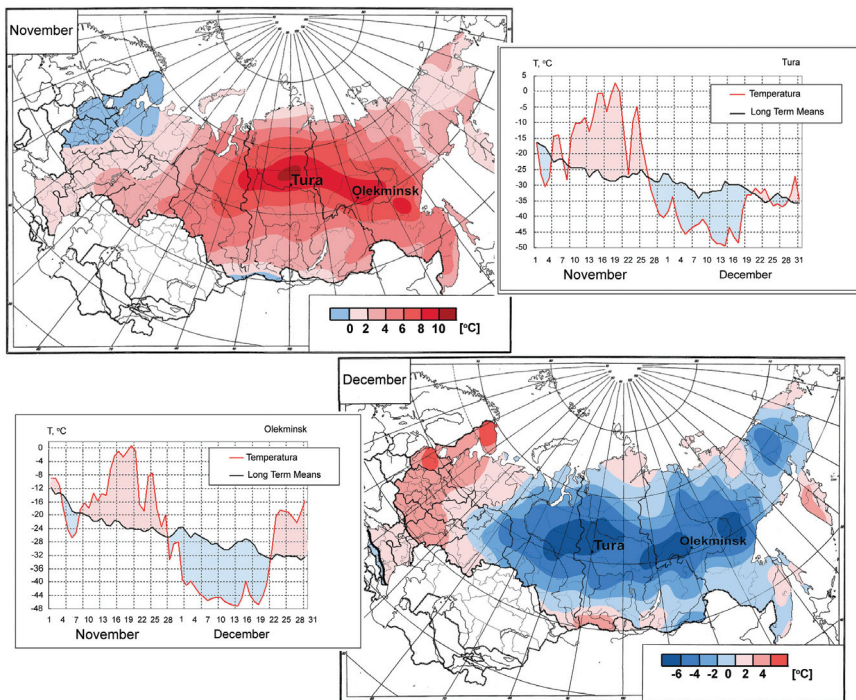


FIG. 6.40. Monthly surface air temperature anomalies (departures from long-term averages (°C) for 2004: (top) Nov, and (bottom) Dec. Inset graphs: mean daily air temperature (black line) and the daily mean temperature during Nov and Dec at Tura and Olekminsk meteorological stations.

cific coast, bringing heavy rains and hurricane-force winds (~32–34 m s⁻¹; ~62–66 kt) to the region [see section 4bii(i)].

In August, air temperatures in Russia were near the long-term average, while the largest precipitation anomalies were measured in the Northern Caucasus region. Twice in August (during both the 10th–12th and the 19th–21st of the month) showers accompanied by hail and wind gusts of up to 23–28 m s⁻¹ were reported. These events led to flooding on the Terek, Laba, and Upper Kuban Rivers, and mudflows in the mountains of northern Osetia.

(iv) Autumn

Over most of the territory of Russia in early autumn temperatures were near normal. The only exceptions were in European Russia (the Northeast, Middle Volga, and Orenburg regions), and the Chukotka and Khabarovsk Territory, where temperatures were 2°C above normal. Typhoon Songda impacted the southern sections of the Far East (the Maritime Territory and Sakhalin) in mid-September. In the city of Vladivostok, wind gusts associated with Songda were as strong as 28 m s⁻¹ (~54 kt), and in Sakhalin heavy rains caused rising water levels in the regions' rivers [see section 4bii(i)].

In October, surface air temperatures departures ~7°C below normal developed in Yakutia. In the Urals, record precipitation totals were reported as the region experienced heavy snowfall, accompanied by winds of up to 15–20 m s⁻¹ on 12–13 October. These storms developed much earlier than normal, as the frequency of snow occurrence in October in the Urals is typically only once in 5–6 yr. In Chelyabinsk, the snowfall was likely the heaviest in the last 30 yr, and in Ekaterinburg it was the heaviest snow event in the last 20 yr.

Above-average temperatures were observed over most of the territory of Russia in November (Fig. 6.40). The largest temperature anomalies occurred over the

Evenki autonomous area, where the monthly anomalies exceeded 10°C and the mean daily air temperatures were more than 20°C above the long-term average. Excessive precipitation was also observed during the month. For example, European Russia, the Krasnodar Territory, and Adygeia received from 46 to 239 mm of precipitation (300%–600% of their monthly means).

For Asian Russia, the end of the year was anomalously cold. Over most of the territory the surface air temperature was 4°–6°C below normal, and the coldest temperature anomalies reached –7.1°C in Tura and –7.4°C in Olekminsk (inset in Fig. 6.40). In Evenkia, a minimum daily air temperature below –52°C was reported during December.

IV) SOUTH ASIAN MONSOON— K. Rupa Kumar²³ and M. Rajeevan³⁰

The South Asian monsoon produced deficient rainfall in 2004, leading to drought conditions in several areas of the Indian subcontinent, particularly over the northwestern parts of the region. This closely followed another unanticipated failure of the Indian summer monsoon in 2002 (Lyon et al. 2003), intervened by a near-normal monsoon in 2003 (Kolli 2004) that provided relief to the region. However, the relief

was short lived, with the Indian summer monsoon rainfall (ISMR) recording 87% of the long period average (LPA) in 2004. Summer monsoon rainfall was also deficient in Pakistan and Sri Lanka, leading to drought conditions.

An important aspect of the monsoon was its early onset over the Indian subcontinent, but also its slow and interrupted progress toward northern parts of India. The early monsoon onset was associated with the formation of a tropical storm over the Bay of Bengal. A strong surge of monsoon westerlies associated with the tropical cyclone heralded the commencement of monsoon rains over the Kerala coast on 18 May, two weeks earlier than the normal date of onset. However, once the cyclone moved away and dissipated, further advance to the north did not take place until the first week of June. Afterward, the monsoon advanced rapidly, covering nearly two-thirds of the country by 18 June. Following this period of rapid advance, there was a lull in monsoon activity until the first week of July. This weak revival was not sustained for long, lasting only a couple of days. Ultimately, the monsoon covered all of south Asia by 18 July. Therefore, despite the early onset process in the initial stages in 2004, two fairly long-duration monsoon breaks occurred as the advance was halted twice—for about 17 days from 18 June to 4 July, and for 13 days from 5 July to 18 July. However, the redevelopment of the monsoon after both of these breaks was not strong enough to sustain rainfall activity in the north.

In 2004, summer monsoon rainfall over India was not uniformly distributed, both spatially and temporally. For example, the rainfall over the country as a whole was close to the average in June and August, but well below average in July and September (100% of the LPA in June, 83% in July, 95% in August, and 71% in September). In June, rainfall was uniformly distributed over the country. However, in July, which is typically the wettest month of the season, rainfall was confined only to southeastern parts of the country. Despite the development of three low pressure systems over Bay of Bengal during the month, none of these moved into the central and northwest parts of the country due to an anomalous anticyclonic circulation that persisted over northwest India. In August, rainfall activity had substantially expanded over central and northwest India due to several westward-propagating low pressure systems across the central parts of the country. In September, rainfall activity over the country was again suppressed, except over the southeastern parts.

There was a strong intraseasonal variation in the rainfall activity during the season, as shown in

Fig. 6.41. While rainfall activity over the country during the third and fourth weeks of June was above normal, it was suppressed for the following 5 weeks from late June to late July. By the end of July, cumulative seasonal rainfall dropped to 85% of the LPA. This rapid decline generated widespread concern across all sections of Indian society, with fears of a repeat of another severe drought similar to 2002. With the revival of monsoon rainfall in August, the situation improved as the cumulative seasonal rainfall increased to 94% of the LPA by 25 August. However, below-normal rainfall activity throughout September (with an overall monthly deficiency reaching 29%) led to an overall seasonal rainfall deficiency of 13%.

Monsoon low pressure systems and depressions that form over the northern Bay of Bengal, and move northwestward across the central parts of the subcontinent, typically contribute significant rainfall over the country. In the background of a significant decline in the number of monsoon depressions during the past few years, a welcome change in the 2004 monsoon was the formation of three deep depressions and one depression over land, which contributed a significant part of the summer monsoon rainfall (Fig. 6.42). In addition, nine areas of low pressure formed over the Bay of Bengal—four each in July and August and one in September. However, most of these low pressure systems remained weak and did not move into northwestern parts of the country, resulting in large rainfall deficiencies over this region.

The cumulative rainfall distribution across India in 2004 is shown in Fig. 6.43c, along with two recent years with deficient summer monsoon rainfall (2000

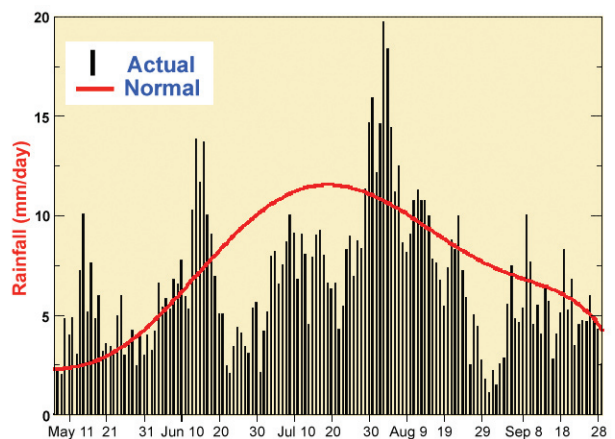


FIG. 6.41. The evolution of the all-India mean daily summer monsoon rainfall (mm day^{-1}), during Jun–Sep 2004. The smooth curve indicates the long-term average (source: Monsoon On-Line; <http://www.tropmet.res.in/~kolli/mol>).

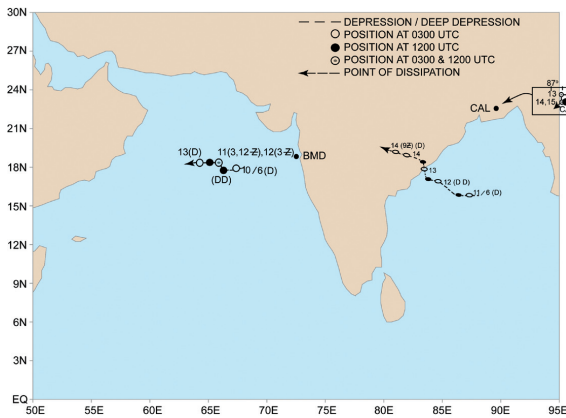


FIG. 6.42. The observed tracks of monsoon depressions that formed during 2004.

and 2002; Figs. 6.43a–b). The rainfall anomalies are depicted by a subdivision in six classes based on their respective standard deviations, ranging from deficient to excessive (-1σ through $+1\sigma$). It should be noted that, while the rainfall anomalies were negative across a major part of South Asia, severely deficient conditions were scattered, with mildly deficient conditions over a major part of the country in 2004 (Fig. 6.43c). In contrast to the severe drought in 2002 when rainfall deficits spread over the entire country (Fig. 6.43b), the 2004 monsoon, although technically termed a drought year, had only marginal impacts on various sectors. The largest negative rainfall anomaly in 2004 was observed over northwest India (-40%). The west coast region, covering the catchments of most Indian peninsular rivers, received copious rainfall, providing relief to the areas that have experienced water stress over the past 3–4 yr. The rainfall defi-

ciency over northeast India was only 6%, but this was likely a drought when considering the low variability in the region. Notwithstanding this deficiency, the Indian states of Assam and Meghalaya experienced severe floods, which highlights the role of intraseasonal variability. Out of the 524 meteorological districts in India, 57 (11%) received excess rainfall, 233 (45%) normal rainfall, 210 (41%) deficient rainfall, and 16 (3%) scanty rainfall.

The withdrawal of the monsoon was delayed in 2004, primarily due to the prevalence of an atmospheric circulation pattern that generated rainfall over northwest India until the end of September. The monsoon withdrew from extreme west Rajasthan on 24 September. It further withdrew from most parts of northwest India and parts of west-central India on the 27th.

Summer monsoon rainfall in 2004 was also deficient in Pakistan and Sri Lanka, leading to drought conditions in these countries. During the summer monsoon, Pakistan received only 59% of its normal rainfall. The rainfall deficiency was the largest over the Balochistan and Sindh Provinces, which caused a water crisis over these regions. Most of Sri Lanka has experienced drought conditions since the end of 2003, which were aggravated during the summer monsoon due to deficient rainfall.

On the other hand, the Asian summer monsoon during June–September brought heavy rain and flooding to parts of northeastern India, Nepal, and Bangladesh. Approximately 1800 deaths were blamed on flooding brought by heavy monsoon rains in these areas, while flooding in Bangladesh was the worst in over a decade.

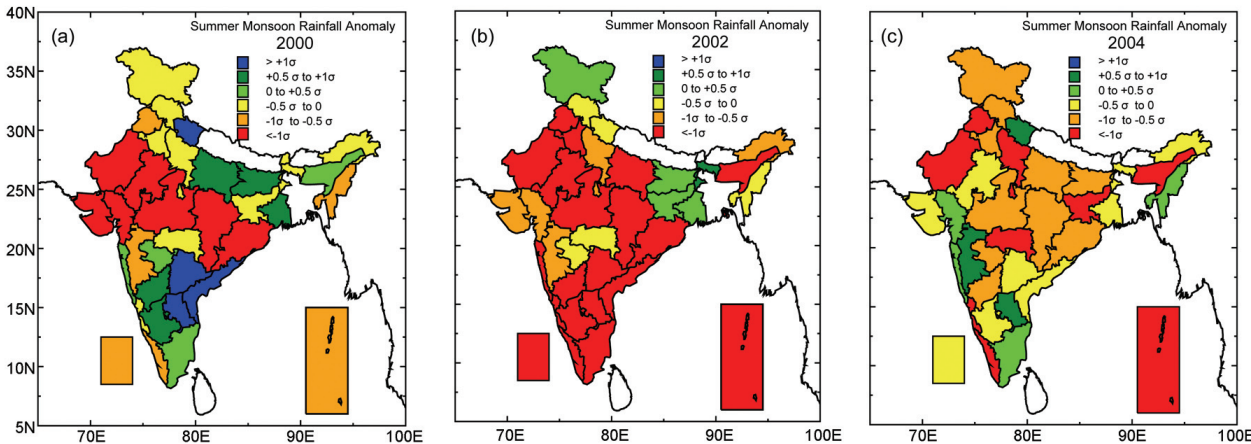


FIG. 6.43. Spatial distribution of summer monsoon seasonal rainfall anomalies in the last three deficient summer monsoon years: (a) 2000, (b) 2002 and (c) 2004. The classification is based on the standard deviations (σ) of the respective subdivisions.

The poor performance of the Indian monsoon was contrary to the official forecast for a near-normal monsoon issued by the India Meteorological Department (IMD). The causes of the poor monsoon performance in 2004 are currently not well understood. The simultaneous evolution of weak El Niño conditions over the equatorial central Pacific, the anomalous northward movement of typhoons over the Northwest Pacific, and southward intrusions of cold and dry midlatitude westerlies, especially in July, were blamed as the possible causes for the below-average monsoon rains this year. More specifically, the extremely poor monsoon performance in September (deficiency of 29%) may be attributed to the weak El Niño conditions that prevailed over the central Pacific.

g. Australasia and the southwest Pacific

1) AUSTRALIA—A. B. Watkins⁴¹ and B. Trewin⁴¹

Neutral to slightly warm conditions in both the equatorial Indian and Pacific Oceans resulted in competing influences upon the Australian climate in 2004. While warmer-than-normal conditions in the Indian Ocean typically encourage the formation of northwest cloud bands, which can bring rainfall to northwestern and southern Australia, warmer-than-normal conditions in the central to eastern equatorial Pacific Ocean tend to reduce the onshore flow of moisture, and, hence, rainfall, for the southern and eastern states.

During 2004, the northeastern Indian Ocean SSTs ranged from 0.9° (February) to 0°C (November) above normal^{6,3}, while the central tropical Pacific SSTs varied from 0.1° (March) to 0.9°C (September) above

the mean. Despite little atmospheric response directly over the warm anomalies in the equatorial Pacific, the warm SSTs in the Pacific may have hindered any significant recovery from long-term rainfall deficiencies for the eastern half of the continent, which generally received from average to below-average rainfall in 2004.

(i) Temperature

Daytime temperatures were generally above the mean for much of the eastern half of the continent, while minimum temperatures were mixed. The largest maximum temperature anomalies (Fig. 6.44) occurred inland of the central Queensland coast, with values as high as +2.0°C for the year, while much of Queensland experienced anomalies of +1°C or greater. This resulted in the fourth warmest annual maximum temperature anomaly on record for Queensland of +0.86°C (high quality, Australia-wide annual temperature records commenced in 1910). Similarly, eastern Australia was warm, with a maximum temperature anomaly of +0.86°C—the fourth warmest year since the commencement of seasonal records in 1950. New South Wales also experienced very warm conditions during 2004, with a statewide anomaly of +1.10°C—its third warmest year on record. Tasmania was the only Australian state with an annual statewide maximum

^{6,3} The term “mean” or “normal” refers to the average calculated over the World Meteorological Organization standard base period of 1961–90. Similarly, all anomaly values are relative to the 1961–90 normal.

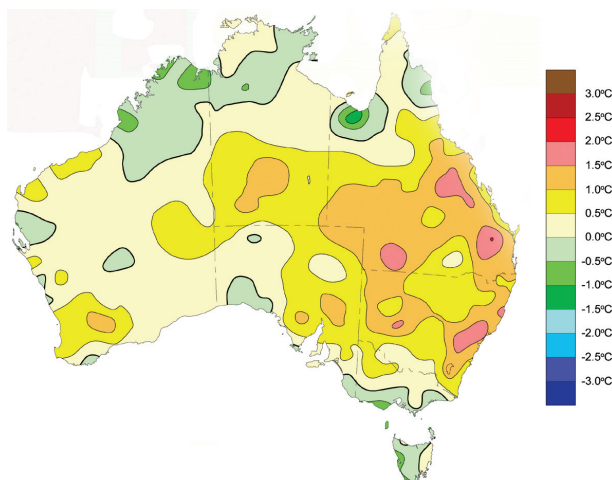


FIG. 6.44. Maximum temperature anomalies (°C) across Australia during 2004. Anomalies were determined with respect to the 1961–90 base period.

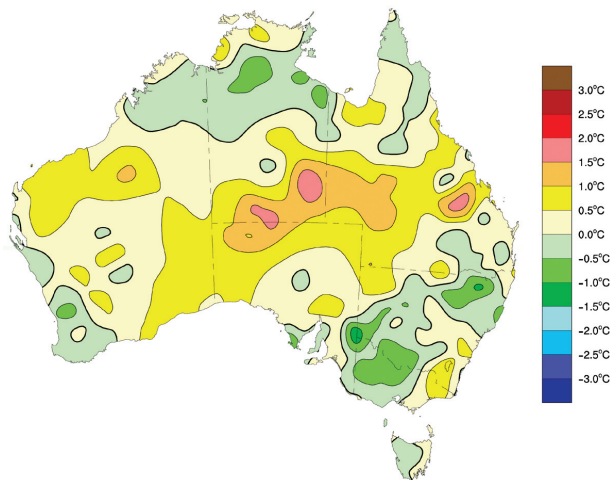


FIG. 6.45. Minimum temperature anomalies (°C) across Australia during 2004. Anomalies were determined with respect to the 1961–90 base period.

temperature for the year that was below normal (-0.09°C). Overall, 2004 maximum temperatures were 0.53°C above the 1961–90 mean, resulting in the eighth warmest daytime temperatures since 1950.

Generally cooler minimum temperatures (Fig. 6.45) over New South Wales reflected the dry conditions, because cloud cover was reduced and daytime heat was rapidly radiated to space at night. The exceptions, however, were over regions near the Australian Capital Territory (ACT), which experienced warmer-than-normal nights, as did most of the central Queensland coast. For some areas in Queensland, minimum temperature anomalies were as high as $+1.5^{\circ}\text{C}$. Anomalies of a similar magnitude were also observed in the southern parts of the Northern Territory. In general, however, most states had minimum temperatures near their long-term mean, which was reflected by the Australia-wide minimum temperature anomaly of $+0.27^{\circ}\text{C}$ —the fourth warmest since 1950. Overall, the mean Australia-wide annual temperature anomaly of $+0.40^{\circ}\text{C}$ in 2004 was the 10th warmest since 1910.

(ii) *Precipitation*

For the eastern half of Queensland, winter was particularly dry, with rainfall in the lowest 10% of recorded totals (i.e., decile 1). This resulted in a state-wide average rainfall of only 13.9 mm for winter—the fifth driest on record (high-quality rainfall records commenced in 1900). Similarly, southern New South Wales, the Australian Capital Territory, and northern Victoria experienced decile 1 (and for the ACT, the lowest on record) rainfall during autumn. In the nation’s capital, Canberra, the January–July total of only 106 mm was 69% below the long-term average.

In contrast, spring, the season with the strongest east Australian rainfall relationship to Pacific Ocean temperatures, brought average to above-average rainfall to most parts of eastern Australia despite the anomalously warm SSTs in the Pacific basin.

For Australia’s western half, dry conditions were experienced in the southwest, while inland and to the north above-average rainfall dominated. In the southwest part of western Australia, rainfall in 2004 was below the long-term average (13th driest since 1900)—a continuation of the trend observed since the mid-1970s when a shift to consistently drier-than-normal winter conditions first occurred. For 2004, rainfall in southwest Western Australian was anomalously low during autumn and early winter. It has been suggested that this long-term shift in the region is consistent with a combination of natural variability and anthropogenic climate change (IOCI 2002; Pitman et al. 2004).

The dry conditions in the southwest were in stark contrast to the well above average rainfall totals experienced over the inland and northwest section of Western Australia, as well as for large parts of the Northern Territory. This was partly due to a monsoon depression that moved over the Pilbara and Gascoyne regions, as well as Tropical Cyclone Monty in February, followed by Fay in March (see section 4bIII). Wet conditions also occurred during May, which were the result of a number of cold fronts that stalled over the inland. The wetter-than-normal conditions for inland and northern Western Australia during 2004 closely matches the spatial pattern of the trend in increasing rainfall observed since 1950.

The large region of above-average rainfall over much of Western and inland Australia led to 64.9%

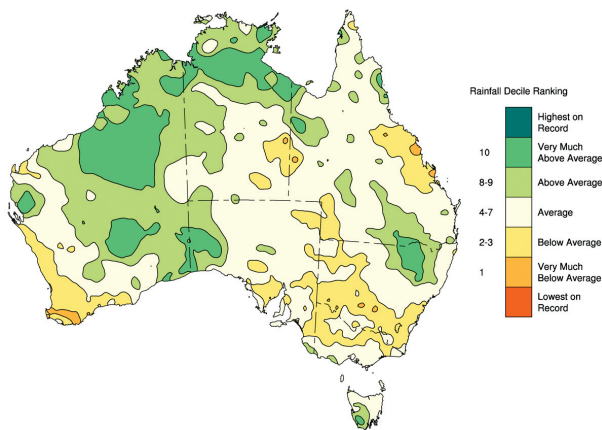


FIG. 6.46. Rainfall deciles across Australia for the period 1 Jan through 31 Dec 2004.

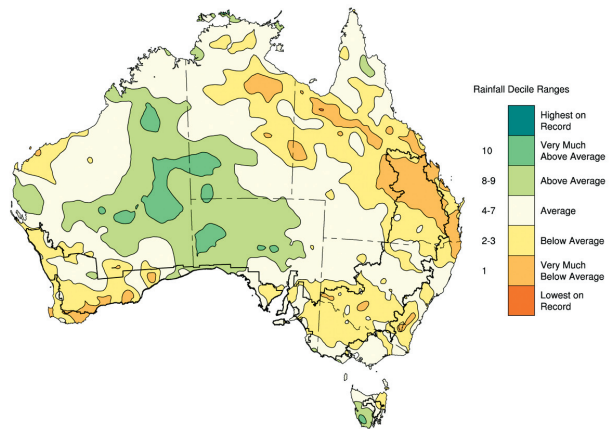


FIG. 6.47. Rainfall deciles for the Australian cropping season (Apr–Oct, inclusive) in 2004 (crop-growing regions are outlined in bold).

of the Australian continent receiving above-normal rainfall, with a mean percentile value of 61. The resulting Australia-wide mean rainfall total for 2004 was 513 mm (Fig. 6.46), making 2004 the 25th wettest year since records commenced in 1900 (the 1961–90 mean for Australia is 472 mm).

For Australia's main crop and pasture growing season from April to October (Fig. 6.47), the Australia-wide average rainfall was 141 mm, which made 2004 the 39th driest growing season since records commenced in 1900. However, eastern Australia was drier in comparative terms than the continent as a whole, recording its 14th driest season on record, with an average of only 167 mm.

Australia's cropping regions were equally dry. The average annual rainfall for the cropping zone (see Fig. 6.47) was 214 mm for the April–October period, making 2004 the 15th driest cropping season since records commenced in 1900. Interestingly, the eight driest cropping seasons have all coincided with El Niño events (1994, 1982, 1902, 1940, 2002, 1914, 1957, 1946), as did 11 of the driest 15 seasons.

ii) NEW ZEALAND—M. J. Salinger³⁶

The nationally averaged temperature in 2004, calculated by New Zealand's NIWA, was 12.3°C, which was 0.3°C below the 1971–2000 normal, and the lowest since 1993. For New Zealand as a whole, there were seven cooler-than-average months (February through April, July through September, and December), four warmer-than-average months (January, May, June, and November), and one month with mean temperatures close to the climatological average (October). The warmest locale was Whangarei, with a mean temperature for the year of 15.3°C (0.3°C below average). Sunshine hours were more than 105% of normal in coastal Otago; less than 95% of normal in Waikato, Taupo, Manawatu, south Taranaki, and the Southern Lakes; and were near normal in all other regions.

In 2004, more low pressure systems over and east of the South Island prevailed during the year, with stronger westerly and southwesterly flow over the country (Fig. 6.48). Anticyclones were prevalent in January, which lead to warmer-than-average conditions. However, this mild pattern gave way to very stormy westerly and southwesterly flow across the country, which produced the most extreme rainfall and flooding experienced in the Manawatu–Taranaki area since at least the 1920s. Anticyclones predominated in April and July, with northerlies or northwesterlies in May and June. Strong southwesterlies, and deep extratropical depressions in the Chatham Islands area,

dominated the remainder of the year from August through to December. The persistent southwesterly flow anomalies were, in part, the result of the weak El Niño that prevailed in the equatorial Pacific from August onward (see section 4a for details).

At many sites, the year was one of the wettest on record, especially in parts of the Bay of Plenty, Manawatu, Kapiti, Upper Hutt, and the Wairarapa. Rainfall was more than 125% of normal in Manawatu, Wanganui, the eastern Bay of Plenty, Horowhenua, and Wairarapa, and at least 110% of normal in Waikato, King Country, south Taranaki, Wellington, the western Bay of Plenty, Gisborne, Nelson, and Southland. Anomalously dry conditions, with rainfall totals only 75% to 90% of average, were measured in coastal Marlborough and eastern Otago.

A number of extreme events occurred in New Zealand in 2004. The year began with very high temperatures accompanied by strong winds, which produced forest fires in early January in Canterbury. These gave way to record rainfall in Taranaki–Wanganui, which produced flooding by the end of February. June was anomalously warm, and July brought more flooding in the Bay of Plenty, while the south stayed anomalously dry. Persistent cold southerlies in August produced blizzards and high winds, as the cold and stormy weather dominated the remainder of the year. December was unusually cold, and measured the strongest southerly circulation over the New Zealand region for any calendar month on record.

iii) SOUTHWEST PACIFIC—M. J. Salinger³⁶

Conditions associated with the ENSO evolved from a neutral state during the first half of the year, to a weak El Niño event in the central equatorial Pacific

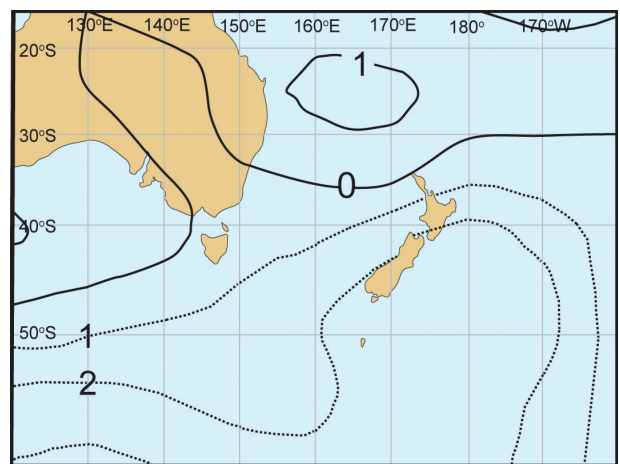


FIG. 6.48. MSLP anomaly map for 2004 for the New Zealand region showing departures from average in hPa.

in the second half of the year (Fig. 6.49; see section 4a for further details). The trade winds were near normal in strength at the start of the year, but equatorial westerly wind bursts occurred from June onward, and these often propagated westward to the date line. Apart from these events, and warmer temperatures for the region, El Niño had little impact on the climate of most southwest Pacific islands in 2004. However, much of New Caledonia and Vanuatu, and to a lesser extent, Fiji and Tonga, had several drier-than-normal months toward the end of the year.

The weak El Niño event was expressed more obviously in SST anomalies. Above-average SSTs occurred throughout the region during 2004 (Fig. 6.50): ~1.0°C above average around Western Kiribati, and 0.5°–0.9°C above average in many other island nations, especially those east of the date line. New Caledonia, Vanuatu, the main island of Fiji, and Tonga, were all surrounded by near-average SSTs.

As with SSTs, air temperatures were 0.5°C or more above average throughout much of the tropical southwest Pacific in 2004, especially along the equator from Nauru to western Kiribati where they were ~1.0°C above average (not shown). Air temperatures were near average in many areas southwest of the date line, including Vanuatu, New Caledonia, and parts of Fiji. It was also one of the warmest years on record at Fua'amotu Airport in southern Tonga,

where the mean air temperature was +0.7°C above average.

From April onward, mean sea level pressures (MSLPs) were generally above average west of the date line, and below average in the east (Fig. 6.48). Areas of enhanced convection affected the region in the vicinity and north of the Solomon Islands, and also near Pitcairn Island, while suppressed convection occurred along the equator and east of the date line. West of the date line, the SPCZ was a little further north and east than usual, especially during the first 6 months of 2004. East of the date line, the SPCZ was further north and east than usual during the first 4 months of the year, after which it remained south of its normal location. Atmospheric convection was slightly suppressed over Samoa and the Society Islands, which is atypical of the normal ENSO climate response.

The synoptic pattern associated with the SPCZ affected the year's rainfall distribution, which was ~110% of average over much of the Solomon Islands, Tonga, Niue, and parts of Tuvalu, and more than 150% of average in the Marquesas Islands of northern French Polynesia, as well as in Pitcairn Island. Rainfall was less than 80% of the average in parts of New Caledonia, and less than 90% of the average in Fiji's Western Division, parts of Samoa, and the Society Islands of central French Polynesia.

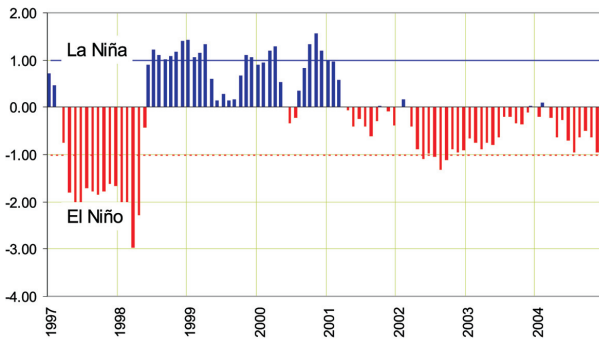


FIG. 6.49. The Southern Oscillation Index, which is the normalized pressure difference between Darwin, Australia, and Papeete, Tahiti. The index displayed neutral values for the first half of 2004, and then drifted negative into the weak El Niño range for the remainder of the year.

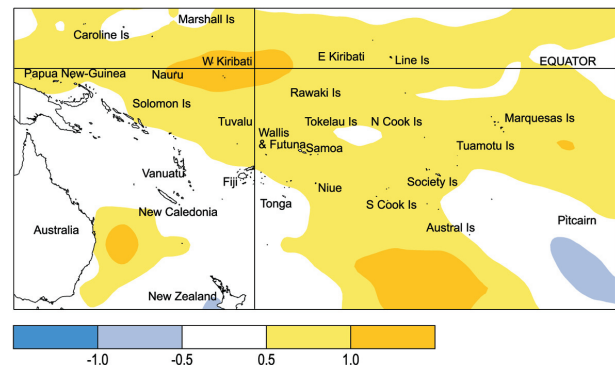


FIG. 6.50. SST anomalies (departure from average, in °C) for the southwest Pacific. Yellow- or orange-shaded areas represent warmer-than-average SSTs.

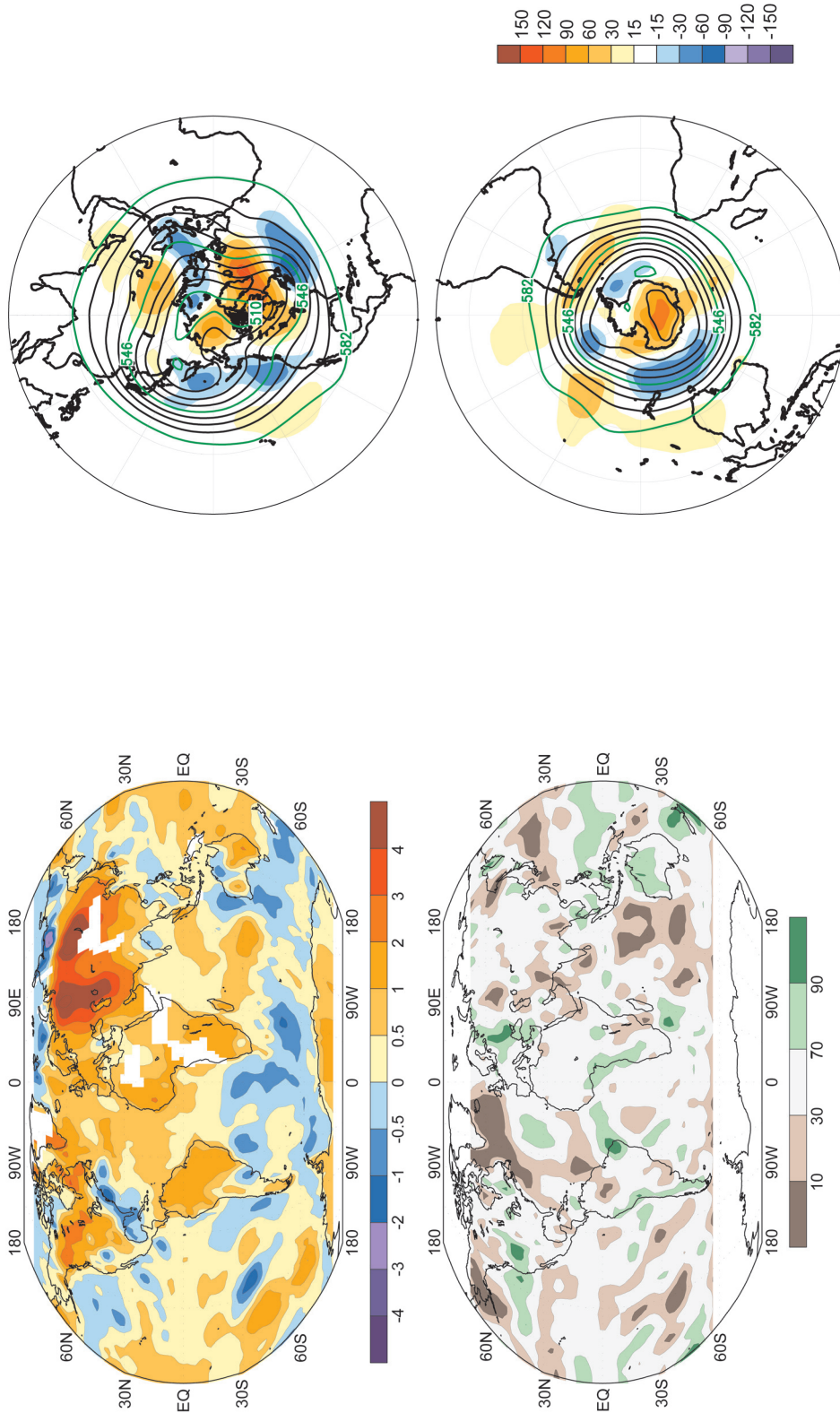


FIG. 7.1. Dec 2003–Feb 2004 (top) surface temperature anomalies and (bottom) precipitation percentiles based on a gamma distribution fit to the 1979–2000 base period. Temperature anomalies (1971–2000 base period) were based on station data over land and sea surface temperature over water. Precipitation data were obtained from a combination of rain gauge observations and satellite-derived precipitation estimates (Janowiak and Xie 1999). The analysis was omitted in data-sparse regions (white areas).

FIG. 7.2. Dec 2003–Feb 2004 (top) Northern Hemisphere and (bottom) Southern Hemisphere 500-hPa geopotential heights (contour interval is 9 dam) and anomalies (shading). Anomalies are departures from the 1979–2000 base period means.

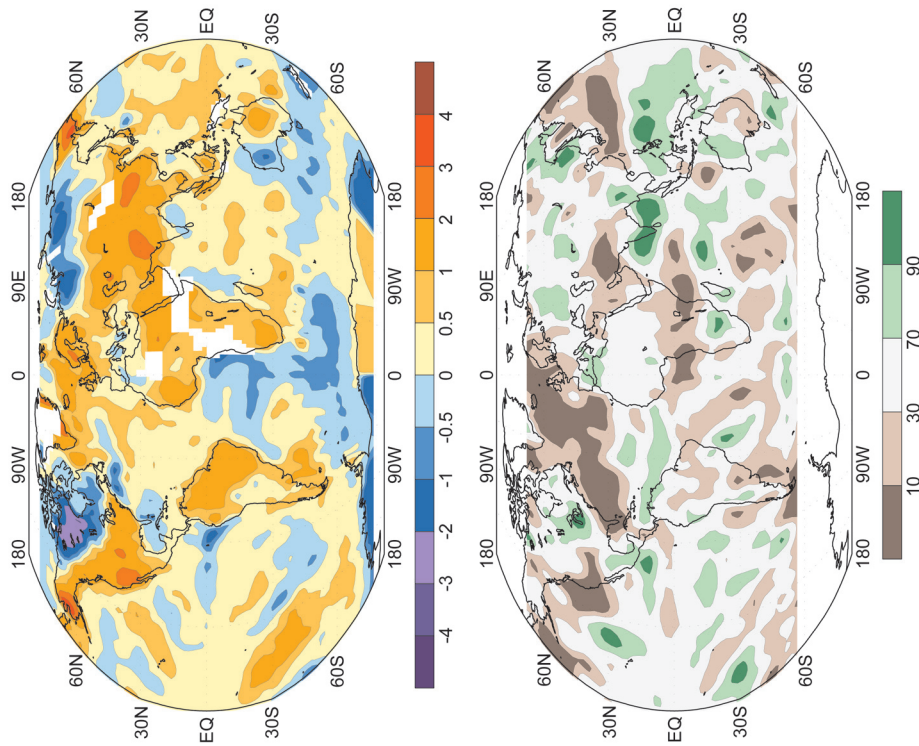


FIG. 7.3. Mar–May 2004 (top) (°C) surface temperature anomalies and (bottom) precipitation percentiles based on a gamma distribution fit to the 1979–2000 base period. Temperature anomalies (1971–2000 base period) were based on station data over land and sea surface temperature over water. Precipitation data were obtained from a combination of rain gauge observations and satellite-derived precipitation estimates (Janowiak and Xie 1999). The analysis was omitted in data-sparse regions (white areas).

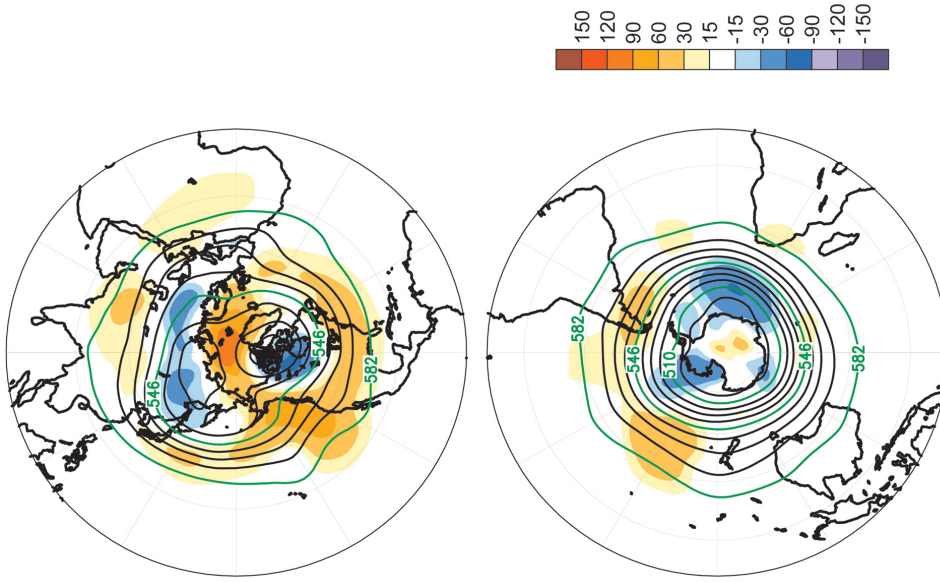


FIG. 7.4. Mar–May 2004 (top) Northern Hemisphere and (bottom) Southern Hemisphere 500-hPa geopotential heights (contour interval is 9 dam) and anomalies (shading). Anomalies are departures from the 1979–2000 base period means.

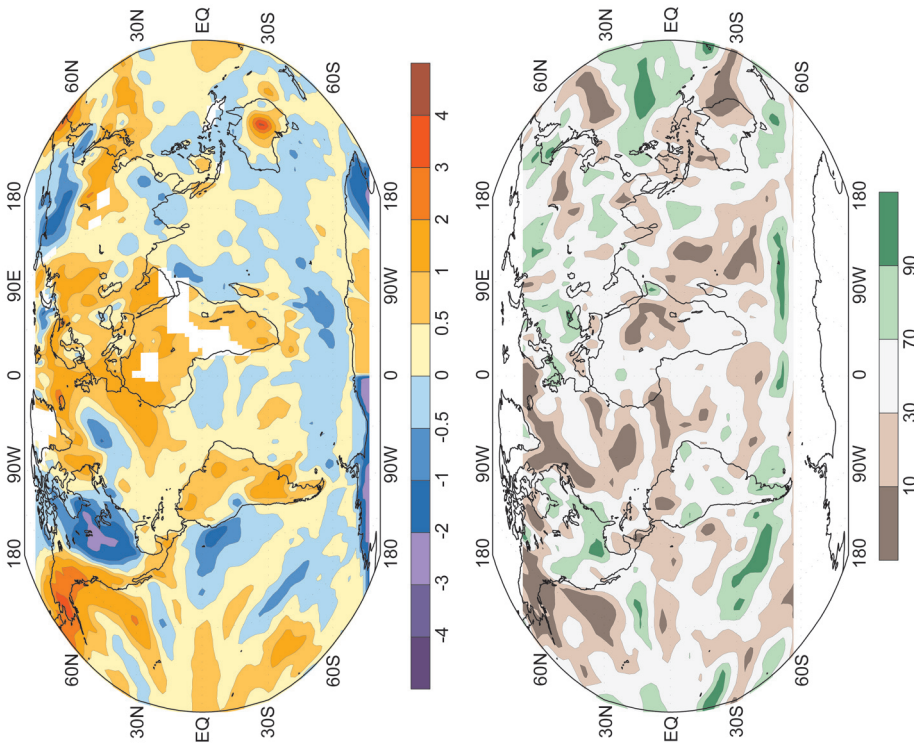


Fig. 7.5 Jun–Aug 2004 (top) (°C) surface temperature anomalies and (bottom) precipitation percentiles based on a gamma distribution fit to the 1979–2000 base period. Temperature anomalies (1971–2000 base period) were based on station data over land and sea surface temperature over water. Precipitation data were obtained from a combination of rain gauge observations and satellite-derived precipitation estimates (Janowiak and Xie 1999). The analysis was omitted in data-sparse regions (white areas).

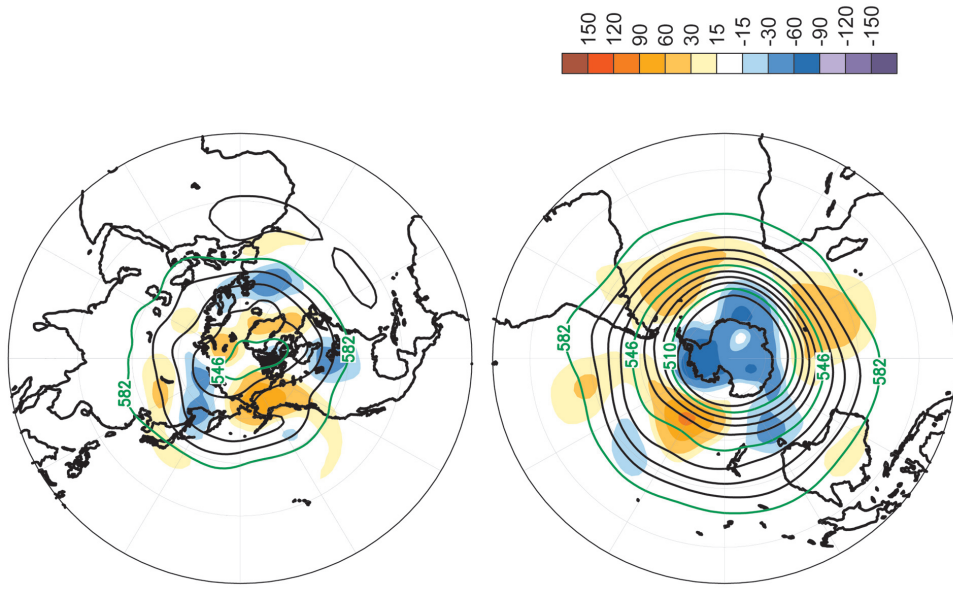


Fig. 7.6 Jun–Aug 2004 (top) Northern Hemisphere and (bottom) Southern Hemisphere 500-hPa geopotential heights (contour interval is 9 dam) and anomalies (shading). Anomalies are departures from the 1979–2000 base period means.

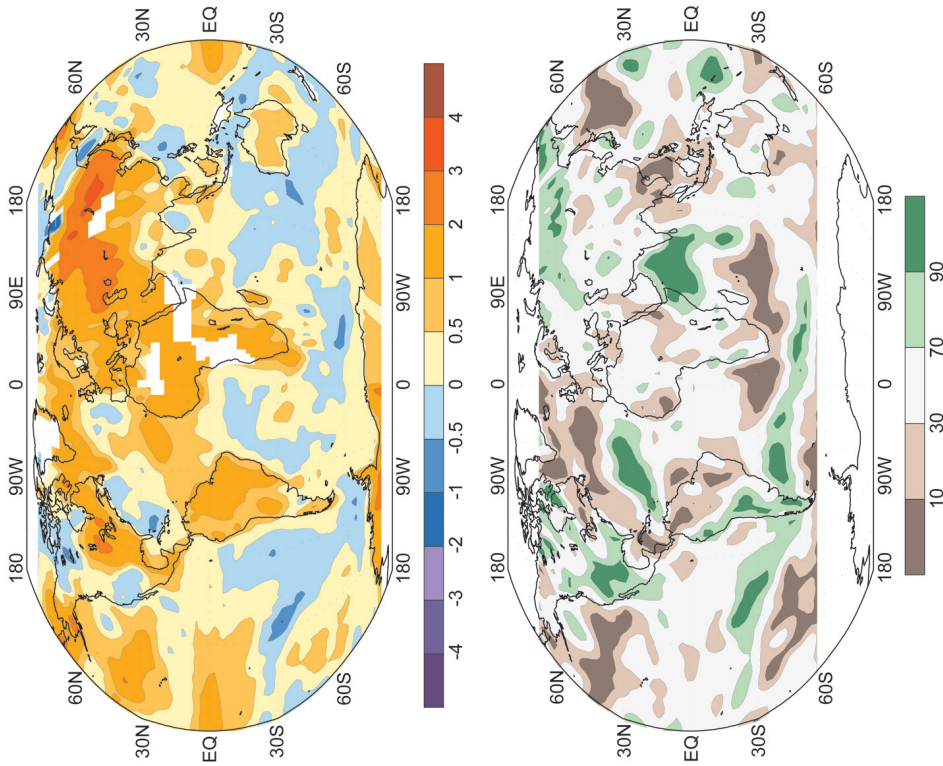


FIG. 7.7. Sep–Nov 2004 (top) surface temperature anomalies and (bottom) precipitation percentiles based on a gamma distribution fit to the 1979–2000 base period. Temperature anomalies (1971–2000 base period) were based on station data over land and sea surface temperature over water. Precipitation data were obtained from a combination of rain gauge observations and satellite-derived precipitation estimates (Janowiak and Xie 1999). The analysis was omitted in data-sparse regions

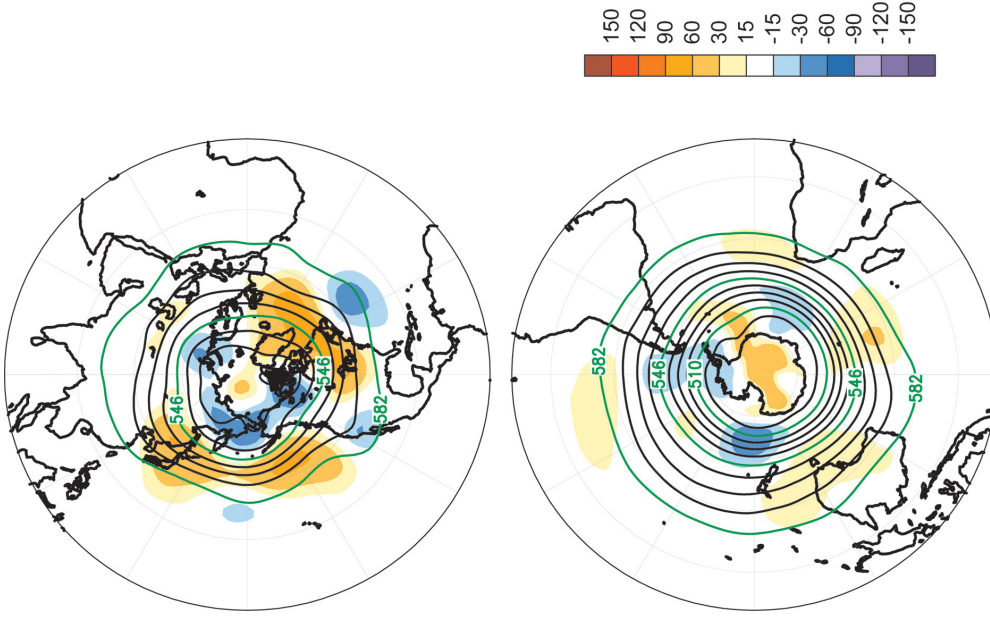


FIG. 7.8. Sep–Nov 2004 (top) Northern Hemisphere and (bottom) Southern Hemisphere 500-hPa geopotential heights (contour interval is 9 dam) and anomalies (shading). Anomalies are departures from the 1979–2000 base period means.

ACKNOWLEDGMENTS. This climate assessment would not have been possible without the assistance and contributions of many scientists from around the world. In addition to the cited authors, numerous contributors are named in the appendix below, and include a broad cross section of expertise from within the NOAA community, various federal laboratories, universities, and other institutions worldwide. We would like to thank all of them for their timely and valuable input. We would also like to thank the comments and suggestions provided by a cadre of reviewers at NCDC that greatly improved this article: Imke Durre, David Easterling, Grant Goodge, Jay Lawrimore, Sharon Leduc, Neal Lott, Scott Stephens, Russ Vose, Trevor Wallis, Anne Waple, David Wuertz, and Huai-min Zhang. Special acknowledgment must be given to Deborah Riddle and Sara Veasey at NCDC for the extensive time and graphical expertise they used in preparing this document. This assessment was supported by a grant from the NOAA Office of Global Program's Climate Change Data and Detection Program.

APPENDIX: CONTRIBUTORS

National Climatic Data Center

- Richard Heim
- Stuart Hinson
- Tom Smith
- Candace Tankersley
- Trevor Wallis

Hadley Centre for Climate Prediction and Research

- Nick Rayner

British Antarctic Survey

- Gareth Marshall

University of Illinois at Urbana–Champaign

- Bill Chapman

NOAA/Climate Monitoring and Diagnostics Laboratory/OAR

- J. H. Butler
- T. J. Conway
- E. J. Dlugokencky
- G. Dutton
- J. W. Elkins
- C. D. Keeling
- B. Johnson
- D. Mondeel
- S. A. Montzka
- P. C. Novelli
- S. Oltmans
- T. Thompson
- K. Thoning

National Snow and Ice Data Center

- Julianne Stroeve

Rutgers University

- Thomas Estilow

South African Weather Service

- Charlotte McBride

REFERENCES

- ACIA, 2004: *Impacts of a Warming Arctic: Arctic Climate Impacts Assessment*. Cambridge University Press, 139 pp.
- Alexander, L. V., and P. D. Jones, 2001: Updated precipitation series for the U.K. and discussion of recent extremes. *Atmos. Sci. Lett.*, **1**, doi:10.1006/asle.2000.0016.
- Antonov, J. I., S. Levitus, and T. P. Boyer, 2002: Steric sea level variations during 1957–1994: Importance of salinity. *J. Geophys. Res.*, **107**, 8103, doi:10.1029/2001JC000964.
- Atkinson, G. D., 1971: Forecasters' guide to tropical meteorology. U.S. Air Force Tech. Rep. 240, 360 pp.
- Australian Bureau of Meteorology, cited 2005: Tropical cyclones in Western Australia—Climatology. 6 pp. [Available online at www.bom.gov.au/weather/wa/cyclone/about/climatology.shtml.]
- Barlow, M., H. Cullen, and B. Lyon, 2002: Drought in central and southwest Asia: La Niña, the warm pool and Indian Ocean precipitation. *J. Climate*, **15**, 697–700.
- BAS, cited 2004: British Antarctic Survey. [Available online at www.antarctic.ac.uk.]
- Behringer, D. W., M. Ji, and A. Leetmaa, 1998: An improved coupled model for ENSO prediction and implications for ocean initialization. Part I: The ocean data assimilation system. *Mon. Wea. Rev.*, **126**, 1013–1021.
- Belchansky, G. I., D. C. Douglas, I. A. Alpatsky, and N. G. Platonov, 2004a: Spatial and temporal multiyear sea ice distributions in the Arctic: A neural network analysis of SSM/I data, 1988–2001. *J. Geophys. Res.*, **109**, C10017, doi:10.1029/2004JC002388.
- , —, and N. G. Platonov, 2004b: Duration of the Arctic sea ice melt season: Regional and interannual variability, 1979–2001. *J. Climate*, **17**, 67–80.
- Bell, G. D., 2003: Atlantic hurricane season. *State of the Climate in 2002*, A. M. Waple and J. H. Lawrimore, Eds., *Bull. Amer. Meteor. Soc.*, **84** (6), S19–S24.
- , and Coauthors, 2000: Climate assessment for 1999. *Bull. Amer. Meteor. Soc.*, **81**, S1–S50.
- , S. Goldenberg, C. Landsea, E. Blake, R. Pasch, M. Chelliah, and K. Mo, 2004: Atlantic hurricane season. *State of the Climate in 2003*, D. H. Levinson and A. M. Waple, Eds., *Bull. Amer. Meteor. Soc.*, **85**, S20–S24.

- Bonatti, J. P., V. B. Rao, and P. L. Silva-Dias, 2004: Estudo observacional da propagação para leste do fenômeno Catarina e sua simulação com modelo global de alta resolução. *Proc., XIII Congresso Brasileiro de Meteorologia*, Fortaleza, Ceara, Brazil, Brazilian Society of Meteorology, CD-ROM. [Available from Sociedade Brasileira de Meteorologia, Rua México, 41, Sala 1304, Centro 20031-144, Rio de Janeiro, Brazil.]
- Box, J. E., D. H. Bromwich, and L.-S. Bai, 2004: Greenland ice sheet surface mass balance for 1991–2000: Application of Polar MM5 mesoscale model and in-situ data. *J. Geophys. Res.*, **109**, D16105, doi:10.1029/2003JD004451.
- Bromwich D. H., J. Cassano, T. Klein, G. Heinemann, K. Hines, K. Steffen, and J. E. Box, 2001: Mesoscale modeling of katabatic winds over Greenland with the Polar MM5. *Mon. Wea. Rev.*, **129**, 2290–2309.
- Cabanes, C., A. Cazenave, and C. LeProvost, 2001: Sea level rise during the past 40 years determined from satellite and in-situ observations. *Science*, **294**, 840–842.
- Camargo, S. J., and A. H. Sobel, 2004: Western North Pacific tropical cyclone intensity and ENSO. International Research Institute for Climate Prediction, IRI Tech. Rep. 04-03, 25 pp.
- , and —, 2005: Western North Pacific tropical cyclone intensity and ENSO. *J. Climate*, in press.
- Cassano, J., J. E. Box, D. H. Bromwich, L. Li, and K. Steffen, 2001: Verification of Polar MM5 simulations of Greenland's atmospheric circulation, *J. Geophys. Res.*, **106** (D24), 33 867–33 890.
- Centurioni, L. R., P. P. Niiler, and D.-K. Lee, 2004: Observations of inflow of the Philippine Sea surface water into the South China Sea through the Luzon Strait. *J. Phys. Oceanogr.*, **34**, 113–121.
- Christy, J. R., and W. B. Norris, 2004: What may we conclude about global tropospheric temperature trends? *Geophys. Res. Lett.*, **31**, L06211, doi:10.1029/2003GL019361.
- , R. W. Spencer, W. B. Norris, W. D. Braswell, and D. E. Parker, 2003: Error estimates of Version 5.0 of MSU/AMSU bulk atmospheric temperatures. *J. Atmos. Oceanic Technol.*, **20**, 613–629.
- Church, J. A., N. J. White, R. Coleman, K. Lambeck, and J. X. Mitrovica, 2004: Estimates of the regional distribution of sea level rise over the 1950–2000 period. *J. Climate*, **17**, 2609–2624.
- Conway, T. J., P. P. Tans, L. S. Waterman, K. W. Thoning, D. R. Kitzis, K. A. Masarie, and N. Zhang, 1994: Evidence for interannual variability of the carbon cycle from the NOAA CMDL global air sampling network. *J. Geophys. Res.*, **99**, 22 831–22 855.
- Cook, E. R., D. M. Meko, D. W. Stahle, and M. K. Cleaveland, 1999: Drought reconstructions for the continental United States. *J. Climate*, **12**, 1145–1162.
- , C. Woodhouse, C. M. Eakin, D. M. Meko, and D. W. Stahle, 2004: Long-term aridity changes in the western United States. *Science*, **306**, 1015–1018 (plus supplementary material).
- Curry, R., B. Dickson, and I. Yashayaev, 2003: A change in the freshwater balance of the Atlantic Ocean over the past four decades. *Nature*, **426**, 826–829.
- Dai, A., I. Y. Fung, and A. D. Del Genio, 1997: Surface observed global land precipitation variations during 1900–88. *J. Climate*, **10**, 2943–2962.
- Daniel, J. S., and S. Solomon, 1998: On the climate forcing of carbon monoxide. *J. Geophys. Res.*, **103** (D11), 13 249–13 260.
- Dickson, R. R., R. Curry, and I. Yashayaev, 2003: Recent changes in the North Atlantic. *Phil. Trans. Roy. Soc. London A*, **361**, 18 pp, doi:10.1098/rsta.2003.1237.
- Dlugokencky, E. J., S. Houweling, L. Bruhwiler, K. A. Masarie, P. M. Lang, J. B. Miller, and P. P. Tans, 2003: Atmospheric methane levels off: Temporary pause or new steady state? *Geophys. Res. Lett.*, **30**, 1992, doi:10.1029/2003GL018126.
- Douglas, B. C., 1997: Global sea rise: A redetermination. *Surv. Geophys.*, **18**, 279–292.
- Drobot, S. D., and J. A. Maslanik, 2003: Interannual variability in summer Beaufort sea ice conditions: Relationship to spring and summer surface and atmospheric variability. *J. Geophys. Res.*, **108**, 3233, doi:10.1029/2002JC001537.
- FAO, cited 2004: Desert Locust Information Service. [Available online at <http://www.fao.org/news/global/LOCUSTS/locuhome.htm>.]
- Folland, C. K., and Coauthors, 2001: Global temperature change and its uncertainties since 1861. *Geophys. Res. Lett.*, **28**, 2621–2624.
- Fujita, T. T., 1971: Proposed characterization of tornadoes and hurricanes by area and intensity. University of Chicago, SMRP Research Paper 91, 42 pp.
- Geller, L. S., J. W. Elkins, J. M. Lobert, A. D. Clarke, D. F. Hurst, J. H. Butler, and R. C. Myers, 1997: Tropospheric SF₆: Observed latitudinal distribution and trends, derived emissions, and interhemispheric exchange time. *Geophys. Res. Lett.*, **24**, 675–678.
- Goldenberg, S. B., and L. J. Shapiro, 1996: Physical mechanisms for the association of El Niño and West African rainfall with Atlantic major hurricanes. *J. Climate*, **9**, 1169–1187.
- , C. W. Landsea, A. M. Mestas-Núñez, and W. M. Gray, 2001: The recent increase in Atlantic hurricane activity: Causes and implications. *Science*, **293**, 474–479.

- GPCC, cited 2004: Global Precipitation Climatology Centre. [Available online at <http://gpcc.dwd.de>; 1994–2004.]
- Gray, W. M., 1984: Atlantic seasonal hurricane frequency. Part I: El Niño and 30 mb quasi-biennial oscillation influences. *Mon. Wea. Rev.*, **112**, 1649–1668.
- Gusso, A., 2004: Aspectos Físicos Preliminares do Ciclone Extra-Tropical Anômalo Catarina na Perspectiva do Sistema de Satélites NOAA. *Proc. XIII Congresso Brasileiro De Meteorologia*, Fortaleza, Ceara, Brazil, Brazilian Society of Meteorology, CD-ROM. [Available from Sociedade Brasileira de Meteorologia, Rua México, 41, Sala 1304, Centro 20031-144, Rio de Janeiro, Brazil.]
- Hastenrath, S., L. Greischar, and J. Van Heerden, 1995: Prediction of the summer rainfall over South Africa. *J. Climate*, **8**, 1511–1518.
- Heim, R. R., Jr., 2002: A review of 20th century drought indices used in the United States. *Bull. Amer. Meteor. Soc.*, **83**, 1149–1165.
- Higgins, R. W., J. K. Schemm, W. Shi, and A. Leetmaa, 2000: Extreme precipitation events in the western United States related to tropical forcing. *J. Climate*, **13**, 793–820.
- Holgate, S. J., and P. L. Woodworth, 2004: Evidence for enhanced coastal sea level rise during the 1990s. *Geophys. Res. Lett.*, **31**, L07305, doi:10.1029/2004GL019626.
- Holland, G. J., 1981: On the quality of the Australian tropical cyclone data base. *Aust. Meteor. Mag.*, **29**, 169–181.
- , 1993: Ready reckoner. Global Guide to Tropical Cyclone Forecasting, World Meteorological Organization WMO/TC-No. 560, Rep. TCP-31. [Available online at http://www.bom.gov.au/bmrc/pubs/tc-guide/globa_guide_intro.htm.]
- Horton, E. B., C. K. Folland, and D. E. Parker, 2001: The changing incidence of extremes in worldwide and Central England temperatures to the end of the twentieth century. *Climatic Change*, **50**, 267–295.
- IOCI, 2002: Climate variability and change in southwest Western Australia. Department of Environment, Water, and Catchment Protection, 43 pp.
- Janowiak, J. E., and P. Xie, 1999: CAMS_OPI: A global satellite–rain gauge merged product for real-time precipitation monitoring applications. *J. Climate*, **12**, 3335–3342.
- Jauregui, E., 2003: Climatology of landfalling hurricanes and tropical storms in Mexico. *Atmosfera*, **16**, 193–204.
- Jones, P. D., 1994: Hemispheric surface air temperature variations: A reanalysis and an update to 1993. *J. Climate*, **7**, 1794–1802.
- , and D. Conway, 1997: Precipitation in the British Isles: An analysis of area-average data updated to 1995. *Int. J. Climatol.*, **17**, 427–438.
- , and A. Moberg, 2003: Hemispheric and large-scale surface air temperature variations: An extensive revision and an update to 2001. *J. Climate*, **16**, 206–223.
- , M. New, D. E. Parker, S. Martin, and I. G. Rigor, 1999: Surface air temperature and its changes over the past 150 years. *Rev. Geophys.*, **37**, 173–200.
- , T. J. Osborn, K. R. Briffa, C. K. Folland, B. Horton, L. V. Alexander, D. E. Parker, and N. A. Rayner, 2001: Adjusting for sampling density in grid-box land and ocean surface temperature time series. *J. Geophys. Res.*, **106**, 3371–3380.
- JTWC, cited 2005: JTWC (Joint Typhoon Warning Center) best track dataset. [Available online at https://metoc.npmoc.navy.mil/jtwc/best_tracks/.]
- Karl, T. R., C. N. Williams, F. T. Quinlan, and T. A. Boden, 1990: United States historical climatology Network. Carbon Dioxide Information and Analysis Center (CDIAC), Environmental Science Division Publication 3404, 389 pp.
- Kasischke, E. S., and Coauthors, 2000: Contributions of 1998 fires in the boreal forest to atmospheric concentrations of carbon monoxide and methane. *EOS Trans. Amer. Geophys. Union*, **81**, 260.
- Kessler, W. S., M. J. McPhaden, and K. M. Weickmann, 1995: Forcing of intraseasonal Kelvin waves in the equatorial Pacific. *J. Geophys. Res.*, **100**, 10 613–10 631.
- Kousky, V. E., and M. T. Kayano 1994: Principal modes of outgoing long-wave radiation and 250-mb circulation for the South American sector. *J. Climate*, **7**, 1131–1143.
- Kuleshov, Y., 2003: Tropical cyclones in the Southern Hemisphere: Influence of the El Niño/Southern Oscillation. *Proc. Seventh Int. Conf. on Southern Hemisphere Meteorology and Oceanography*, Wellington, New Zealand, Amer. Meteor. Soc., 202–203.
- , and G. de Hoedt, 2003: Tropical Cyclone Activity in the Southern Hemisphere. *Bull. Aust. Meteor. Oceanogr. Soc.*, **16**, 135–137.
- Landsea, C. W., G. D. Bell, W. M. Gray, and S. B. Goldenberg, 1998: The extremely active 1995 Atlantic hurricane season: Environmental conditions and verification of seasonal forecasts. *Mon. Wea. Rev.*, **126**, 1174–1193.
- , R. A. Pielke Jr., A. M. Mestas-Núñez, and J. A. Knaff, 1999: Atlantic basin hurricanes: Indices of climate changes. *Climatic Change*, **42**, 89–129.
- Langenfelds, R. L., R. J. Francey, B. C. Pak, L. P. Steele, J. Lloyd, C. M. Trudinger, and C. E. Allison, 2002: Interannual growth rate variations of atmospheric

- CO₂ and its $\delta^{13}\text{C}$, H₂, CH₄, and CO between 1992 and 1999 linked to biomass burning. *Global Biogeochem. Cycles*, **16**, 1048, doi:10.1029/2001GB001466.
- Lanzante, J. R., S. A. Klein, and D. J. Seidel, 2003: Temporal homogenization of monthly radiosonde temperature data. Part I: Methodology. *J. Climate*, **16**, 224–240.
- Lawrence, M. B., L. A. Avila, J. L. Beven, J. L. Franklin, R. J. Pasch, and S. R. Stewart, 2005: Atlantic hurricane season of 2003. *Mon. Wea. Rev.*, **133**, 1744–1773.
- Leuliette, E. W., R. S. Nerem, and G. T. Mitchum, 2004: Calibration of TOPEX/Poseidon and Jason altimeter data to construct a continuous record of mean sea level change. *Mar. Geodesy*, **27** (1–2), 79–94.
- Levinson, D. H., and A. M. Waple, Eds., 2004: State of the Climate in 2003. *Bull. Amer. Meteor. Soc.*, **85** (6), S1–S72.
- Lourensz, R. S., 1981: *Tropical cyclones in the Australian region July 1909 to June 1980*. Australian Government Publishing Service, 94 pp.
- Lyon, B., 2004: The strength of El Niño and the spatial extent of tropical drought. *Geophys. Res. Lett.*, **31**, L21204, doi:10.1029/2004GL020901.
- Madden, R. A., and P. R. Julian, 1971: Detection of a 40–50 day oscillation in the zonal wind in the tropical Pacific. *J. Atmos. Sci.*, **28**, 702–708.
- , and —, 1972: Description of global-scale circulation cells in the Tropics with 40–50 day period. *J. Atmos. Sci.*, **29**, 1109–1123.
- , and —, 1994: Observations of the 40–50 day tropical oscillation—A review. *Mon. Wea. Rev.*, **122**, 814–837.
- Mann, M. E., and P. D. Jones, 2003: Global surface temperatures over the past two millennia. *Geophys. Res. Lett.*, **30**, 1820, doi:10.1029/2003GL017814.
- Mattos L. F., and P. Satyamurty, 2004: Catarina 2004: um Sistema Meteorológico raro no Litoral Brasileiro. *Proc. XIII Congresso Brasileiro De Meteorologia*, Fortaleza, Ceara, Brazil, Brazilian Society of Meteorology, CD-ROM. [Available from Sociedade Brasileira de Meteorologia, Rua México, 41, Sala 1304, Centro 20031-144, Rio de Janeiro, Brazil.]
- McBride, J. L., 2004: Relationships between tropical cyclones and sea surface temperature in the Australian region: Implications for anthropogenic climate change. *Proc. Int. Conf. on Storms*, Brisbane, Australia, Australian Meteorological and Oceanographic Society, 238–239.
- McPhaden, M. J., 2004: Evolution of the 2002–03 El Niño. *Bull. Amer. Meteor. Soc.*, **85**, 677–695.
- Mears, C. A., M. C. Schabel, and F. J. Wentz, 2003: A reanalysis of the MSU channel 2 tropospheric temperature record. *J. Climate*, **16**, 3650–3664.
- Menezes, W., and P. L. Silva-Dias, 2004: Um estudo do impacto das opções físicas do modelo RAMS na simulação numérica do ciclone Catarina. *Proc. XIII Congresso Brasileiro de Meteorologia*, Fortaleza, Ceara, Brasil, Brazilian Society of Meteorology, CD-ROM. [Available from Sociedade Brasileira de Meteorologia, Rua México, 41, Sala 1304, Centro 20031-144, Rio de Janeiro, Brazil.]
- Mestas-Nuñez, A. M., and D. B. Enfield, 1999: Rotated global modes of non-ENSO sea surface temperature variability. *J. Climate*, **12**, 2734–2746.
- Miller, L., and B. C. Douglas, 2004: Mass and volume contributions to 20th-century global sea level rise. *Nature*, **428**, 406–409.
- Mo, K. C., and V. E. Kousky, 1993: Further analysis of the relationship between circulation anomaly patterns and tropical convection. *J. Geophys. Res.*, **98**, 5103–5113.
- Montzka, S. A., and Coauthors, 2003a: Controlled substances and other source gases. Scientific Assessment of Ozone Depletion: 2002, Global Ozone Research and Monitoring Project, WMO/UNEP Rep. 47, 1–83.
- , J. H. Butler, B. D. Hall, J. W. Elkins, and D. J. Mondeel, 2003b: A decline in tropospheric organic bromine. *Geophys. Res. Lett.*, **30**, 1826, doi:10.1029/2003GL017745.
- Neumann, C. J., B. R. Jarvinen, C. J. McAdie, and J. D. Elms, 1993: *Tropical Cyclones of the North Atlantic Ocean, 1871–1992*. NOAA National Climatic Data Center, in cooperation with the National Hurricane Center, 193 pp.
- Niiler, P., 2001: The World Ocean surface circulation. *Ocean Circulation and Climate-Observing and Modeling the Global Ocean*, J. Church, G. Siedler, and J. Gould, Eds., Academic Press, 715 pp.
- Novelli, P. C., K. A. Masarie, P. M. Lang, B. D. Hall, R. C. Myers, and J. C. Elkins, 2003: Reanalysis of tropospheric CO trends: Effects of the 1997–1998 wildfires. *J. Geophys. Res.*, **108**, 4464, doi:10.1029/2002JD003031.
- NSIDC, cited 2004: Arctic sea ice decline continues. [Available online at http://nsidc.org/news/press/20041004_decline.html.]
- Padgett, G., cited 2005: Tropical cyclone summaries [Available online at <ftp://ftp.aoml.noaa.gov/hrd/pub/landsea/padgett/>.]
- Palmer, W. C., 1965: *Meteorological Drought*. U.S. Weather Bureau Research Paper 45, 58 pp. [Available from NOAA Library and Information Services Division, Washington, DC 20852.]

- Parker, D. E., T. P. Legg, and C. K. Folland, 1992: A new daily central England temperature series, 1772–1991. *Int. J. Climatol.*, **12**, 317–342.
- , C. K. Folland, and M. Jackson, 1995: Marine surface temperature: Observed variations and data requirements. *Climatic Change*, **31**, 559–600.
- Pasch, R. J., M. B. Lawrence, L. A. Avila, J. L. Beven, J. L. Franklin, and S. R. Stewart, 2004: Atlantic hurricane season of 2002. *Mon. Wea. Rev.*, **132**, 1829–1859.
- Peltier, W. R., 2001: Global glacial isostatic adjustment and modern instrumental records of relative sea level history. *Sea Level Rise, History and Consequences*, B. C. Douglas, M. S. Kearney, and S. P. Leatherman, Eds., Academic Press, 65–95.
- Peterson, T. C., and R. S. Vose, 1997: An overview of the Global Historical Climatology Network temperature database. *Bull. Amer. Meteor. Soc.*, **78**, 2837–2849.
- Pitman, A. J., G. T. Narisma, R. A. Pielke, and N. J. Holbrook, 2004: Impact of land-cover change on the climate of southwest Western Australia. *J. Geophys. Res.*, **109**, D18109, doi:10.1029/2003JD004347.
- Prather, M. J., 1996: Natural modes and time scales in atmospheric chemistry: Theory, GWPs for CH₄ and CO, and runaway growth. *Geophys. Res. Lett.*, **23**, 2597–2600.
- Prentice, I. C., and Coauthors, 2001: The carbon cycle and atmospheric carbon dioxide. *Climate Change 2001: The Scientific Basis*, J. T. Houghton et al., Eds., Cambridge University Press, p. 190.
- Quayle, R. G., T. C. Peterson, A. N. Basist, and C. S. Godfrey, 1999: An operational near-real-time global temperature index. *Geophys. Res. Lett.*, **26**, 333–335.
- Reale, O., and R. Atlas, 2001: Tropical cyclone-like vortices in the extratropics: Observational evidence and synoptic analysis. *Wea. Forecasting*, **16**, 7–34.
- Reynolds, R. W., N. A. Rayner, T. M. Smith, D. C. Stokes and W. Wang, 2002: An improved in situ and satellite SST analysis for climate. *J. Climate*, **15**, 1609–1625.
- Rigor, I. G., and J. M. Wallace, 2004: Variations in the age of Arctic sea-ice and summer sea-ice extent. *Geophys. Res. Lett.*, **31**, L09401, doi:10.1029/2004GL019492.
- , R. L. Colony, and S. Martin, 2000: Variations in surface air temperature in the Arctic from 1979–1997. *J. Climate*, **13**, 896–914.
- Ropelewski, C. F., and M. S. Halpert, 1987: Global and regional scale precipitation patterns associated with the El Niño/Southern Oscillation. *Mon. Wea. Rev.*, **115**, 1606–1626.
- , and —, 1989: Precipitation patterns associated with the high index phase of the Southern Oscillation. *J. Climate*, **2**, 268–284.
- , and —, 1996: Quantifying Southern Oscillation–precipitation relationships. *J. Climate*, **9**, 1043–1059.
- Rothrock, D. A., and J. Zhang, 2005: Arctic Ocean sea ice volume: What explains its recent depletion? *J. Geophys. Res.*, **110**, C01002, doi:10.1029/2004JC002282.
- Rudolf, B., H. Hauschild, W. Rueth, and U. Schneider, 1994: Terrestrial precipitation analysis: Operational method and required density of point measurements. *Global Precipitation and Climate Change*, M. Desbois and F. Desalmond, Eds., NATO ASI Series I, Vol. 26, Springer-Verlag, 173–186.
- , T. Fuchs, U. Schneider, and A. Meyer-Christoffer, 2003: Introduction of the Global Precipitation Climatology Centre (GPCC). Deutscher Wetterdienst, 16 pp. [Available on request via e-mail at gpcc@dwd.de.]
- Rusticucci, M., and W. Vargas, 1995: Synoptic situations related to spells of extreme temperatures over Argentina. *Meteor. Appl.*, **2**, 291–300.
- Sabine, and Coauthors, 2004: The oceanic sink for anthropogenic CO₂. *Science*, **305**, 367–371.
- Sampaio-Calearo, D., and Coauthors, 2004: Monitoramento do Catarina no Centro Operacional da Epagri/Climerh. *Proc. XIII Congresso Brasileiro De Meteorologia*, Fortaleza, Ceara, Brazil, Brazilian Society of Meteorology, CD-ROM. [Available from Sociedade Brasileira de Meteorologia, Rua México, 41, Sala 1304, Centro 20031-144, Rio de Janeiro, Brazil.]
- Seidel, D. J., and Coauthors, 2004: Uncertainty in signals of large-scale climate variations in radiosonde and satellite upper-air temperature datasets. *J. Climate*, **17**, 2225–2240.
- Serreze, M. C., and Coauthors, 2003: A record minimum arctic sea ice extent and area in 2002. *Geophys. Res. Lett.*, **30**, 1110, doi:10.1029/2002GL016406.
- Shapiro, L. J., 1989: The relationship of the quasi-biennial oscillation to Atlantic tropical storm activity. *Mon. Wea. Rev.*, **117**, 1545–1552.
- Silva-Dias, P. L., M. A. Silva-Dias, M. Seluchi, and F. O. Assis-Diniz, 2004: Ciclone Catarina: Análise Preliminar da Estrutura, Dinâmica e Previsibilidade. *Proc. XIII Congresso Brasileiro De Meteorologia*, Fortaleza, Ceara, Brazil, Brazilian Society of Meteorology, CD-ROM. [Available from Sociedade Brasileira de Meteorologia, Rua México, 41, Sala 1304, Centro 20031-144, Rio de Janeiro, Brazil.]
- Simpson, R. H., 1974: The hurricane disaster potential scale. *Weatherwise*, **27**, 169–186.
- Smith, T. M., and R. W. Reynolds, 1998: A high-resolution global sea surface temperature climatology for the 1961–90 base period. *J. Climate*, **11**, 3320–3323.
- , and —, 2004: Improved extended reconstruction of SST (1854–1997). *J. Climate*, **17**, 2466–2477.
- , and —, 2005: A global merged land–air–sea surface temperature reconstruction based on historical observations (1880–1997). *J. Climate*, in press.

- Stone, R. S., E. G. Dutton, J. M. Harris, and D. Longenecker, 2002: Earlier spring snowmelt in northern Alaska as an indicator of climate change. *J. Geophys. Res.*, **107**, 10.1029/2000JD000286.
- , D. C. Douglas, G. I. Belchansky, S. D. Drobot, and J. Harris, 2005: Cause and effect of variations in western Arctic snow and sea ice cover. Preprints, *Eighth Conf. on Polar Meteorology and Oceanography*, San Diego, CA, Amer. Meteor. Soc., CD-ROM, 8.3.
- Stroeve, J. C., M. C. Serreze, F. Fetterer, T. Arbetter, W. Meier, J. A. Maslanik, and K. Knowles, 2005: Tracking the Arctic's shrinking sea ice cover: Another extreme minimum in 2004. *Geophys. Res. Lett.*, **32**, L04501, doi:10.1029/2004GL021810.
- Steffen, K., and J. E. Box, 2001: Surface climatology of the Greenland ice sheet: Greenland climate network 1995–1999. *J. Geophys. Res.*, **106** (D24), 33 951–33 964.
- Tans, P. P., 1997: The CO₂ lifetime concept should be banished, an editorial comment. *Climatic Change*, **37**, 487–490.
- , and P. S. Bakwin, 1995: Climate change and carbon dioxide forever. *Ambio*, **24**, 376–378.
- , and J. W. C. White, 1998: In balance, with a little help from the plants. *Science*, **282**, 183–184.
- Thiaw, W. M., A. B. Barnston, and V. Kumar, 1999: Predictions of African rainfall on the seasonal time scale. *J. Geophys. Res.*, **104**, 31 589–31 597.
- Thompson, D. W. J., and J. M. Wallace, 1998: The Arctic Oscillation signature in the wintertime geopotential height and temperature fields. *Geophys. Res. Lett.*, **25**, 1297–1300.
- Thompson, T. M., and Coauthors, 2004: Halocarbons and other atmospheric trace species. Climate Monitoring and Diagnostics Laboratory Summary Report 2002–2003, NOAA Oceanic and Atmospheric Research CMDL No. 27, 115–135.
- Thorne, P. W., D. E. Parker, S. F. B. Tett, P. D. Jones, M. McCarthy, H. Coleman, P. Brohan, and J. R. Knight, 2005b: Revisiting radiosonde upper-air temperatures from 1958 to 2002. *J. Geophys. Res.*, in press.
- Vaughan, D. G., and C. S. M. Doake, 1996: Recent atmospheric warming and retreat of ice shelves on the Antarctic Peninsula. *Nature*, **379**, 328–331.
- Vose, R. S., R. L. Schmoyer, P. M. Steurer, T. C. Peterson, R. Heim, T. R. Karl, and J. Eischeid, 1992: The Global Historical Climatology Network: Long-term monthly temperature, precipitation, sea level pressure, and station pressure data. Carbon Dioxide Information Analysis Center (CDIAC), Oak Ridge National Laboratory, Rep. ORNL/CDIAC-53, NDP-041, 315 pp.
- White, N. J., J. A. Church, and J. M. Gregory, 2005: Coastal and global averaged sea level rise for 1950 to 2000. *Geophys. Res. Lett.*, **32**, L01601, doi:10.1029/2004GL021391.
- Whitney, L. D., and J. S. Hobgood, 1997: The relationship between sea surface temperatures and maximum intensities of tropical cyclones in the eastern North Pacific Ocean. *J. Climate*, **10**, 2921–2930.
- Willis, J. K., D. Roemmich, and B. Cornuelle, 2004: Interannual variability in upper ocean heat content, temperature, and thermocline expansion on global scales. *J. Geophys. Res.*, **109**, C12036, doi:10.1029/2003JC002260.
- Zhang, C., H. Hendon, W. Kessler, and A. Rosati, 2001: A workshop on the MJO and ENSO. *Bull. Amer. Meteor. Soc.*, **82**, 971–976.
- Zwally, H. J., W. Abdalati, T. Herring, K. Larson, J. Saba, and K. Steffen, 2002: Surface melt-induced acceleration of Greenland ice-sheet flow. *Science*, **297**, 218–222.